The HYDRUS Code for Simulating the One-Dimensional Movement of Water, Heat, and Multiple Solutes in Variably-Saturated Media

Version 6.0

Research Report No. 144

May 1998

U. S. SALINITY LABORATORY
AGRICULTURAL RESEARCH SERVICE
U. S. DEPARTMENT OF AGRICULTURE
RIVERSIDE, CALIFORNIA

The HYDRUS Code for Simulating the One-Dimensional Movement of Water, Heat, and Multiple Solutes in Variably-Saturated Media

Version 6.0

by

J. Šimůnek, K. Huang, and M. Th. van Genuchten

Research Report No. 144

May 1998

U. S. SALINITY LABORATORY
AGRICULTURAL RESEARCH SERVICE
U. S. DEPARTMENT OF AGRICULTURE
RIVERSIDE, CALIFORNIA

DISCLAIMER

This report documents version 6.0 of HYDRUS, a computer program for simulating water, heat and solute movement in one-dimensional variably-saturated media. The code has been verified against a large number of test cases. However, no warranty is given that the program is completely error-free. If you do encounter problems with the code, find errors, or have suggestions for improvement, please contact one of the authors at

U. S. Salinity Laboratory
USDA, ARS
450 West Big Springs Road
Riverside, CA 92507

Tel. 909-369-4865 (J. Šimůnek)
Tel. 909-369-4846 (M. Th. van Genuchten)
Fax. 909-342-4964
E-mail. jsimunek@ussl.ars.usda.gov
rvang@ussl.ars.usda.gov

ABSTRACT

Šimůnek, J., K. Huang, and M. Th. van Genuchten. 1998. The HYDRUS Code for Simulating the Movement of Water, Heat, and Multiple Solutes in Variably Saturated Media, Version 6.0, Research Report No. 144, U.S. Salinity Laboratory, USDA, ARS, Riverside, California.

This report documents version 6.0 of HYDRUS, a computer program for simulating water, heat and solute movement in one-dimensional variably saturated media. The HYDRUS 6.0 program numerically solves the Richards' equation for variably-saturated water flow and convection-dispersion type equations for heat and solute transport. The flow equation incorporates a sink term to account for water uptake by plant roots. The heat transport equation considers transport due to conduction and convection with flowing water. The solute transport equations consider convective-dispersive transport in the liquid phase, as well as diffusion in the gaseous phase. The transport equations also include provisions for nonlinear nonequilibrium reactions between the solid and liquid phases, linear equilibrium reactions between the liquid and gaseous phases, zero-order production, and two first-order degradation reactions: one which is independent of other solutes, and one which provides the coupling between solutes involved in sequential first-order decay reactions. The program may be used to analyze water and solute movement in unsaturated, partially saturated, or fully saturated porous media. The flow region may be composed of nonuniform soils. Flow and transport can occur in the vertical, horizontal, or a generally inclined direction. The water flow part of the model can deal with prescribed head and flux boundaries, boundaries controlled by atmospheric conditions, as well as free drainage boundary conditions. The governing flow and transport equations are solved numerically using Galerkin-type linear finite element schemes.

This report serves as both a user manual and reference document. Detailed instructions are given for data input preparation. The program is written in FORTRAN 77 and compiled and linked with Microsoft Fortran PowerStation. Example input and output files are also provided.

TABLE OF CONTENTS

LIST OF FIGURES

LIST OF TABLES

LIST OF ALL VARIABLES

$\bar{a}$	ion activity on the exchange surfaces [-]
a^*	parameter in the exponential depth distribution function [L^{-1}]
a_i	conversion factor from concentration to osmotic head [L^4M^{-1}]
a_r	value of coefficient a at reference temperature T_r^A
a_T	value of coefficient a at temperature T^A
a_v	air content [L^3L^{-3}]
A	amplitude of temperature sine wave at the soil surface [K]
A_{qh}	empirical parameter in the deep drainage function, Eq. (7.1) [LT^{-1}]
b	normalized root water uptake distribution [L^{-1}]
b'	arbitrary root water uptake distribution [L^{-1}]
b_i	coefficients in the global matrix equations for water flow [T^{-1}] and solute transport [$L T^{-1}$]
b_1,b_2,b_3	empirical parameters to calculate the soil thermal conductivity, λ_0 [$MLT^{-3}K^{-1}$] (e.g. W $m^{-1}K^{-1}$)
B	convective term in the solute transport equation [LT^{-1}]
B_{qh}	empirical parameter in the deep drainage function, Eq. (7.1) [L^{-1}]
c	solution concentration [ML^{-3}]
c'	finite element approximation of c [ML^{-3}]
c_i	initial solution concentration [ML^{-3}]
c_n	value of the concentration at node n [ML^{-3}]
c_r	concentration of the sink term [ML^{-3}]
c_0	prescribed concentration boundary condition [ML^{-3}]
C	soil water capacity [L^{-1}]
C_a	volumetric heat capacity of the gas phase [$ML^{-1}T^{-2}K^{-1}$] (e.g. $Jm^{-3}K^{-1}$)
C_n	volumetric heat capacity of the solid phase [$ML^{-1}T^{-2}K^{-1}$] (e.g. $Jm^{-3}K^{-1}$)
C_o	volumetric heat capacity of the organic matter [$ML^{-1}T^{-2}K^{-1}$] (e.g. $Jm^{-3}K^{-1}$)
C_p	volumetric heat capacity of the porous medium [$ML^{-1}T^{-2}K^{-1}$] (e.g. $Jm^{-3}K^{-1}$)
C_T	total solution concentration [ML^{-3}] ($mmol_c l^{-1}$)

C_w volumetric heat capacity of the liquid phase [$ML^{-1}T^{-2}K^{-1}$] (e.g. $Jm^{-3}K^{-1}$)

Cr_i^e local Courant number for element e [-]

d thickness of stagnant boundary layer above soil surface [L]

d_i coefficients in the global matrix equations for water flow [T^{-1}] and solute transport [$L T^{-1}$]

D effective dispersion coefficient of the soil matrix [L^2T^{-1}]

D^-, D^+ effective dispersion coefficients corrected for higher-order approximation [L^2T^{-1}]

D^g diffusion coefficient for the gas phase [L^2T^{-1}]

D^w solute dispersion coefficient for the liquid phase [L^2T^{-1}]

D_g molecular diffusion coefficient of the gas phase [L^2T^{-1}]

D_L longitudinal dispersivity [L]

$\bar{D}_L$ additional longitudinal dispersivity [L] to fulfill the performance index ω_s

D_w molecular diffusion coefficient in free water [L^2T^{-1}]

e element number [-]

e_i coefficients in the global matrix equations for water flow [T^{-1}] and solute transport [$L T^{-1}$]

e_R elements located in the root zone [-]

E maximum (potential) rate of infiltration or evaporation under the prevailing atmospheric conditions [LT^{-1}]

E dispersive term in the solute transport equation [L^2T^{-1}]

E_a activation energy of a chemical reaction or process [$ML^2T^{-2}M^{-1}$] ($m^2s^{-2}mol^{-1}$)

f fraction of exchange sites assumed to be at equilibrium with the solution concentration [-]

f_i coefficients in the global matrix equations for water flow [LT^{-1}] and solute transport [$ML^{-2}T^{-1}$]

f_r root growth coefficient [-]

$\{f\}$ vector in the global matrix equation for solute transport [$MT^{-1}L^{-2}$]

F first-order decay term in the solute transport equation [T^{-1}]

$\{F_w\}$ coefficient vector in the global matrix equation for water flow [LT^{-1}]

g gas phase concentration [ML^{-3}]

g_{atm} gas phase concentration above the stagnant boundary layer [ML^{-3}]

G zero-order decay term in the solute transport equation [$ML^{-3}T^{-1}$]

h pressure head [L]

h^* scaled pressure head [L]

h' finite element approximation of h [L]

h_A minimum pressure head allowed at the soil surface [L]

h_i initial condition for the pressure head [L]

h_n nodal value of the pressure head [L]

h_{ref} pressure head at reference temperature T_{ref} [L]

h_s air-entry value in the Brooks and Corey soil water retention function [L]

h_S maximum pressure head allowed at the soil surface [L]

h_T pressure head at soil temperature T [L]

h_0 surface boundary condition for the pressure head [L]

h_{50} pressure head at which root water uptake is reduced by 50 % [L]

h_ϕ osmotic head [L]

$h_{\phi 50}$ osmotic head at which root water uptake is reduced by 50 % [L]

h_Δ pressure head at the reversal point in a hysteretic retention function [L]

k kth chain number [-]

k_g empirical constant relating the solution and gas phase concentrations [-]

k_s empirical constant relating the solution and adsorbed concentrations [L^3M^{-1}]

K unsaturated soil hydraulic conductivity [LT^{-1}]

K^* scaled unsaturated soil hydraulic conductivity [LT^{-1}]

K^d unsaturated hydraulic conductivity of the main drying branch [LT^{-1}]

K^w unsaturated hydraulic conductivity of the main wetting branch [LT^{-1}]

K_{ex} dimensionless thermodynamic equilibrium constant [-]

K_H Henry's law constant [$MT^2M^{-1}L^{-2}$]

K_k measured value of the unsaturated soil hydraulic conductivity at θ_k [LT^{-1}]

K_r relative soil hydraulic conductivity [-]

K_{ref} hydraulic conductivity at reference temperature T_{ref} [LT^{-1}]

K_s saturated hydraulic conductivity [LT^{-1}]

K_s^d saturated hydraulic conductivity associated with the main drying branch [LT^{-1}]

K_s^w saturated hydraulic conductivity associated with the main wetting branch [LT^{-1}]

K_T hydraulic conductivity at soil temperature T [LT^{-1}]

K_v Vanselow selectivity coefficient [-]

K_{12} selectivity coefficient [-]

K_Δ unsaturated hydraulic conductivity at the reversal point in a hysteretic conductivity function [LT^{-1}]

l pore-connectivity parameter [-]

L x-coordinate (depth of the soil profile) of the soil surface above a certain reference plane [L]

L_m maximum rooting depth [L]

L_R root depth [L]

L_0 initial value of the rooting depth at the beginning of the growth period [L]

m parameter in the soil water retention function [-]

M total amount of mass in the entire flow domain [ML^{-2}]

M^0 cumulative amount of solute removed from the flow region by zero-order reactions [ML^{-2}]

M^1 cumulative amount of solute removed from the flow region by first-order reactions [ML^{-2}]

M_r cumulative amount of solute removed from the flow region by root water uptake [ML^{-2}]

M_t total amount of solute in the flow region at time t [ML^{-2}]

M_t^e amount of solute in element e at time t [ML^{-2}]

M_0 amount of solute in the flow region at the beginning of the simulation [ML^{-2}]

M_0^e amount of solute in element e at the beginning of the simulation [ML^{-2}]

n exponent in the soil water retention function [-]

n^d exponent in the soil water retention function; drying branch [-]

n^w exponent in the soil water retention function; wetting branch [-]

n_s number of solutes involved in the consecutive solute chain [-]

N total number of nodes [-]

O actual rate of inflow/outflow to/from a subregion [LT^{-1}]

p exponent in the water and osmotic stress response function [-]

p_t period of time necessary to complete one temperature cycle (1 day) [T]

p_1 exponent in the water stress response function [-]

p_2 exponent in the osmotic stress response function [-]

Pe_i^e local Peclet number for element e [-]

$[P_s]$ coefficient matrix in the global matrix equation for solute transport [LT^{-1}]

$[P_w]$ coefficient matrix in the global matrix equation for water flow [T^{-1}]

q Darcian fluid flux density [LT^{-1}]

q_N water flux boundary condition at the soil surface [LT^{-1}]

q_s solute flux [$ML^{-2}T^{-1}$]

q_{s0} solute flux boundary condition at the bottom of the soil profile [LT^{-1}]

q_{sN} solute flux boundary condition at the soil surface [LT^{-1}]

q_0 water flux boundary condition at the bottom of the soil profile [LT^{-1}]

$[Q]$ coefficient matrix in the global matrix equation for solute transport [L]

r growth rate [T^{-1}]

r_i coefficients in the global matrix equation for solute transport [$ML^{-2}T^{-1}$]

R solute retardation factor [-]

R_u universal gas constant [$ML^2T^{-2}K^{-1}M^{-1}$] (= 8.314kg $m^2s^{-2}K^{-1}mol^{-1}$)

$\{R\}$ vector in the global matrix equation for solute transport [$ML^{-2}T^{-1}$]

s adsorbed solute concentration [-]

s^e adsorbed solute concentration on type-1 sites [-]

s_i initial value of adsorbed solute concentration [-]

s^k adsorbed solute concentration on type-2 sites [-]

S sink term in the flow equation [T^{-1}]

S_e effective saturation [-]

S_{ek} effective saturation at θ_k [-]

S_p spatial distribution of the potential transpiration rate over the soil profile [T^{-1}]

S_T cation exchange capacity [MM^{-1}] ($mmol_c kg^{-1}$)

$[S]$ coefficient matrix in the global matrix equation for solute transport [LT^{-1}]

t time [T]

t_0 time when simulation begins [T]

t_p period of time covering one complete cycle of the temperature sine wave [T]

T temperature [K]

$\overline{T}$ average temperature at the soil surface during period t_p [K]

T^A absolute temperature [K]

T_a actual transpiration rate per unit soil surface [LT^{-1}]

T_i initial temperature [K]

T_p potential transpiration rate [LT^{-1}]

T_r^A reference absolute temperature [K] (293.15K = 20°C)

T_{ref} reference temperature [K]

T_0 prescribed temperature boundary condition [K]

$[T]$ coefficient matrix in the global matrix equation for solute transport [LT^{-1}]

v average pore-water velocity [LT^{-1}]

V volume of water in each subregion [L]

V_{new} volume of water in each subregion at the new time level [L]

V_{old} volume of water in each subregion at the previous time level [L]

V_t volume of water in the flow domain at time t [L]

V_t^e volume of water in element e at time t [L]

V_0 volume of water in the flow domain at initial time t_0 [L]

V_0^e volume of water in element e at initial time t_0 [L]

W total amount of energy in the flow region [MT^{-2}]

x spatial coordinate [L] (positive upward)

α dimensionless water stress response function [-]

α parameter in the soil water retention function [L^{-1}]

α^d value of α for a drying branch of the soil water retention function [L^{-1}]

α^w value of α for a wetting branch of the soil water retention function [L^{-1}]

α^w weighing factor [-]

α_h scaling factor for the pressure head [-]

α_h^* temperature scaling factor for the pressure head [-]

α_K scaling factor for the hydraulic conductivity [-]

α_K^* temperature scaling factor for the hydraulic conductivity [-]

α_θ scaling factor for the water content [-]

β empirical constant in the adsorption isotherm [-]

β_t thermal dispersivity [L]

γ_g zero-order rate constant for solutes in the gas phase [$ML^{-3}T^{-1}$]

γ_i activity coefficient in the soil solution [L^3M^{-1}] (l mol^{-1})

γ_s zero-order rate constant for solutes adsorbed onto the solid phase [T^{-1}]

γ_w zero-order rate constants for solutes in the liquid phase [$ML^{-3}T^{-1}$]

δ_{ij} Kronecker delta [-]

Δt time increment [T]

Δt_{max} maximum permitted time increment [T]

Δt_{min} minimum permitted time increment [T]

Δx size of the elements [L]

ϵ temporal weighing factor [-]

ϵ_a^c absolute error in the solute mass balance [ML^{-2}]

ϵ_a^w absolute error in the water mass balance [L]

ϵ_r^c relative error in the solute mass balance [%]

ϵ_r^w relative error in the water mass balance [%]

η empirical constant in the adsorption isotherm [L^3M^{-1}]

θ volumetric water content [L^3L^{-3}]

θ^* scaled volumetric water content [L^3L^{-3}]

θ_a parameter in the soil water retention function [L^3L^{-3}]

θ_k volumetric water content corresponding to K_k [L^3L^{-3}]

θ_m parameter in the soil water retention function [L^3L^{-3}]

θ_m^d parameter in soil water retention function; drying branch [L^3L^{-3}]

θ_m^w parameter in soil water retention function; wetting branch [L^3L^{-3}]

θ_n volumetric solid phase fraction [L^3L^{-3}]

θ_o volumetric organic matter fraction [L^3L^{-3}]

θ_r residual soil water content [L^3L^{-3}]

θ_r^* scaled residual soil water content [L^3L^{-3}]

θ_r^d residual soil water content of the main drying branch [L^3L^{-3}]

θ_r^w residual soil water content of the main wetting branch [L^3L^{-3}]

θ_s saturated soil water content [L^3L^{-3}]

θ_s^d saturated soil water content of the main drying branch [L^3L^{-3}]

θ_s^w saturated soil water content of the main wetting branch [L^3L^{-3}]

θ_Δ water content at the reversal point of a hysteretic retention function [L^3L^{-3}]

λ apparent thermal conductivity of the soil [$MLT^{-3}K^{-1}$] (e.g. $Wm^{-1}K^{-1}$)

λ_0 thermal conductivity of porous medium in the absence of water flow [$MLT^{-3}K^{-1}$] (e.g. $Wm^{-1}K^{-1}$)

μ_g first-order rate constant for solutes in the gas phase [T^{-1}]

μ_{ref} dynamic viscosity at reference temperature T_{ref} [$MT^{-1}L^{-1}$]

μ_s first-order rate constant for solutes adsorbed onto the solid phase [T^{-1}]

μ_T dynamic viscosity at temperature T [$MT^{-1}L^{-1}$]

μ_w first-order rate constant for solutes in the liquid phase [T^{-1}]

μ_g' first-order rate constant for decay chain solutes in the gas phase [T^{-1}]

μ_s' first-order rate constant for decay chain solutes adsorbed onto the solid phase [T^{-1}]

μ_w' first-order rate constant for decay chain solutes in the liquid phase [T^{-1}]

ξ_i activity coefficient for the exchange surfaces [MM^{-1}] (kg mol^{-1})

ρ bulk density of porous medium [ML^{-3}]

ρ_{ref} density of soil water at reference temperature T_{ref} [ML^{-3}]

ρ_T density of soil water at temperature T [ML^{-3}]

σ surface tension [MT^{-2}]

σ_{ref} surface tension at reference temperature T_{ref} [MT^{-2}]

σ_T surface tension at temperature T [MT^{-2}]

τ_g tortuosity factor in the gas phase [-]

τ_w tortuosity factor in the liquid phase [-]

ϕ_n linear basis functions [-]

ϕ_n^u upstream weighted basis functions [-]

ω first-order adsorption rate constant [T^{-1}]

ω_s performance index for minimizing or eliminating numerical oscillations [-]

ξ local coordinate [-]

1. INTRODUCTION

The importance of the unsaturated zone as an integral part of the hydrological cycle has long been recognized. The zone plays an inextricable role in many aspects of hydrology, including infiltration, soil moisture storage, evaporation, plant water uptake, groundwater recharge, runoff and erosion. Initial studies of the unsaturated (vadose) zone focused primarily on water supply studies, inspired in part by attempts to optimally manage the root zone of agricultural soils for maximum crop production. Interest in the unsaturated zone has dramatically increased in recent years because of growing concern that the quality of the subsurface environment is being adversely affected by agricultural, industrial and municipal activities. Federal, state and local action and planning agencies, as well as the public at large, are now scrutinizing the intentional or accidental release of surface-applied and soil-incorporated chemicals into the environment. Fertilizers and pesticides applied to agricultural lands inevitably move below the soil root zone and may contaminate underlying groundwater reservoirs. Chemicals migrating from municipal and industrial disposal sites also represent environmental hazards. The same is true for radionuclides emanating from energy waste disposal facilities.

The past several decades has seen considerable progress in the conceptual understanding and mathematical description of water flow and solute transport processes in the unsaturated zone. A variety of analytical and numerical models are now available to predict water and/or solute transfer processes between the soil surface and the groundwater table. The most popular models remain the Richards' equation for variably saturated flow, and the Fickian-based convection-dispersion equation for solute transport. Deterministic solutions of these classical equations have been used, and likely will continue to be used in the near future, for predicting water and solute movement in the vadose zone, and for analyzing specific laboratory or field experiments involving unsaturated water flow and/or solute transport. Models of this type are also helpful tools for extrapolating information from a limited number of field experiments to different soil, crop and climatic conditions, as well as to different tillage and water management schemes.

Once released into the subsurface environment, industrial and agricultural chemicals are generally subjected to a large number of simultaneous physical, chemical, and biological processes, including sorption-desorption, volatilization, photolysis, and biodegradation, as well

as their kinetics. The extent of degradation, sorption and volatilization largely determines the persistence of a pollutant in the subsurface [*Chiou*, 1989]. For example, the fate of organic chemicals in soils is known to be strongly affected by the kinetics of biological degradation. *Alexander and Scow* [1989] gave a review of some of the equations used to represent the kinetics of biodegradation. These equations include zero-order, half-order, first-order, three-half-order, mixed-order, logistic, logarithmic, Michaelis-Menton, and Monod type (with or without growth) expressions. While most of these expressions have a theoretical bases, they are commonly used only in an empirical fashion by fitting the equations to observed data. Zero- and first-order kinetic equations remain the most popular for describing biodegradation of organic compounds, mostly because of their simplicity and the ease at which they can be incorporated in solute transport models. Conditions for the application of these two equations are described by *Alexander and Scow* [1989].

One special group of degradation reactions involves decay chains in which solutes are subject to sequential (or consecutive) decay reactions. Problems of solute transport involving sequential first-order decay reactions frequently occur in soil and groundwater systems. Examples are the migration of various radionuclides [*Lester et al.*, 1975; *Rogers,* 1978; *Gureghian*, 1981; *Gureghian and Jansen*, 1983], the simultaneous movement of interacting nitrogen species [*Cho*, 1971; *Misra et al.*, 1974; *Wagenet et al.*, 1976; *Tillotson et al.*, 1980], organic phosphate transport [*Castro and Rolston*, 1977], and the transport of certain pesticides and their metabolites [*Bromilow and Leistra,* 1980; *Wagenet and Hutson*, 1987].

While in the past most pesticides were regarded as involatile, volatilization is now increasingly recognized as being an important process affecting the fate of pesticides in field soils [*Glotfelty and Schomburg*, 1989; *Spencer*, 1991]. Another process affecting pesticide fate and transport is the relative reactivity of solutes in the sorbed and solution phases. Several processes such as gaseous and liquid phase molecular diffusion, and convective-dispersive transport, act only on solutes that are not adsorbed. Degradation of organic compounds likely occurs mainly, or even exclusively, in the liquid phase [*Pignatello*, 1989]. On the other side, radioactive decay takes place equally in the solution and adsorbed phases, while other reactions or transformations may occur only or primarily in the sorbed phase.

Several analytical solutions have been published for simplified transport systems involving consecutive decay reactions [*Cho*, 1971; *Wagenet et al.*, 1976; *Harada et al.*, 1980; *Higashi and Pigford,* 1980; *van Genuchten*, 1985]. Unfortunately, analytical solutions for more complex situations, such as for transient water flow or the nonequilibrium solute transport with nonlinear reactions, are not available and/or cannot be derived, in which case numerical models must be employed. To be useful, such numerical models must allow for different reaction rates to take place in the solid, liquid, and gaseous phases, as well as for a correct distribution of the solutes among the different phases.

The purpose of this report is to document version 6.0 of the HYDRUS computer program simulating one-dimensional variably-saturated water flow, heat movement, and the transport of solutes involved in sequential first-order decay reactions. Program numerically solves the Richards' equation for saturated-unsaturated water flow and convection-dispersion type equations for heat and solute transport. The water flow equation incorporates a sink term to account for water uptake by plant roots. The heat transport equation considers movement by conduction as well as convection with flowing water. The governing convection-dispersion solute transport equations are written in a very general form by including provisions for nonlinear nonequilibrium reactions between the solid and liquid phases, and linear equilibrium reaction between the liquid and gaseous phases. Hence, both adsorbed and volatile solutes such as pesticides can be considered. The solute transport equations also incorporate the effects of zero-order production, first-order degradation independent of other solutes, and first-order decay/production reactions that provides the required coupling between the solutes involved in the sequential first-order chain. The transport models also account for convection and dispersion in the liquid phase, as well as for diffusion in the gas phase, thus permitting one to simulate solute transport simultaneously in both the liquid and gaseous phases. HYDRUS at present considers up to five solutes which can be either coupled in a unidirectional chain or may move independently of each other.

The HYDRUS code may be used to analyze water and solute movement in unsaturated, partially saturated, or fully saturated porous media. The flow region itself may be composed of nonuniform soils. Flow and transport can occur in the vertical, horizontal, or in a generally inclined direction. The water flow part of the model considers prescribed head and flux

boundaries, as well as boundaries controlled by atmospheric conditions or free drainage. First and third-type boundary conditions can be implemented in both the solute and heat transport parts of the model.

The governing flow and transport equations are solved numerically using standard Galerkin-type linear finite element schemes, or modification thereof. The program is a one-dimensional version of the CHAIN-2D code simulating water, heat and solute movement in two-dimensional variably saturated media [*Šimůnek and van Genuchten*, 1994], and an extension of the one-dimensional variably saturated flow and solute transport code SWMI_ST of *Šimůnek* [1993], which in turn was based in part on the variably saturated flow code SWMI of *Vogel* [1990]. The method of incorporating hysteresis in the soil hydraulic properties, as well as several other features, was adopted from HYDRUS 5.0 [*Vogel et al.*, 1996]. The source code was developed and tested on a P5 using Microsoft's Fortran PowerStation compiler. Several extensions of the MS Fortran beyond the ANSI standard were used.

The HYDRUS code is distributed on 3½ inch floppy diskettes containing the source code, the input and output files of five examples discussed in this report, several examples included with HYDRUS 5.0, and the computer code itself.

2. VARIABLY SATURATED WATER FLOW

2.1. *Governing Flow Equation*

One-dimensional water movement in a partially saturated rigid porous medium is described by a modified form of the Richards' equation using the assumptions that the air phase plays an insignificant role in the liquid flow process and that water flow due to thermal gradients can be neglected:

$$\frac{\partial \theta}{\partial t} = \frac{\partial}{\partial x}[K(\frac{\partial h}{\partial x} + \cos\alpha)] - S \tag{2.1}$$

where h is the water pressure head [L], θ is the volumetric water content [L^3L^{-3}], t is time [T], x is the spatial coordinate [L] (positive upward), S is the sink term [$L^3L^{-3}T^{-1}$], α is the angle between the flow direction and the vertical axis (i.e., $\alpha = 0^0$ for vertical flow, 90^0 for horizontal flow, and $0^0 < \alpha < 90^0$ for inclined flow), and K is the unsaturated hydraulic conductivity function [LT^{-1}] given by

$$K(h,x) = K_s(x)\, K_r(h,x) \tag{2.2}$$

where K_r is the relative hydraulic conductivity [-] and K_s the saturated hydraulic conductivity [LT^{-1}].

2.2. *Root Water Uptake*

The sink term, S, is defined as the volume of water removed from a unit volume of soil per unit time due to plant water uptake. *Feddes et al.* [1978] defined S as

$$S(h) = \alpha(h) S_p \tag{2.3}$$

where the root-water uptake water stress response function $\alpha(h)$ is a prescribed dimensionless function (Fig. 2.1) of the soil water pressure head ($0 \le \alpha \le 1$), and S_p the potential water uptake rate [T^{-1}]. Figure 2.1. gives a schematic plot of the stress response function as used by *Feddes et al.*

[1978]. Notice that water uptake is assumed to be zero close to saturation (i.e., wetter than some arbitrary "anaerobiosis point", h_1). For $h<h_4$ (the wilting point pressure head), water uptake is also assumed to be zero. Water uptake is considered optimal between pressure heads h_2 and h_3, whereas for pressure head between h_3 and h_4 (or h_1 and h_2), water uptake decreases (or increases) linearly with h. The variable S_p in (2.3) is equal to the water uptake rate during periods of no water stress when $a(h)=1$. *van Genuchten* [1987] expanded formulation of Feddes by including osmotic stress as follows

$$S(h,h_\phi) = \alpha(h,h_\phi)S_p \tag{2.4}$$

where h_ϕ is the osmotic head [L], which is assumed here to be given by a linear combination of the concentrations, c_i, of all solutes present, i.e.,

$$h_\phi = a_i c_i \tag{2.5}$$

in which a_i are experimental coefficients [L^4M] converting concentrations into osmotic heads. *van Genuchten* [1987] proposed an alternative S-shaped function to describe the water uptake stress response function (Fig. 2.1), and suggested that the influence of the osmotic head reduction can be either additive or multiplicative as follows

$$\alpha(h,h_\phi) = \frac{1}{1 + \left[\dfrac{h + h_\phi}{h_{50}}\right]^p} \tag{2.6}$$

or

$$\alpha(h,h_\phi) = \frac{1}{1 + (h/h_{50})^{p_1}} \frac{1}{1 + (h_\phi/h_{\phi_{50}})^{p_2}} \tag{2.7}$$

respectively, where p, p_1, and p_2 are experimental constants. The exponent p was found to be approximately 3 when applied to salinity stress data only [*van Genuchten*, 1987]. The parameter h_{50} in (2.6) and (2.7) represents the pressure head at which the water extraction rate is reduced by 50% during conditions of negligible osmotic stress. Similarly, $h_{\phi 50}$ represents the osmotic head

at which the water extraction rate is reduced by 50% during conditions of negligible water stress. Note that, in contrast to the expression of *Feddes et al.* [1978], this formulation of the stress response function, $\alpha(h,h_\phi)$, does not consider the transpiration reduction near saturation. Such a simplification seems justified at or near saturation for only relatively short periods of time.

When the potential water uptake rate is equally distributed over the root zone, S_p becomes

$$S_p = \frac{1}{L_R} T_p \tag{2.8}$$

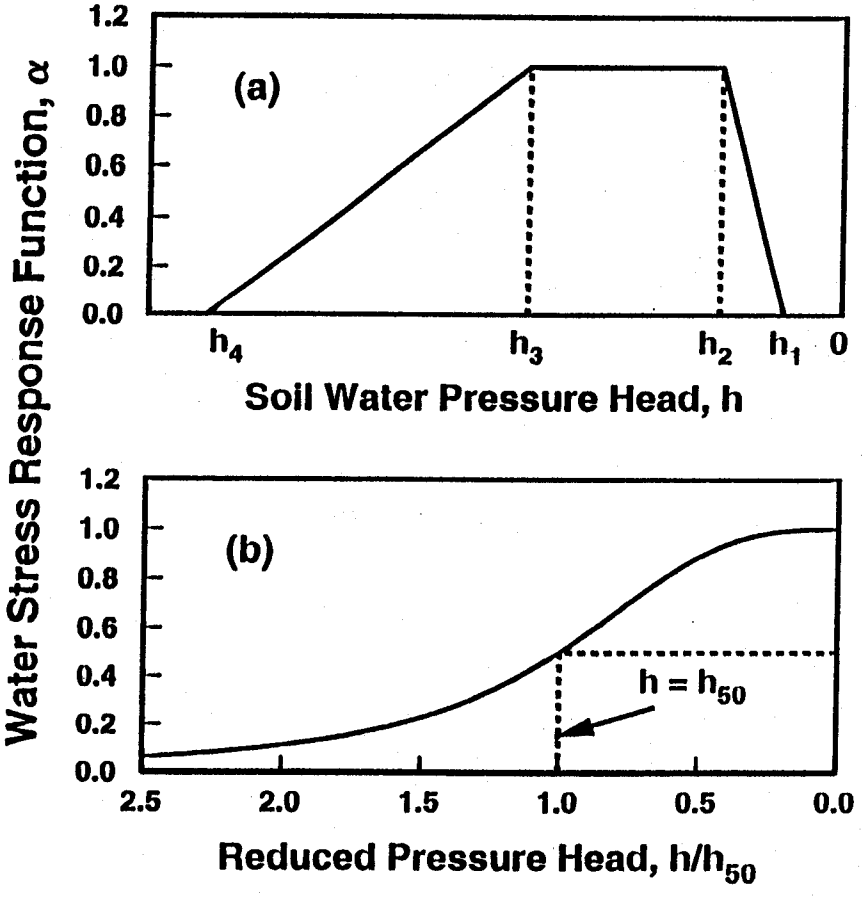

Fig. 2.1. Schematic of the plant water stress response function, $\alpha(h)$, as used by a) *Feddes et al.* [1978] and b) *van Genuchten* [1987].

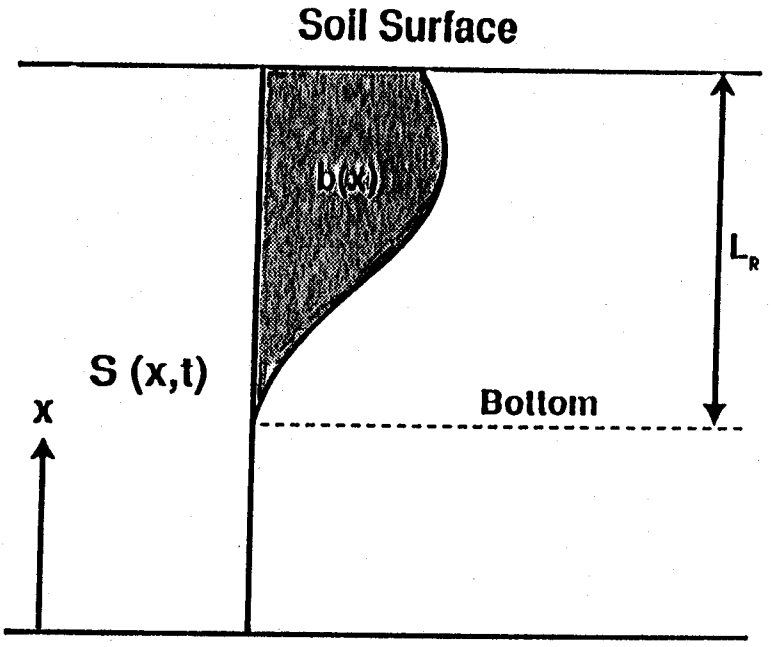

Fig. 2.2. Schematic of the potential water uptake distribution function, $b(x)$, in the soil root zone.

where T_p is the potential transpiration rate [LT^{-1}] and L_R the depth [L] of the root zone. Equation (2.8) may be generalized by introducing a non-uniform distribution of the potential water uptake rate over a root zone of arbitrary shape:

$$S_p = b(x)\, T_p \tag{2.9}$$

where $b(x)$ is the normalized water uptake distribution [L^{-1}]. This function describes the spatial variation of the potential extraction term, S_p, over the root zone (Fig. 2.2), and is obtained by normalizing any arbitrarily measured or prescribed root distribution function, $b'(x)$, as follows

$$b(x) = \frac{b'(x)}{\int_{L_R} b'(x)\,dx} \tag{2.10}$$

where L_R is the region occupied by the root zone. Normalizing the uptake distribution ensures that $b(x)$ integrates to unity over the flow domain, i.e.,

$$\int_{L_R} b(x)\,dx = 1 \tag{2.11}$$

There are many ways to express the function $b(x)$; constant with depth, linear [*Feddes et al.*, 1978], or an exponential function with a maximum at the soil surface [*Raats*, 1974]:

$$b(x) = a^* e^{-a^*(L-x)} \tag{2.12}$$

where L is the x-coordinate of the soil surface [L] and a^* an empirical constant [L^{-1}]. HYDRUS allows a user to prescribe virtually any shape of the water uptake distribution function, provided that this function is constant during the simulation. When the rooting depth varies in time (as described later), only the exponential function is allowed. Note that in the above development, and throughout this manual, the bottom of the soil profile is located at $x = 0$ and the soil surface at $x = L$.

From (2.9) and (2.11) it follows that S_p is related to T_p by the expression

$$\int_{L_R} S_p dx = T_p \tag{2.13}$$

The actual water uptake distribution is obtained by substituting (2.9) into (2.3):

$$S(h,h_\phi,x) = \alpha(h,h_\phi,x)\, b(x)\, T_p \tag{2.14}$$

whereas the actual transpiration rate, T_a, is obtained by integrating (2.14) as follows

$$T_a = \int_{L_R} S(h,h_\phi,x)\,dx = T_p \int_{L_R} a(h,h_\phi,x)\, b(x)\,dx \tag{2.15}$$

The root depth, L_R, can be either constant or variable during the simulation. For annual vegetation a growth model is required to simulate the change in rooting depth with time. HYDRUS assumes that the actual root depth is the product of the maximum rooting depth, L_m [L], and a root growth coefficient, $f_r(t)$ [-] [*Šimůnek and Suarez*, 1993a]:

$$L_R(t) = L_m f_r(t) \tag{2.16}$$

For the root growth coefficient, $f_r(t)$, we use the classical Verhulst-Pearl logistic growth

function

$$f_r(t) = \frac{L_0}{L_0 + (L_m - L_0)e^{-rt}} \tag{2.17}$$

where L_0 is the initial value of the rooting depth at the beginning of the growing season [L], and r the growth rate [T^{-1}]. The growth rate is calculated either from the assumption that 50% of the rooting depth will be reached after 50% of the growing season has elapsed, or from given data.

2.3. *The Unsaturated Soil Hydraulic Properties*

The unsaturated soil hydraulic properties, $\theta(h)$ and $K(h)$, in (2.1) are in general highly nonlinear functions of the pressure head. HYDRUS permits the use of three different analytical models for the hydraulic properties [*Brooks and Corey*, 1964; *van Genuchten*, 1980; and *Vogel and Císlerová*, 1988].

The soil water retention, $\theta(h)$, and hydraulic conductivity, $K(h)$, functions according to *Brooks and Corey* [1964] are given by

$$S_e = \begin{cases} |\alpha h|^{-n} & h < -1/\alpha \\ 1 & h \geq -1/\alpha \end{cases} \tag{2.18}$$

$$K = K_s S_e^{2/n+l+2} \tag{2.19}$$

respectively, where S_e is the effective water content,

$$S_e = \frac{\theta - \theta_r}{\theta_s - \theta_r} \tag{2.20}$$

in which θ_r and θ_s denote the residual and saturated water content, respectively; K_s is the saturated hydraulic conductivity, α is the inverse of the air-entry value (or bubbling pressure), n is a pore-size distribution index, and l is a pore-connectivity parameter assumed to be 2.0 in the original study of *Brooks and Corey* [1964]. The parameters α, n and l in HYDRUS are considered to be

empirical coefficients affecting the shape of the hydraulic functions.

HYDRUS also implements the soil-hydraulic functions of *van Genuchten* [1980] who used the statistical pore-size distribution model of *Mualem* [1976] to obtain a predictive equation for the unsaturated hydraulic conductivity function in terms of soil water retention parameters. The expressions of *van Genuchten* [1980] are given by

$$\theta(h) = \begin{cases} \theta_r + \dfrac{\theta_s - \theta_r}{[1 + |\alpha h|^n]^m} & h<0 \\ \theta_s & h \geq 0 \end{cases} \tag{2.21}$$

$$K(h) = K_s S_e^l [1 - (1 - S_e^{1/m})^m]^2 \tag{2.22}$$

where

$$m = 1 - 1/n \quad , \qquad n > 1 \tag{2.23}$$

The above equations contain five independent parameters: θ_r, θ_s, α, n, and K_s. The pore-connectivity parameter l in the hydraulic conductivity function was estimated [*Mualem*, 1976] to be about 0.5 as an average for many soils.

A third set of hydraulic equations implemented in HYDRUS are those by *Vogel and Císlerová* [1988] who modified the equations of *van Genuchten* [1980] to add flexibility in the description of the hydraulic properties near saturation. The soil water retention, $\theta(h)$, and hydraulic conductivity, $K(h)$, functions of *Vogel and Císlerová* [1988] are given by (Fig. 2.3)

$$\theta(h) = \begin{cases} \theta_a + \dfrac{\theta_m - \theta_a}{(1 + |\alpha h|^n)^m} & h<h_s \\ \theta_s & h \geq h_s \end{cases} \tag{2.24}$$

and

$$K(h) = \begin{cases} K_s K_r(h) & h \le h_k \\ K_k + \dfrac{(h - h_k)(K_s - K_k)}{h_s - h_k} & h_k < h < h_s \\ K_s & h \ge h_s \end{cases} \tag{2.25}$$

respectively, where

$$K_r = \frac{K_k}{K_s} \left[\frac{S_e}{S_{ek}} \right]^l \left[\frac{F(\theta_r) - F(\theta)}{F(\theta_r) - F(\theta_k)} \right]^2 \tag{2.26}$$

$$F(\theta) = \left[1 - \left[\frac{\theta - \theta_a}{\theta_m - \theta_a} \right]^{1/m} \right]^m \tag{2.27}$$

$$S_{ek} = \frac{\theta_k - \theta_r}{\theta_s - \theta_r} \tag{2.28}$$

The above equations allow for a non-zero minimum capillary height, h_s, by replacing the parameter θ_s in van Genuchten's retention function by a fictitious (extrapolated) parameter θ_m slightly larger than θ_s as shown in Fig. 2.3. While this change from θ_s to θ_m has little or no effect on the retention curve, the effect on the shape and value of the hydraulic conductivity function can be considerable, especially for fine-textured soils when n is relatively small (e.g., $1.0 < n < 1.3$). To increase the flexibility of the analytical expressions, the parameter θ_r in the retention function was replaced by the fictitious (extrapolated) parameter $\theta_a \le \theta_r$. The approach maintains the physical meaning of θ_r and θ_s as measurable quantities. Equation (2.26) assumes that the predicted hydraulic conductivity function is matched to a measured value of the hydraulic conductivity, $K_k = K(\theta_k)$, at some water content, θ_k, less that or equal to the saturated water content, i.e., $\theta_k \le \theta_s$ and $K_k \le K_s$ [*Vogel and Cislerová*, 1988; *Luckner et al.*, 1989]. Inspection of (2.24) through (2.28) shows that the hydraulic characteristics contain 9 unknown parameters: θ_r, θ_s, θ_a, θ_m, α, n, K_s, K_k, and θ_k. When $\theta_a = \theta_r$, $\theta_m = \theta_k = \theta_s$ and $K_k = K_s$, the soil hydraulic functions of

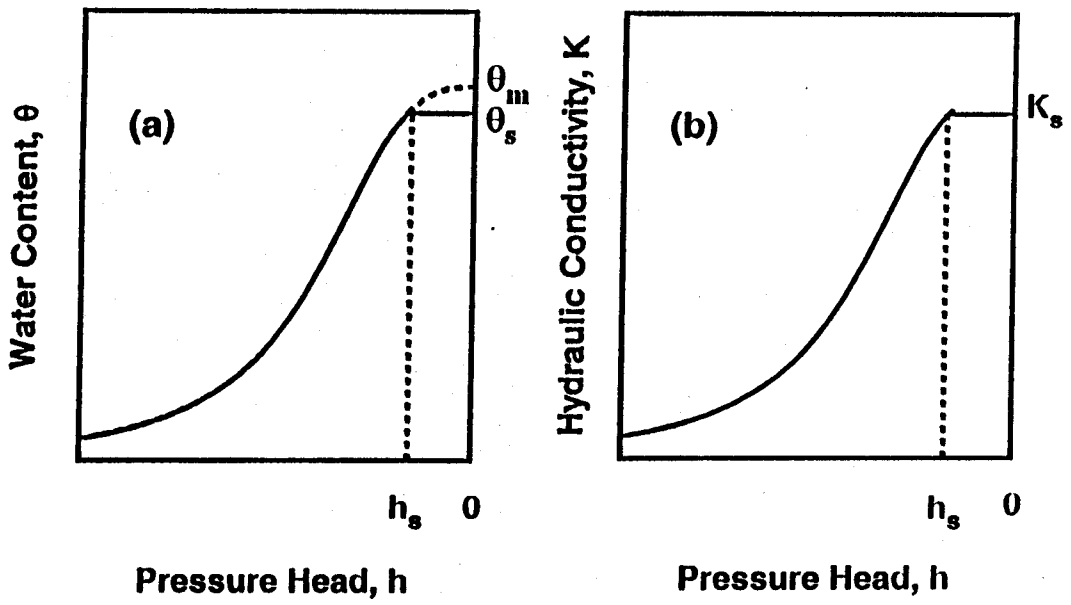

Fig. 2.3. Schematics of the soil water retention (a) and hydraulic conductivity (b) functions as given by equations (2.24) and (2.25), respectively.

Vogel and Císlerová [1988] reduce to the original expressions of *van Genuchten* [1980].

2.4. *Scaling in the Soil Hydraulic Functions*

HYDRUS implements a scaling procedure designed to simplify the description of the spatial variability in the unsaturated soil hydraulic properties in the flow domain. The code assumes that variability in the hydraulic properties of a given soil profile can be approximated by means of a set of linear scaling transformations which relate the soil hydraulic characteristics $\theta(h)$ and $K(h)$ of the individual soil layers to reference characteristics $\theta^*(h^*)$ and $K^*(h^*)$. The technique is based on the similar media concept introduced by *Miller and Miller* [1956] for porous media which differ only in the scale of their internal geometry. The concept was extended by *Simmons et al.* [1979] to materials which differ in morphological properties, but which exhibit 'scale-similar' soil hydraulic functions. Three independent scaling factors are embodied in HYDRUS. These three scaling parameters may be used to define a linear model of the actual spatial variability in the soil hydraulic properties as follows [*Vogel et al.*, 1991]:

$$K(h) = \alpha_K K^*(h^*)$$

$$\theta(h) = \theta_r + \alpha_\theta [\theta^*(h^*) - \theta_r^*] \tag{2.29}$$

$$h = \alpha_h h^*$$

in which, for the most general case, α_θ, α_h and α_K are mutually independent scaling factors for the water content, the pressure head and the hydraulic conductivity, respectively. Less general scaling methods arise by invoking certain relationships between α_θ, α_h and/or α_K. For example, the original Miller-Miller scaling procedure is obtained by assuming α_θ=1 (with $\theta_r^* = \theta_r$), and α_K=α_h^{-2}. A detailed discussion of the scaling relationships given by (2.29), and their application to the hydraulic description of heterogeneous soil profiles, is given by *Vogel et al.* [1991].

2.5. *Temperature Dependence of the Soil Hydraulic Functions*

A similar scaling technique as described above is used in HYDRUS to express the temperature dependence of the soil hydraulic functions. Based on capillary theory that assumes that the influence of temperature on the soil water pressure head can be quantitatively predicted from the influence of temperature on surface tension, *Philip and de Vries* [1957] derived the following equation

$$\frac{dh}{dT} = \frac{h}{\sigma}\frac{d\sigma}{dT} \tag{2.30}$$

where T is temperature [K] and σ is the surface tension at the air-water interface [MT^{-2}]. From (2.30) it follows that

$$h_T = \frac{\sigma_T}{\sigma_{ref}} h_{ref} = \alpha_h^* h_{ref} \tag{2.31}$$

where h_T and h_{ref} (σ_T and σ_{ref}) are pressure heads (surface tensions) at temperature T and reference temperature T_{ref}, respectively; and α_h^* is the temperature scaling factor for the pressure head.

Following *Constantz* [1982], the temperature dependence of the hydraulic conductivity can be expressed as

$$K_T(\theta) = \frac{\mu_{ref}}{\mu_T}\frac{\rho_T}{\rho_{ref}} K_{ref}(\theta) = \alpha_K^* K_{ref}(\theta) \tag{2.32}$$

where K_{ref} and K_T denote hydraulic conductivities at the reference temperature T_{ref} and soil temperature T, respectively; μ_{ref} and μ_T (ρ_{ref} and ρ_T) represent the dynamic viscosity [$ML^{-1}T^{-1}$] (density of soil water [ML^{-3}]) at temperatures T_{ref} and T, respectively; and α_K^* is the temperature scaling factor for the hydraulic conductivity.

2.6. *Hysteresis in the Soil Hydraulic Properties*

Applications of unsaturated flow models often assume unique, single-valued (non-hysteretic) functions for $\theta(h)$ and $K(h)$ to characterize the hydraulic properties at a certain point in the soil profile. While such a simplification may be acceptable for many flow simulations, other cases require a more realistic description involving hysteresis in the soil hydraulic properties. The HYDRUS code incorporates hysteresis by using the empirical model introduced by *Scott et al.* [1983]. This model was also employed by *Kool and Parker* [1987], who modified the formulation to account for air entrapment. The present version of HYDRUS further extends the model of *Kool and Parker* according to *Vogel et al.* [1996] by considering also hysteresis in the hydraulic conductivity function.

The adopted procedure for modeling hysteresis in the retention function requires that both the main drying and main wetting curves be known (Fig. 2.4). These two curves are described with (2.24) using the parameter vectors (θ_r^d, θ_s^d, θ_m^d, α^d, n^d) and (θ_r^w, θ_s^w, θ_m^w, α^w, n^w), respectively, where the subscripts d and w indicate wetting and drying, respectively. The following restrictions are expected to hold in most practical applications:

$$\theta_r^d = \theta_r^w \;; \quad \alpha^d \le \alpha^w \tag{2.33}$$

We also invoke the often assumed restriction

$$n^d = n^w \tag{2.34}$$

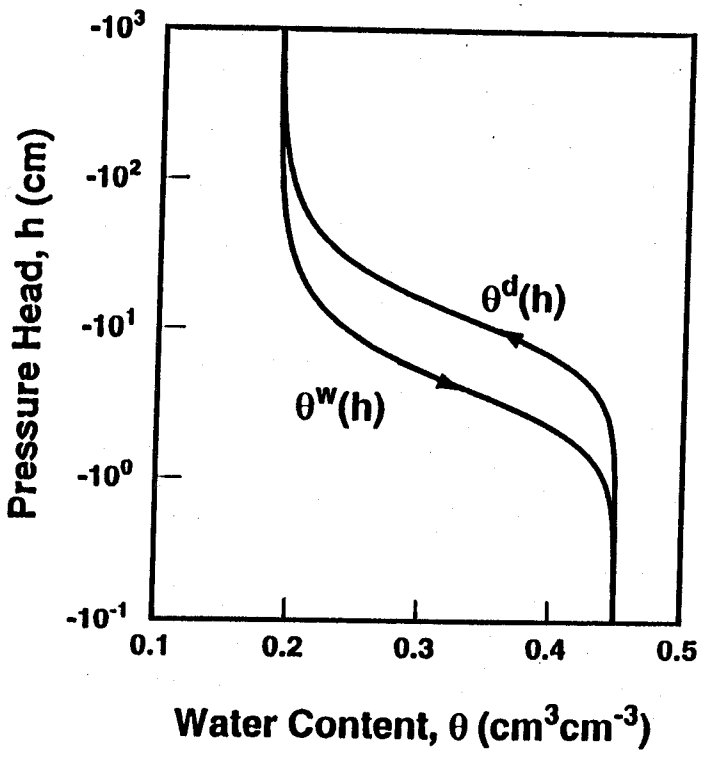

Fig. 2.4. Example of a water retention curve showing hysteresis. Shown are the boundary wetting curve, $\theta^w(h)$, and the boundary drying curve, $\theta^d(h)$.

If data are lacking, one may use $\alpha^w = 2\alpha^d$ as a reasonable first approximation [*Kool and Parker*, 1987; *Nielsen and Luckner*, 1992]. We further assume

$$\theta_m^w = \theta_r + \frac{\theta_s^w - \theta_r}{\theta_s^d - \theta_r}(\theta_m^d - \theta_r) \tag{2.35}$$

so that the parameters θ_s and α are the only independent parameters describing hysteresis in the retention function. According to the hysteresis model, drying scanning curves are scaled from the main drying curve, and wetting scanning curves from the main wetting curve. The scaling factors for the drying scanning curves can be obtained by considering the main drying curve as a reference curve in scaling equation (2.29) (keeping $\alpha_h = 1$ to scale only in the water content

direction), i.e.:

$$\theta(h) = \theta_r' + \alpha_\theta[\theta^d(h) - \theta_r^d] \tag{2.36}$$

and forcing each scanning curve, $\theta(h)$, to pass through the point $(\theta_\Delta, h_\Delta)$ characterizing the latest reversal from wetting to drying. Substituting this reversal point into (2.36), and assuming that $\theta_r = \theta_r^d$, leads to

$$\alpha_\theta = \frac{\theta_\Delta - \theta_r}{\theta^d(h_\Delta) - \theta_r} \tag{2.37}$$

Note that the scaling procedure results in a fictitious value of the parameter θ_s' for the drying scanning curve (this parameter may be located outside of the main hysteresis loop). The scaling relationship is similarly for the wetting scanning curves

$$\theta(h) = \theta_r' + \alpha_\theta[\theta^w(h) - \theta_r] \tag{2.38}$$

in which the fictitious parameter θ_r' is now used (again possibly scaled outside of the main loop). The scaling factor α_θ for a particular scanning curve can be obtained by substituting the reversal point $(\theta_\Delta, h_\Delta)$ and the full saturation point $(\theta_s, 0)$ into (2.38), and subtracting the two resulting equations to eliminate θ_r' to give

$$\alpha_\theta = \frac{\theta_\Delta - \theta_s}{\theta^w(h_\Delta) - \theta_s^w} \tag{2.39}$$

The parameter θ_r' is subsequently determined from (2.38) as $\theta_r' = \theta_s - \alpha_\theta(\theta_s^w - \theta_r)$. If the main hysteresis loop is not closed at saturation, the water content at saturation for a particular wetting scanning curve is evaluated using the empirical relationship of *Aziz and Settari* [1979]

$$\theta_s = \theta_s^d - \frac{\theta_s^d - \theta_\Delta}{1 + R(\theta_s^d - \theta_\Delta)}; \qquad R = \frac{1}{\theta_s^d - \theta_s^w} - \frac{1}{\theta_s^d - \theta_r^d} \tag{2.40}$$

An analogous hysteretic procedure can be applied to the unsaturated hydraulic conductivity function $K(h)$. The main branches $K^d(h)$ and $K^w(h)$ of the hysteresis loop are characterized by

the same set of parameters as the corresponding retention curves $\theta^d(h)$ and $\theta^w(h)$, and by the saturated conductivities K_s^d and K_s^w according to Eq. (2.22). For drying scanning curves we obtain from (2.29)

$$K(h) = \alpha_K K^d(h) \tag{2.41}$$

From knowledge of the reversal point (h_Δ, K_Δ) we obtain

$$\alpha_K = \frac{K_\Delta}{K^d(h_\Delta)} \tag{2.42}$$

For a wetting scanning curve we have now

$$K(h) = K_r' + \alpha_K K^w(h) \tag{2.43}$$

where K_r' is a fictitious parameter. Substituting the reversal point (h_Δ, K_Δ) and the saturation point (0, K_s) into (2.43) and solving for α_K yields

$$\alpha_K = \frac{K_\Delta - K_s}{K^w(h_\Delta) - K_s^w} \tag{2.44}$$

The fictitious conductivity parameter K_r' may be obtained from (2.43) as $K_r' = K_s - \alpha_K K_s^w$. If the main hysteresis loop is not closed at saturation, the hydraulic conductivity at saturation for a wetting scanning curve is evaluated using equations similar to (2.40), i.e.,

$$K_s = K_s^d - \frac{K_s^d - K_\Delta}{1 + R(K_s^d - K_\Delta)} \quad ; \quad R = \frac{1}{K_s^d - K_s^w} - \frac{1}{K_s^d} \tag{2.45}$$

2.7. *Initial and Boundary Conditions*

The solution of Eq. (2.1) requires knowledge of the initial distribution of the pressure head within the flow domain:

$$h(x,t) = h_i(x) \qquad t = t_0 \tag{2.46}$$

where h_i [L] is a prescribed function of x, and t_o is the time when the simulation begins.

One of the following boundary conditions must be specified at the soil surface (x=L) or at the bottom of the soil profile (x=0):

$$\begin{aligned} h(x,t) &= h_0(t) && \text{at} \quad x = 0 \quad \text{or} \quad x = L \\ -K\left(\frac{\partial h}{\partial x} + \cos\alpha\right) &= q_0(t) && \text{at} \quad x = 0 \quad \text{or} \quad x = L \\ \frac{\partial h}{\partial x} &= 0 && \text{at} \quad x = 0 \end{aligned} \tag{2.47}$$

where h_0 [L] and q_0 [LT^{-1}] are the prescribed values of the pressure head and the soil water flux at the boundary, respectively.

In addition to the system-independent boundary conditions given by (2.47), we consider two system-dependent boundary conditions which cannot be defined a priori. One of these involves the soil-air interface which is exposed to atmospheric conditions. The potential fluid flux across this interface is controlled exclusively by external conditions. However, the actual flux depends also on the prevailing (transient) soil moisture conditions near the surface. The soil surface boundary condition may change from a prescribed flux to a prescribed head type condition (and vice-versa). The numerical solution of (2.1) is obtained by limiting the absolute value of the surface flux by the following two conditions [*Neuman et al.*, 1974]:

$$\left| -K\frac{\partial h}{\partial x} - K \right| \le E \qquad \text{at} \quad x = L \tag{2.48}$$

and

$$h_A \le h \le h_S \qquad \text{at} \quad x = L \tag{2.49}$$

where E is the maximum potential rate of infiltration or evaporation under the current atmospheric conditions [LT^{-1}], and h_A and h_S are, respectively, minimum and maximum pressure head at the soil surface allowed under the prevailing soil conditions [L]. The value for h_A is

determined from the equilibrium conditions between soil water and atmospheric water vapor, whereas h_S is usually set equal to zero; if positive, h_S represents a small layer of water ponded which can form on top of the soil surface during heavy rains before initiation of runoff. One options in HYDRUS is to assume that any excess water on the soil surface above zero will be immediately removed. When one of the end points of (2.48) is reached, a prescribed head boundary condition will be used to calculate the actual surface flux. Methods of calculating E and h_A on the basis of atmospheric data have been discussed by *Feddes et al.* [1974].

Another option in HYDRUS is to permit water to build up on the surface. If surface ponding is expected to develop, a "surface reservoir" boundary condition of the type [*Mls*, 1982]

$$-K(\frac{\partial h}{\partial z} + \cos\alpha) = q_0(t) - \frac{dh}{dt} \qquad \text{at} \quad x = L \tag{2.50}$$

may be applied. The flux q_0 in this equation is the net infiltration rate, i.e., the difference between precipitation and evaporation. Equation (2.50) shows that the height $h(L,t)$ of the surface water layer increases due to precipitation, and reduces because of infiltration and evaporation.

A third system-dependent type boundary condition considered in HYDRUS is a seepage face at the bottom of the soil profile through which water can leave the saturated part of the flow domain. This type of boundary condition assumes that a zero-flux boundary condition applies as long as the local pressure head at the bottom of the soil profile ($x = 0$) is negative. However, a zero pressure head will be used as soon as the bottom of the profile becomes saturated. This type of boundary condition often applies to finite lysimeters which are allowed to drain under gravity.

Another system-dependent lower boundary condition may be imposed in cases where a functional relationship between the position of the water table and drainage from the soil profile can be established. One possible relationship of this type is discussed in Section 7.3.

3. NONEQUILIBRIUM TRANSPORT OF SOLUTES INVOLVED IN SEQUENTIAL FIRST-ORDER DECAY REACTIONS

3.1. *Governing Solute Transport Equations*

We assume that solutes can exist in all three phases (liquid, solid, and gaseous) and that the decay and production processes can be different in each phase. Interactions between the solid and liquid phases may be described by nonlinear nonequilibrium equations, while interactions between the liquid and gaseous phases are assumed to be linear and instantaneous. We further assume that the solutes are transported by convection and dispersion in the liquid phase, as well as by diffusion in the gas phase. A general structure of the system of first-order decay reactions for three solutes (A, B and C) is as follows [*Šimůnek and van Genuchten*, 1995]:

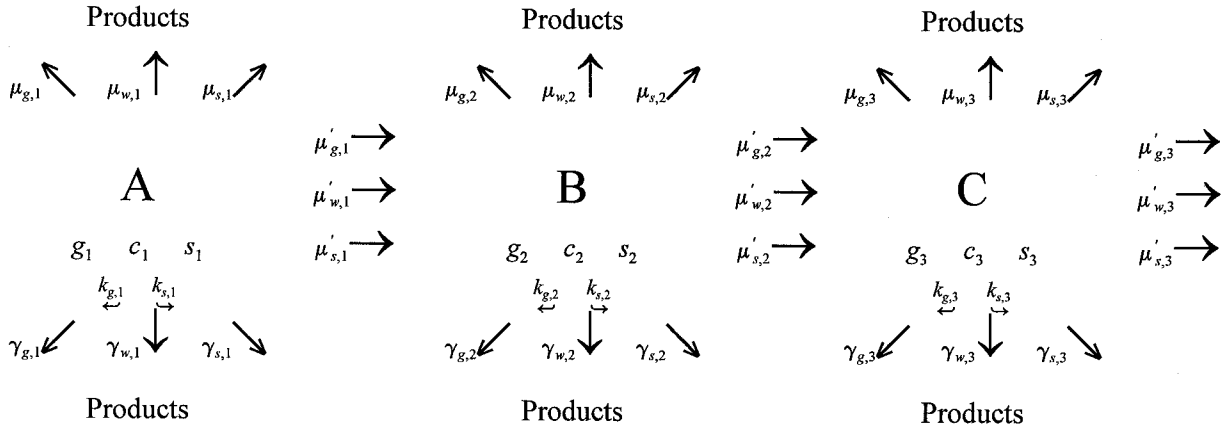

where c, s, and g represent concentrations in the liquid, solid, and gaseous phases, respectively; the subscripts s, w, and g refer to solid, liquid and gaseous phases, respectively; straight arrows represent the different zero-order (γ) and first-order (μ, μ') rate reactions, and circular arrows (k_g, k_s) indicate equilibrium distribution coefficients between phases.

Typical examples of sequential first-order decay chains are:

1. Radionuclides [*van Genuchten*, 1985]

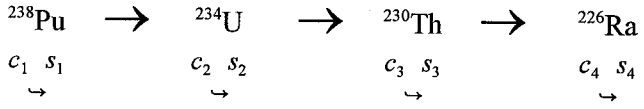

2. Nitrogen [*Tillotson et al.*, 1980]

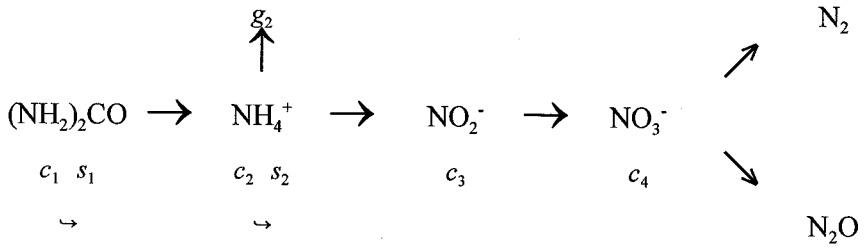

3. Pesticides [*Wagenet and Hutson*, 1987]:

a) Uninterrupted chain - one reaction path:

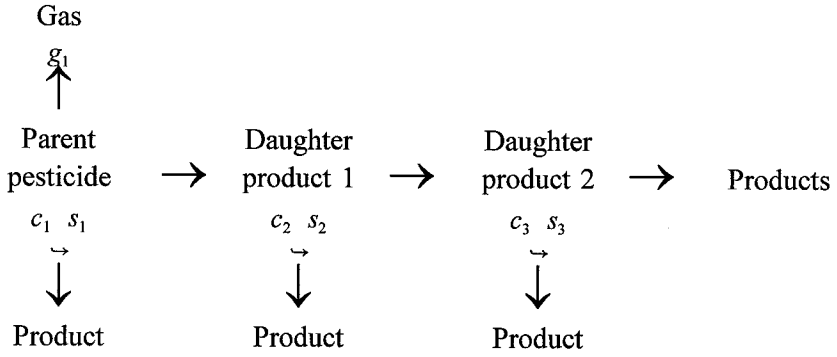

b) Interrupted chain - two independent reaction paths:

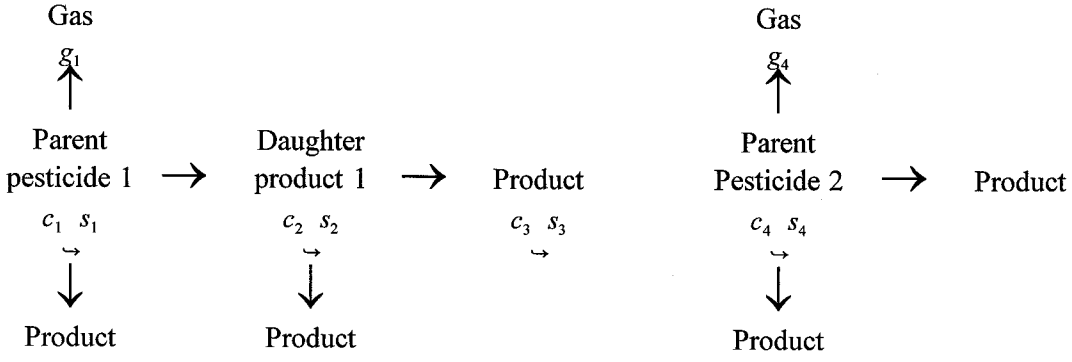

HYDRUS at present considers up to six solutes which can be either coupled in a unidirectional chain or may move independently of each other.

The partial differential equations governing one-dimensional nonequilibrium chemical transport of solutes involved in a sequential first-order decay chain during transient water flow in a variably saturated rigid porous medium are taken as [*Šimůnek and van Genuchten*, 1995]:

$$\frac{\partial \theta c_1}{\partial t} + \frac{\partial \rho s_1}{\partial t} + \frac{\partial a_v g_1}{\partial t} = \frac{\partial}{\partial x}(\theta D_1^{\,w} \frac{\partial c_1}{\partial x}) + \frac{\partial}{\partial x}(a_v D_1^{\,g} \frac{\partial g_1}{\partial x}) - \frac{\partial q c_1}{\partial x} - Sc_{r,1} -$$
$$-(\mu_{w,1} + \mu'_{w,1})\theta c_1 - (\mu_{s,1} + \mu'_{s,1})\rho s_1 - (\mu_{g,1} + \mu'_{g,1}) a_v g_1 + \gamma_{w,1}\theta + \gamma_{s,1}\rho + \gamma_{g,1} a_v \tag{3.1}$$

$$\frac{\partial \theta c_k}{\partial t} + \frac{\partial \rho s_k}{\partial t} + \frac{\partial a_v g_k}{\partial t} = \frac{\partial}{\partial x}(\theta D_k^{\,w} \frac{\partial c_k}{\partial x}) + \frac{\partial}{\partial x}(a_v D_k^{\,g} \frac{\partial g_k}{\partial x}) - \frac{\partial q c_k}{\partial x} -$$
$$-(\mu_{w,k} + \mu'_{w,k})\theta c_k - (\mu_{s,k} + \mu'_{s,k})\rho s_k - (\mu_{g,k} + \mu_{g,k}) a_v g_k + \mu'_{w,k-1}\theta c_{k-1} \tag{3.2}$$
$$+\mu'_{s,k-1}\rho s_{k-1} + \mu'_{g,k-1} a_v g_{k-1} + \gamma_{w,k}\theta + \gamma_{s,k}\rho + \gamma_{g,k} a_v - Sc_{r,k} \qquad k \in (2, n_s)$$

where c, s, and g are solute concentrations in the liquid [ML^{-3}], solid [MM^{-1}], and gaseous [ML^{-3}], phases, respectively; q is the volumetric flux density [LT^{-1}], μ_w, μ_s, and μ_g are first-order rate constants for solutes in the liquid, solid, and gas phases [T^{-1}], respectively; μ_w', μ_s', and μ_g' are similar first-order rate constants providing connections between individual chain species, γ_w, γ_s, and γ_g are zero-order rate constants for the liquid [$ML^{-3}T^{-1}$], solid [T^{-1}], and gas [$ML^{-3}T^{-1}$] phases, respectively; ρ is the soil bulk density [$M\,L^{-3}$], a_v is the air content [L^3L^{-3}], S is the sink term in the water flow equation (2.1), c_r is the concentration of the sink term [ML^{-3}], D^w is the dispersion coefficient [L^2T^{-1}] for the liquid phase, and D^g is the diffusion coefficient [L^2T^{-1}] for the gas phase. As before, the subscripts w, s, and g correspond with the liquid, solid and gas phases, respectively; while the subscript k represents the kth chain number, and n_s is the number of solutes involved in the chain reaction. The nine zero- and first-order rate constants in (3.1) and (3.2) may be used to represent a variety of reactions or transformations including biodegradation, volatilization, and precipitation.

HYDRUS assumes nonequilibrium interaction between the solution (c) and adsorbed (s)

concentrations, and equilibrium interaction between the solution (c) and gas (g) concentrations of the solute in the soil system. The adsorption isotherm relating s_k and c_k is described by a generalized nonlinear equation of the form

$$s_k = \frac{k_{s,k} c_k^{\beta_k}}{1 + \eta_k c_k^{\beta_k}} \qquad k \epsilon (1, n_s)$$

$$\frac{\partial s_k}{\partial t} = \frac{k_{s,k}\beta_k c_k^{\beta_k - 1}}{(1 + \eta_k c_k^{\beta_k})^2} \frac{\partial c_k}{\partial t} + \frac{c_k^{\beta_k}}{1 + \eta_k c_k^{\beta_k}} \frac{\partial k_{s,k}}{\partial t} - \frac{k_{s,k} c_k^{2\beta_k}}{(1 + \eta_k c_k^{\beta_k})^2} \frac{\partial \eta_k}{\partial t} + \frac{k_{s,k} c_k^{\beta_k} \ln c_k}{(1 + \eta_k c_k^{\beta_k})^2} \frac{\partial \beta_k}{\partial t} \qquad (3.3)$$

where $k_{s,k}$ [L^3M^{-1}], β_k [-] and η_k [L^3M^{-1}] are empirical coefficients. The Freundlich, Langmuir, and linear adsorption equations are special cases of equation (3.3). When β_k=1, equation (3.3) becomes the Langmuir equation, when η_k=0, equation (3.3) becomes the Freundlich equation, and when both β_k=1 and η_k=0, equation (3.3) leads to a linear adsorption isotherm. Solute transport without adsorption is described with $k_{s,k}$=0. While the coefficients $k_{s,k}$, β_k, and η_k in equation (3.3) are assumed to be independent of concentration, they are permitted to change as a function of time through their dependency on temperature. This feature will be discussed later.

The concept of two-site sorption [*Selim et al.*, 1977; *van Genuchten and Wagenet*, 1989] is implemented in HYDRUS to permit consideration of nonequilibrium adsorption-desorption reactions. The two-site sorption concept assumes that the sorption sites can be divided into two fractions:

$$s_k = s_k^e + s_k^k \qquad k \epsilon (1, n_s) \qquad (3.4)$$

Sorption, s_k^e [MM^{-1}], on one fraction of the sites (the type-1 sites) is assumed to be instantaneous, while sorption, s_k^k [MM^{-1}], on the remaining (type-2) sites is considered to be time-dependent. At equilibrium we have for the type-1 (equilibrium) and type-2 (kinetic) sites, respectively

$$s_k^e = f s_k \qquad k \epsilon (1, n_s) \qquad (3.5)$$

$$s_k^k = (1 - f) s_k \qquad k \epsilon (1, n_s) \qquad (3.6)$$

where f is the fraction of exchange sites assumed to be in equilibrium with the solution phase [-].

Because type-1 sorption sites are always at equilibrium, differentiation of (3.5) gives immediately the sorption rate for the type-1 equilibrium sites:

$$\frac{\partial s_k^e}{\partial t} = f\frac{\partial s_k}{\partial t} \qquad k \in (1, n_s) \tag{3.7}$$

Sorption on the type-2 nonequilibrium sites is assumed to be a first-order kinetic rate process. Following *Toride et al.* [1993], the mass balance equation for the type-2 sites in the presence of production and degradation is given by

$$\frac{\partial s_k^k}{\partial t} = \omega_k \left[(1-f)\frac{k_{s,k} c_k^{\beta_k}}{1 + \eta_k c_k^{\beta_k}} - s_k^k \right] - (\mu_{s,k} + \mu'_{s,k}) s_k^k + (1-f)\gamma_{s,k} \qquad k \in (1, n_s) \tag{3.8}$$

where ω_k is the first-order rate constant for the kth solute [T^{-1}].

The concentrations g_k and c_k are related by a linear expression of the form

$$g_k = k_{g,k} c_k \qquad k \in (1, n_s) \tag{3.9}$$

where $k_{g,k}$ is an empirical constant [-] equal to $(K_H R_u T^A)^{-1}$ [*Stumm and Morgan*, 1981] in which K_H is Henry's Law constant [$MT^2M^{-1}L^{-2}$], R_u is the universal gas constant [$ML^2T^{-2}K^{-1}M^{-1}$] and T^A is absolute temperature [K].

Substituting (3.3) through (3.9) into (3.1) and (3.2) leads to the following equation

$$\frac{\partial \theta R_{k1} c_k}{\partial t} + \theta R_{k2}\frac{\partial c_k}{\partial t} = \frac{\partial}{\partial x}\left(E_k \frac{\partial c_k}{\partial x}\right) - \frac{\partial B_k c_k}{\partial x} + F_k c_k + G_k = 0 \qquad k \in (1, n_s) \tag{3.10}$$

in which E_k [L^2T^{-1}] and B_k [LT^{-1}] are an effective dispersion coefficient and effective velocity given by

$$E_k = \theta D_k^w + a_v D_k^g k_{g,k} \qquad k \in (1, n_s) \tag{3.11}$$

$$B_k = q - a_v D_k^g \frac{\partial k_{g,k}}{\partial x} \qquad k \in (1, n_s) \tag{3.12}$$

respectively. The coefficients F_k and G_k in (3.10) are defined as

$$F_k(c_k) = -(\mu_{w,k} + \mu'_{w,k})\theta - (\mu_{s,k} + \mu'_{s,k})\rho f \frac{k_{s,k} c_k^{\beta_k - 1}}{1 + \eta_k c_k^{\beta_k}} - (\mu_{g,k} + \mu'_{g,k}) a_v k_{g,k} \qquad (3.13)$$

$$G_1(c_1) = \gamma_{w,1}\theta + \gamma_{s,1} f\rho + \gamma_{g,1} a_v - Sc_{r,1} - \omega_1 \rho \left[\frac{(1-f) k_{s,1} c_1^{\beta_1}}{1 + \eta_1 c_1^{\beta_1}} - s_1^{\,k} \right] - g_1(c_1)$$

$$G_k(c_k) = (\mu'_{w,k-1}\theta + \mu'_{s,k-1} f\rho \frac{k_{s,k-1} c_{k-1}^{\beta_{k-1} - 1}}{1 + \eta_{k-1} c_{k-1}^{\beta_{k-1}}} + \mu_{g,k-1} a_v k_{g,k-1}) c_{k-1} + \mu'_{s,k-1} \rho s_{k-1}^{\,k} + \gamma_{w,k}\theta + \qquad (3.14)$$

$$\gamma_{s,k} f\rho + \gamma_{g,k} a_v - Sc_{r,k} - \omega_k \rho \left[\frac{(1-f) k_{s,k} c_k^{\beta_k}}{1 + \eta_k c_k^{\beta_k}} - s_k^{\,k} \right] - g_k(c_k) \qquad k \in (2, n_s)$$

where the variable g_k accounts for possible changes in the adsorption parameters caused by temperature changes in the system as follows (see also section 3.4):

$$g_k(c_k) = \rho f \left[\frac{c_k^{\beta_k}}{1 + \eta_k c_k^{\beta_k}} \frac{\partial k_{s,k}}{\partial t} - \frac{k_{s,k} c_k^{2\beta_k}}{(1 + \eta_k c_k^{\beta_k})^2} \frac{\partial \eta_k}{\partial t} + \frac{k_{s,k} \ln c_k \, c_k^{\beta_k}}{(1 + \eta_k c_k^{\beta_k})^2} \frac{\partial \beta_k}{\partial t} \right] \qquad k \in (1, n_s) \qquad (3.15)$$

Because of numerical and programming consideration, we divided the total retardation factor R_k [-] for use in (3.10) into one part, R_{k1}, associated with the liquid and gaseous phases, and another part, R_{k2}, associated with the solid phase:

$$R_{k1}(c_k) = 1 + \frac{a_v k_{g,k}}{\theta} \qquad k \in (1, n_s) \qquad (3.16)$$

$$R_{k2}(c_k) = \frac{\rho}{\theta} \frac{f k_{s,k} \beta_k c_k^{\beta_k - 1}}{(1 + \eta_k c_k^{\beta_k})^2} \qquad k \in (1, n_s) \qquad (3.17)$$

In order to solve equation (3.10), it is necessary to know the water content θ and the volumetric flux q. Both variables are obtained from solutions of the Richards' equation. The above equations may appear to be relatively complicated. However, by selecting proper values

of particular coefficients (i.e., γ_w, γ_s, γ_g, μ_w, μ_s, μ_g, μ_w', μ_s', μ_g', η, k_s, k_g, f, β, ω) the entire system can be simplified significantly. Assuming for example that μ_w', μ_s', μ_g', η, and k_g are zero, and f and β are equal to one, the entire system of equations (3.1) through (3.17) simplifies into a set of equations describing the transport of mutually independent solutes, i.e., single-ion transport as applicable to:

$$\frac{\partial \theta R c}{\partial t} = \frac{\partial}{\partial x}(\theta D^{w} \frac{\partial c}{\partial x}) - \frac{\partial q c}{\partial x} + Fc + G = 0 \tag{3.18}$$

3.2. *Initial and Boundary Conditions*

The solution of (3.10) requires knowledge of the initial concentration within the flow region, Ω, i.e.,

$$\begin{aligned} c(x,0) &= c_i(x) \\ s^{k}(x,0) &= s_i^{k}(x) \end{aligned} \tag{3.19}$$

where c_i [ML^{-3}] and s_i^k [-] are prescribed functions of x and z. The initial condition for s_i^k must be specified only when nonequilibrium adsorption is considered. The subscript k is dropped in (3.19) and throughout the remainder of this report, thus assuming that the transport-related equations in the theoretical development and the numerical solution apply to each of the solutes in the decay chain.

Two types of boundary conditions (Dirichlet and Cauchy type conditions) can be applied to the upper or lower boundaries. First-type (or Dirichlet type) boundary conditions prescribe the concentration at a boundary:

$$c(x,t) = c_0(x,t) \qquad \text{at } x = 0 \quad \text{or} \quad x = L \tag{3.20}$$

whereas third-type (Cauchy type) boundary conditions may be used to prescribe the concentration flux at the upper or lower boundary as follows:

$$-\theta D\frac{\partial c}{\partial x} + qc = q_0 c_0 \qquad \text{at} \quad x = 0 \quad \text{or} \quad x = L \tag{3.21}$$

in which q_0 represents the upward fluid flux and c_0 is the concentration of the incoming fluid [ML^{-3}]. In some cases, for example when boundary is impermeable (q_0=0) or when water flow is directed out of the region, (3.21) reduces to a second-type (Neumann type) boundary condition of the form:

$$\theta D\frac{\partial c}{\partial x} = 0 \qquad \text{at} \quad x = 0 \quad \text{or} \quad x = L \tag{3.22}$$

A different type of soil surface boundary condition is needed for volatile solutes when they are present in both the liquid and gas phases. This situation requires a third-type boundary condition as before, but with an additional term to account for gaseous diffusion through a stagnant boundary layer of thickness d [L] on the soil surface. The additional solute flux is proportional to the difference in gas concentrations above and below the boundary layer [*Jury et al.*, 1983]. The modified boundary condition has the form

$$-\theta D\frac{\partial c}{\partial x} + qc = q_0 c_0 + \frac{D_g}{d}(k_g c - g_{atm}) \qquad \text{at} \quad x = L \tag{3.23}$$

where D_g is the molecular diffusion coefficient in the gas phase [L^2T^{-1}] and g_{atm} is the gas concentration above the stagnant boundary layer [ML^{-3}] (*Jury et al.* [1983] assumed g_{atm} to be zero). Similarly as for (3.21), (3.23) reduces to a second-type (or Neumann type) boundary condition when water flow is zero or directed out of the region:

$$-\theta D\frac{\partial c}{\partial x} = \frac{D_g}{d}(k_g c - g_{atm}) \qquad \text{at} \quad x = L \tag{3.24}$$

Equations (3.23) and (3.24) can only be used when the additional gas diffusion flux is positive. *Jury et al.* [1983] discussed how to estimate the thickness of the boundary layer, d; they recommended value of 0.5 cm for d as a good average for a bare surface.

3.3. *Effective Dispersion Coefficient*

The dispersion coefficient in the liquid phase, D^w, is given by [*Bear*, 1972]

$$\theta D^{w} = D_L |q| + \theta D_w \tau_w \tag{3.25}$$

where D_w is the molecular diffusion coefficient in free water [L^2T^{-1}], τ_w is a tortuosity factor in the liquid phase [-], $|q|$ is the absolute value of the Darcian fluid flux density [LT^{-1}], and D_L is the longitudinal dispersivity [L]. After adding the diffusion contribution from the gas phase, the effective dispersion coefficient in the soil matrix for one-dimensional transport is as follows:

$$\theta D = D_L |q| + \theta D_w \tau_w + a_v D_g k_g \tau_g \tag{3.26}$$

where D_g is the molecular diffusion coefficient in the gas phase [L^2T^{-1}] and τ_g is a tortuosity factor in the gas phase [-].

The tortuosity factors for both phases are evaluated in HYDRUS as a function of the water and air contents using the relationship of *Millington and Quirk* [1961]:

$$\tau_w = \frac{\theta^{7/3}}{\theta_s^2}$$
$$\tau_g = \frac{a_v^{7/3}}{\theta_s^2} \tag{3.27}$$

3.4. *Temperature Dependence of Transport and Reaction Coefficients*

Several of the diffusion (D_w, D_g), zero-order production (γ_w, γ_s, γ_g), first-order degradation (μ_w', μ_s', μ_g', μ_w, μ_s, and μ_g), and adsorption (k_s, k_g, β, η, ω) coefficients may be strongly dependent upon temperature. HYDRUS assumes that this dependency can be expressed by the Arrhenius equation [*Stumm and Morgan*, 1981]. After some modification, this equation can be expressed in the general form [*Šimůnek and Suarez,* 1993a]

$$a_T = a_r \exp\left[\frac{E_a(T^A - T_r^A)}{R_u T^A T_r^A}\right] \tag{3.28}$$

where a_r and a_T are the values of the coefficient being considered at a reference absolute temperature T_r^A and absolute temperature T^A, respectively; R_u is the universal gas constant, and E_a [$ML^2T^{-2}M^{-1}$] is the activation energy of the particular reaction or process being modeled.

4. HEAT TRANSPORT

4.1. *Governing Heat Transport Equations*

Neglecting the effect of water vapor diffusion on transport, one-dimensional heat transfer can be described with a convection-dispersion equation of the form

$$\frac{\partial C_p(\theta)T}{\partial t} = \frac{\partial}{\partial x}[\lambda(\theta)\frac{\partial T}{\partial x}] - C_w\frac{\partial qT}{\partial x} - C_w ST \tag{4.1}$$

or equivalently as [*Sophocleous*, 1979]:

$$C_p(\theta)\frac{\partial T}{\partial t} = \frac{\partial}{\partial x}[\lambda(\theta)\frac{\partial T}{\partial x}] - C_w q\frac{\partial T}{\partial x} \tag{4.2}$$

where $\lambda(\theta)$ is the coefficient of the apparent thermal conductivity of the soil [$MLT^{-3}K^{-1}$] and $C_p(\theta)$ and C_w are the volumetric heat capacities [$ML^{-1}T^{-2}K^{-1}$] of the porous medium and the liquid phase, respectively. The volumetric heat capacity is defined as the product of the bulk density and gravimetric heat capacity. The first term on the right-hand side of (4.1) represents heat flow due to conduction, the second term heat transported by flowing water, and the third term energy uptake by plant roots associated with root water uptake. We do not consider the transfer of latent heat by vapor movement. Equation (4.2) is derived from (4.1) by making use of the continuity equation describing isothermal Darcian flow of water in a variably-saturated porous medium

$$\frac{\partial\theta}{\partial t} = -\frac{\partial q}{\partial x} - S \tag{4.3}$$

According to *de Vries* [1963] the volumetric heat capacity can be expressed as

$$C_p(\theta) = C_n\theta_n + C_o\theta_o + C_w\theta + C_a a_v \approx (1.92\,\theta_n + 2.51\,\theta_o + 4.18\,\theta)\,10^6 \quad (\mathrm{J\,m^{-3}\,{}^{o}C^{-1}}) \tag{4.4}$$

where θ refers to a volumetric fraction [L^3L^{-3}], and subscripts *n, o, a, w* represent solid phase, organic matter, gas phase and liquid phase, respectively.

4.2. *Apparent Thermal Conductivity Coefficient*

The apparent thermal conductivity $\lambda(\theta)$ combines the thermal conductivity $\lambda_0(\theta)$ of the porous medium (solid plus water) in the absence of flow and the macrodispersivity, which is a linear function of the velocity [*de Marsily*, 1986]:

$$\lambda(\theta) = \lambda_0(\theta) + \beta_t C_w |q| \tag{4.5}$$

where β_t is the thermal dispersivity [L]. The volumetric heat capacity of the liquid phase is included in the definition of the thermal conductivity in order to have the dimensions of the thermal dispersivity in length units. Thermal conductivity is described by *Chung and Horton* [1987] with the equation

$$\lambda_0(\theta) = b_1 + b_2\theta + b_3\theta^{0.5} \tag{4.6}$$

where b_1, b_2, and b_3 are empirical parameters [$MLT^{-3}K^{-1}$].

4.3. *Initial and Boundary Conditions*

The solution of (4.1) requires knowledge of the initial temperature within the flow region, i.e.,

$$T(x,0) = T_i(x) \qquad t = 0 \tag{4.7}$$

where T_i is a prescribed function of x.

Two types of boundary conditions (Dirichlet and Cauchy type conditions) can be specified at the top and bottom boundaries of the soil profile. First-type (or Dirichlet type) boundary conditions prescribe the temperature:

$$T(x,t) = T_0(t) \qquad \text{at} \quad x = 0 \quad \text{or} \quad x = L \tag{4.8}$$

whereas third-type (or Cauchy type) boundary conditions may be used to prescribe the heat flux as follows

$$-\lambda\frac{\partial T}{\partial x} + TC_w q = T_0 C_w q \qquad \text{at} \quad x = 0 \quad \text{or} \quad x = L \tag{4.9}$$

in which T_0 is either the temperature of the incoming fluid or the temperature at the boundary. In some cases, for example for an impermeable boundary (q=0) or when water flow is directed out of the region, (4.9) reduces to a second-type (Neumann type) boundary condition of the form:

$$\frac{\partial T}{\partial x} = 0 \qquad \text{at} \quad x = 0 \tag{4.10}$$

Atmospheric boundary conditions for daily fluctuations in soil temperature are often represented by a sine function as follows [*Kirkham and Powers*, 1972]:

$$T_0 = \overline{T} + A\sin\left(\frac{2\pi t}{p_t} - \frac{7\pi}{12}\right) \tag{4.11}$$

where p_t is a period of time [T] necessary to complete one cycle of the sine wave (taken to be 1 day), $\overline{T}$ is the average temperature at the soil surface [K] during the period p_t, and A is the amplitude of the sine wave [K]. The second part of the sine term is included to force the maximum in the daily temperature to occur at 1 p.m.

5. NUMERICAL SOLUTION OF THE WATER FLOW EQUATION

5.1. *Space and Time Discretization*

The soil profile is first discretized into N-1 adjoining elements, with the ends of the elements located at the nodal points, and N being the number of nodes. The same spatial discretization is used for water flow, solute transport and heat movement. HYDRUS assumes that the vertical coordinate x is directed positive upward.

A mass-lumped linear finite elements scheme was used for discretization of the mixed form of the Richards' equation (2.1). Since the mass-lumped scheme results in an equivalent and somewhat standard finite difference scheme [e.g., *Vogel et al.*, 1996], we omit the detailed finite element development and give immediately the invoked final finite difference scheme:

$$\frac{\theta_i^{j+1,k+1} - \theta_i^j}{\Delta t} = \frac{1}{\Delta x}\left[K_{i+1/2}^{j+1,k} \frac{h_{i+1}^{j+1,k+1} - h_i^{j+1,k+1}}{\Delta x_i} - K_{i-1/2}^{j+1,k} \frac{h_i^{j+1,k+1} - h_{i-1}^{j+1,k+1}}{\Delta x_{i-1}} \right] + \frac{K_{i+1/2}^{j+1,k} - K_{i-1/2}^{j+1,k}}{\Delta x} - S_i^j \tag{5.1}$$

where

$$\Delta t = t^{j+1} - t^j$$

$$\Delta x = \frac{x_{i+1} - x_{i-1}}{2} \qquad \Delta x_i = x_{i+1} - x_i \qquad \Delta x_{i-1} = x_i - x_{i-1} \tag{5.2}$$

$$K_{i+1/2}^{j+1,k} = \frac{K_{i+1}^{j+1,k} + K_i^{j+1,k}}{2} \qquad K_{i-1/2}^{j+1,k} = \frac{K_i^{j+1,k} + K_{i-1}^{j+1,k}}{2}$$

in which subscripts i-1, i, and i+1 indicate the position in the finite difference mesh; superscripts k and k+1 denote the previous and current iteration levels, respectively; and superscripts j and j+1 represent the previous and current time levels, respectively. Equation (5.1) is based on a fully implicit discretization of the time derivative, and will be solved with a Picard iterative solution scheme. Notice also that the sink term, S, is evaluated at the previous time level. The mass-

conservative method proposed by *Celia et al.* [1990], in which $\theta^{j+1,k+1}$ is expanded in a truncated Taylor series with respect to h about the expansion point $h^{j+1,k}$, is used in the time difference scheme of (5.1):

$$\frac{\theta_i^{j+1,k+1} - \theta_i^j}{\Delta t} = C_i^{j+1,k} \frac{h_i^{j+1,k+1} - h_i^{j+1,k}}{\Delta t} + \frac{\theta_i^{j+1,k} - \theta_i^j}{\Delta t} \tag{5.3}$$

where C_i represents the nodal value of the soil water capacity [L^{-1}]:

$$C_i^{j+1,k} = \left.\frac{d\theta}{dh}\right|^{j+1,k} \tag{5.4}$$

This method has been shown to provide excellent results in terms of minimizing the mass balance error. Notice that the second term on the right hand size of (5.3) is known prior to the current iteration. The first term on the right hand side of (5.3) should vanish at the end of the iteration process if the numerical solution converges. The derivation leads to the following matrix equation with matrix $[P_w]$ and vectors $\{h\}$ and $\{F_w\}$

$$[P_w]^{j+1,k}\{h\}^{j+1,k+1} = \{F_w\} \tag{5.5}$$

The symmetrical tridiagonal matrix $[P_w]$ in (5.5) has the form

$$[P_w] = \begin{vmatrix} d_1 & e_1 & 0 & & & & 0 \\ e_1 & d_2 & e_2 & 0 & & & 0 \\ 0 & e_2 & d_3 & e_3 & 0 & & 0 \\ & \cdot & & \cdot & & \cdot & \\ & \cdot & & \cdot & & \cdot & \\ 0 & & 0 & e_{N-3} & d_{N-2} & e_{N-2} & 0 \\ 0 & & & 0 & e_{N-2} & d_{N-1} & e_{N-1} \\ 0 & & & & 0 & e_{N-1} & d_N \end{vmatrix} \tag{5.6}$$

where the diagonal entries d_i and above-diagonal entries e_i of the matrix $[P_w]$, and the entries f_i of vector $\{F_w\}$, are given by

$$d_i = \frac{\Delta x}{\Delta t} C_i^{j+1,k} + \frac{K_{i+1}^{j+1,k} + K_i^{j+1,k}}{2\Delta x_i} + \frac{K_i^{j+1,k} + K_{i-1}^{j+1,k}}{2\Delta x_{i-1}} \tag{5.7}$$

$$e_i = -\frac{K_i^{j+1,k} + K_{i+1}^{j+1,k}}{2\Delta x_i} \tag{5.8}$$

$$f_i = \frac{\Delta x}{\Delta t} C_i^{j+1,k} h_i^{j+1,k} - \frac{\Delta x}{\Delta t}(\theta_i^{j+1,k} - \theta_i^j) + \frac{K_{i+1}^{j+1,k} - K_{i-1}^{j+1,k}}{2} - S_i^j \Delta x \tag{5.9}$$

The tridiagonal matrix $[P_w]$ is symmetric and therefore the below-diagonal entries are equal to the above-diagonal entries. The entries d_1, e_1, f_1, and e_{N-1}, d_N, f_N are dependent upon the prescribed boundary conditions.

5.2. *Treatment of Pressure Head Boundary Conditions*

If a first-type (Dirichlet) boundary condition is specified at the top or bottom of the soil profile, then the terms d_1 or d_N are equal to unity, e_1 or e_{N-1} reduce to zero, and f_1 or f_N equal to the prescribed pressure head, h_0. Some additional rearrangement of matrix $[P_w]$ is also necessary to preserve its symmetry. The appropriate entries in the second or (N-1)st equations containing the prescribe boundary pressure head h_0 in the left-hand side matrix must then be incorporated into the known vector on the right-hand side of the global matrix equation. When done properly, this rearrangement will restore symmetry in $[P_w]$.

5.3. *Treatment of Flux Boundary Conditions*

If a third-type (Neumann) boundary condition at the bottom of the profile is specified, then the individual entries are obtained by discretization of Darcy's law, i.e.,

$$q = -K\frac{\partial h}{\partial x} - K \tag{5.10}$$

such that d_1 and f_1 in $[P_w]$ attain the values

$$d_1 = \frac{K_1^{j+1,k} + K_2^{j+1,k}}{2\Delta x_1} \tag{5.11}$$

$$f_1 = \frac{K_1^{j+1,k} + K_2^{j+1,k}}{2} + q_0^{j+1} \tag{5.12}$$

where q_0 is the prescribed bottom boundary flux [LT^{-1}] and where e_1 is described by (5.8). A similar discretization of Darcy's law is possible to incorporate flux boundary condition at the top of the soil profile. This approach, however, can quickly lead to relatively unstable solutions when the boundary fluxes at the soil surface vary strongly with time (erratic irrigation or rainfall rates). A more stable and mass-conservative solution results when the mass balance equation

$$\frac{\partial \theta}{\partial t} = -\frac{\partial q}{\partial x} - S \tag{5.13}$$

instead of Darcy's law is discretized. Discretization of (5.13) gives

$$\frac{\theta_N^{j+1,k+1} - \theta_N^j}{\Delta t} = -\frac{2(q_N^{j+1} - q_{N-1/2}^{j+1,k})}{\Delta x_{N-1}} - S_N^j \tag{5.14}$$

Expanding the time derivative on the left hand side of (5.14) as in (5.3), and using the discretized form of Darcy's law for $q_{N-1/2}$ leads to

$$d_N = \frac{\Delta x_{N-1}}{2\Delta t} C_N^{j+1,k} + \frac{K_N^{j+1,k} + K_{N-1}^{j+1,k}}{2\Delta x_{N-1}} \tag{5.15}$$

$$f_N = \frac{\Delta x_{N-1}}{2\Delta t} C_N^{j+1,k} h_N^{j+1,k} - \frac{\Delta x}{2\Delta t}(\theta_N^{j+1,k} - \theta_N^j) - \frac{K_N^{j+1,k} + K_{N-1}^{j+1,k}}{2} - \frac{\Delta x_{N-1}}{2} S_N^j - q_N^{j+1} \tag{5.16}$$

where q_N is the prescribed soil surface boundary flux. Implementation of a third-type boundary condition always preserves symmetry of the matrix $[P_w]$.

5.4. *Numerical Solution Strategy*

5.4.1. *Iterative Process*

Because of the nonlinear nature of (5.5), an iterative process must be used to obtain solutions of the global matrix equation at each new time step. For each iteration a system of linearized algebraic equations is first derived from (5.5) which, after incorporation of the boundary conditions, is solved using Gaussian elimination. The Gaussian elimination process takes advantage of the tridiagonal and symmetric features of the coefficient matrix in (5.5). After solving (5.5) the first time, the coefficients in (5.5) are re-evaluated using this first solution, and the new equations are again solved. The iterative process continues until a satisfactory degree of convergence is obtained, i.e., until at all nodes in the saturated (or unsaturated) region the absolute change in pressure head (or water content) between two successive iterations becomes less than some small value determined by the imposed absolute pressure head (or water content) tolerance. The first estimate (at zero iteration) of the unknown pressure heads at each time step is obtained by extrapolation from the pressure head values at the previous two time levels.

5.4.2. *Time Control*

Three different time discretizations are introduced in HYDRUS: (1) time discretizations associated with the numerical solution, (2) time discretizations associated with the implementation of boundary conditions, and (3) time discretizations which provide printed output of the simulation results (e.g., nodal values of dependent variables, water, solute mass balance components, and other information about the flow regime).

Discretizations 2 and 3 are mutually independent; they generally involve variable time steps as described in the input data file. Discretization 1 starts with a prescribed initial time increment, Δt. This time increment is automatically adjusted at each time level according to the following rules [*Mls*, 1982; *Šimůnek et al.*, 1992]:

a. Discretization 1 must coincide with time values resulting from time discretizations 2 and 3.

b. Time increments cannot become less than a preselected minimum time step, Δt_{min}, nor exceed a maximum time step, Δt_{max} (i.e., $\Delta t_{min} \leq \Delta t \leq \Delta t_{max}$).

c. If, during a particular time step, the number of iterations necessary to reach convergence is ≤ 3, the time increment for the next time step is increased by multiplying Δt by a predetermined constant >1 (usually between 1.1 and 1.5). If the number of iterations is ≥ 7, Δt for the next time level is multiplied by a constant <1 (usually between 0.3 and 0.9).

d. If, during a particular time step, the number of iterations at any time level becomes greater than a prescribed maximum (usually between 10 and 50), the iterative process for that time level is terminated. The time step is subsequently reset to $\Delta t/3$, and the iterative process restarted.

5.4.3. *Atmospheric Boundary Conditions and Seepage Faces*

Atmospheric boundaries are simulated by applying either prescribed head or prescribed flux boundary conditions depending upon whether equation (2.48) or (2.49) is satisfied [*Neuman*, 1974]. If (2.49) is not satisfied, boundary node n becomes a prescribed head boundary. If, at any point in time during the computations, the calculated flux exceeds the specified potential flux in (2.48), the node will be assigned a flux equal to the potential value and treated again as a prescribed flux boundary.

If a seepage face is considered as the lower boundary condition and if during each iteration the lower part of the soil profile is saturated then the last node is treated as a prescribed pressure head boundary with h=0. However, if this node is unsaturated then a prescribed flux boundary with q=0 is imposed at the lower boundary.

5.4.4. *Water Balance Computations*

The HYDRUS code performs water balance computations at prescribed times for several preselected subregions of the flow domain. The water balance information for each subregion consists of the actual volume of water, V, in that subregion, and the rate, O [LT^{-1}], of inflow or

outflow to or from the subregion. These variables V and O are evaluated in HYDRUS by means of

$$V = \sum_e \Delta x_i \frac{\theta_i + \theta_{i+1}}{2} \tag{5.17}$$

and

$$O = \frac{V_{new} - V_{old}}{\Delta t} \tag{5.18}$$

respectively, where θ_i and θ_{i+1} are water contents evaluated at the corner nodes of element e, Δx_i is the size of the element, and V_{new} and V_{old} are volumes of water in the subregion computed at the current and previous time levels, respectively. The summation in (5.17) is taken over all elements within the subregion.

The absolute error in the mass balance of the flow domain is calculated as

$$\epsilon_a^w = V_t - V_0 + \int_0^t T_a dt - \int_0^t (q_0 - q_N) dt \tag{5.19}$$

where V_t and V_0 are the volumes of water in the flow domain, Eq. (5.17), evaluated at times t and zero, respectively. The third term on the right-hand side of (5.19) represents the cumulative root water uptake amount, while the fourth term gives the net cumulative flux through both boundaries.

The accuracy of the numerical solution is evaluated by the relative error, ϵ_r^w [%], in the water mass balance as follows:

$$\epsilon_r^w = \frac{|\epsilon_a^w|}{\max\left[\sum_e |V_t^e - V_0^e|, \int_0^t T_a dt + \int_0^t (|q_N| + |q_0|) dt\right]} 100 \tag{5.20}$$

where V_t^e and V_0^e are the volumes of water in element e at times t and zero, respectively. Note that HYDRUS does not relate the absolute error to the volume of water in the flow domain, but instead to the maximum value of two quantities. The first quantity represents the sum of the

absolute changes in water content over all elements, whereas the second quantity is the sum of the absolute values of all fluxes in and out of the flow domain.

5.4.5. *Computation of Nodal Fluxes*

Components of the Darcian flux are computed at each time level during the simulation only when the water flow and solute (or heat) transport equations are solved simultaneously. When the flow equation is being solved alone, the flux components are calculated only at selected print times. The x-components of the nodal fluxes are computed for each node n according to

$$q_1^{j+1} = -K_{1+1/2}^{j+1}\left[\frac{h_2^{j+1} - h_1^{j+1}}{\Delta x_i} + 1\right]$$

$$q_i^{j+1} = \frac{-K_{i+1/2}^{j+1}\left[\frac{h_{i+1}^{j+1} - h_i^{j+1}}{\Delta x_i} + 1\right]\Delta x_{i-1} \; - \; K_{i-1/2}^{j+1}\left[\frac{h_i^{j+1} - h_{i-1}^{j+1}}{\Delta x_{i-1}} + 1\right]\Delta x_i}{\Delta x_{i-1} + \Delta x_i} \qquad (5.21)$$

$$q_N^{j+1} = -K_{N-1/2}^{j+1}\left[\frac{h_N^{j+1} - h_{N-1}^{j+1}}{\Delta x_{N-1}} + 1\right] - \frac{\Delta x_{N-1}}{2}\left[\frac{\theta_N^{j+1} - \theta_N^{j}}{\Delta t} + S_N^{j}\right]$$

5.4.6. *Water Uptake by Plant Roots*

HYDRUS considers the root zone to consist of all nodes, n, for which the potential root water uptake distribution, b (see Section 2.2), is greater than zero. The root water extraction rate is assumed to vary linearly over each element. The values of actual root extraction rate S_i in (5.1) are evaluated with (2.4). HYDRUS calculates the total rate of transpiration using the equation

$$T_a = \sum_e \Delta x_i \frac{S_i + S_{i+1}}{2} \qquad (5.22)$$

in which the summation takes place over all elements within the root zone, and where S_i and S_{i+1} are the root water uptake rates evaluated at the corner nodes of element e.

5.4.7. *Evaluation of the Soil Hydraulic Properties*

At the beginning of a simulation, HYDRUS generates for each soil type in the flow domain a table of water contents, hydraulic conductivities, and specific water capacities from the specified set of hydraulic parameters [*Vogel*, 1987]. The values of θ_i, K_i and C_i in the table are evaluated at prescribed pressure heads h_i within a specified interval (h_a, h_b). The entries in the table are generated such that

$$\frac{h_{i+1}}{h_i} = constant \tag{5.23}$$

which means that the spacing between two consecutive pressure head values increases in a logarithmic fashion. Values for the hydraulic properties, $\theta(h)$, $K(h)$ and $C(h)$, are computed during the iterative solution process using linear interpolation between the entries in the table. If an argument h falls outside the prescribed interval (h_a, h_b), the hydraulic characteristics are evaluated directly from the hydraulic functions, i.e., without interpolation. The above interpolation technique was found to be much faster computationally than direct evaluation of the hydraulic functions over the entire range of pressure heads, except when very simple hydraulic models are used.

6. NUMERICAL SOLUTION OF THE SOLUTE TRANSPORT EQUATION

The Galerkin finite element method is used to solve the solute and heat transport equations subject to appropriate initial and boundary conditions. Since the heat transport equation (4.1) has the same mathematical form as the (linearized) solute transport equation (3.10), the numerical solution will be given here only for solute transport.

6.1. *Space Discretization*

The finite element method assumes that the dependent variable, the concentration function $c(x,t)$, can be approximated by a finite series $c'(x,t)$ of the form

$$c'(x,t) = \sum_{m=1}^{N} \phi_m(x)\, c_m(t) \tag{6.1}$$

where ϕ_m are the selected linear basis functions that fulfill the condition $\phi_m(x_n)=\delta_{nm}$, δ_{nm} is Kronecker delta ($\delta_{nm}=1$ for $m=n$, and $\delta_{nm}=0$ for $m\neq n$), c_m are the unknown time-dependent coefficients which represent solutions of (3.10) at the finite element nodal points, and N is the total number of nodal points. Linear basis functions have the following form:

$$\begin{aligned} \phi_1 &= 1 - \xi \\ \phi_2 &= \xi \end{aligned} \tag{6.2}$$

where ξ is the distance in the local coordinate system [-]. In the global coordinate system ξ is defined as

$$\xi = \frac{x - x_1}{\Delta x} \qquad\qquad x_1 \le x \le x_2 \tag{6.3}$$

where Δx ($=x_2-x_1$) is the size of a finite element [L], i.e., the distance between two neighboring nodal points. The approximate solution $c'(x,t)$ converges to the correct solution $c(x,t)$ as the number of basis functions N increases.

Application of the Galerkin method which postulates that the differential operator

associated with the transport equation is orthogonal to each of the N basis functions, we obtain the following system of N time-dependent differential equations with N unknown values $c_n(t)$.

$$\int_0^L \left[-\frac{\partial \theta R^1 c}{\partial t} - \theta R^2 \frac{\partial c}{\partial t} + \frac{\partial}{\partial x}\left(E\frac{\partial c}{\partial x} - Bc\right) + Fc + G \right] \phi_n dx = 0 \tag{6.4}$$

where, for notational convenience we have dropped the index k referring to the kth decay chain number. Integrating by parts the terms containing spatial derivatives leads to the following equation

$$\begin{aligned} &\int_0^L \left[-\frac{\partial \theta R^1 c}{\partial t} - \theta R^2 \frac{\partial c}{\partial t} + Fc + G \right] \phi_n dx - \\ &\qquad \int_0^L \left[E\frac{\partial c}{\partial x} - Bc \right] \frac{\partial \phi_n}{\partial x} dx - q_{sL}\phi_n(L) + q_{s0}\phi_n(0) = 0 \end{aligned} \tag{6.5}$$

where q_{s0} and q_{sL} are solute fluxes across the lower and upper boundaries, respectively. By substituting (6.1) for $c(x,t)$ we obtain

$$\begin{aligned} &\sum_e \int_0^{L_e} \left[-\frac{\partial \theta R^1 c_m}{\partial t}\phi_m - \theta R^2 \frac{\partial c_m}{\partial t}\phi_m - Fc_m\phi_m + G \right] \phi_n dx - \\ &\qquad \sum_e \int_0^{L_e} \left[Ec_m \frac{\partial \phi_m}{\partial x} - Bc_m\phi_m \right] \frac{\partial \phi_n}{\partial x} dx - q_{s_L}\phi_n(L) + q_{s_0}\phi_n(0) = 0 \end{aligned} \tag{6.6}$$

Equation (6.6) can be rewritten in matrix form as

$$\frac{d([Q^1]\{c\})}{dt} + [Q^2]\frac{d\{c\}}{dt} + [S]\{c\} = \{f\} \tag{6.7}$$

where the vector $\{c\}$ contains the unknown values of the nodal concentrations, and where

$$Q^1_{nm} = \int_0^{L_e} \theta R^1 \phi_m \phi_n dx \tag{6.8}$$

$$Q_{nm}^2 = \int_0^{L_e} \theta R^2 \phi_m \phi_n dx \tag{6.9}$$

$$S_{nm} = \int_0^{L_e} [E \frac{d\phi_m}{dx} \frac{d\phi_n}{dx} - B \frac{d\phi_n}{dx} \phi_m - F \phi_m \phi_n] dx \tag{6.10}$$

$$f_n = \int_0^{L_e} G \phi_n dx - q_{sL} \phi_n(L) + q_{s0} \phi_n(0) \tag{6.11}$$

$$q_s = -\theta D \frac{\partial c'}{\partial x} + q c' \tag{6.12}$$

In addition to the basic assumptions involving the Galerkin method, several additional assumptions are now made (*van Genuchten* [1978]). First, within each element and at a given time, the different coefficients or groups of coefficients in equations (6.8) through (6.11) (i.e., θR, θD, q, F, and G) are assumed to change linearly according to the expressions:

$$\begin{aligned}
\theta R(t,x) &= \sum_{m=1}^{2} \theta R(t,x_m) \phi_m(x) \\
E(t,x) &= \sum_{m=1}^{2} E(t,x_m) \phi_m(x) \\
B(t,x) &= \sum_{m=1}^{2} B(t,x_m) \phi_m(x) \\
F(t,x) &= \sum_{m=1}^{2} F(t,x_m) \phi_m(x) \\
G(t,x) &= \sum_{m=1}^{2} G(t,x_m) \phi_m(x)
\end{aligned} \tag{6.13}$$

Because of (6.13) it is now not necessary to use numerical integration for evaluating the coefficients from equation (6.7). Second, mass lumping will be invoked by redefining the nodal

values of the time derivative in (6.4) as weighted averages over the entire flow region:

$$\frac{dc_n}{dt} = \frac{\int_0^L \theta R \frac{\partial c'}{\partial t} \phi_n dx}{\int_0^L \theta R \phi_n dx} \tag{6.14}$$

The above expansions lead to the following element matrices associated with global matrix equation (6.7). Note that $[S] = [S_1] + [S_2] + [S_3]$.

$$Q_{nm}{}^e = \int_1^2 \theta R \phi_m \phi_n dx = \frac{\Delta x}{12} \begin{vmatrix} 3\theta_1 R_1 + \theta_2 R_2 & \theta_1 R_1 + \theta_2 R_2 \\ \theta_1 R_1 + \theta_2 R_2 & \theta_2 R_2 + 3\theta_2 R_2 \end{vmatrix} \tag{6.15}$$

$$S_{nm}{}^e{}_1 = \int_1^2 E \frac{d\phi_m}{dx} \frac{d\phi_n}{dx} dx = \frac{1}{2\Delta x} \begin{vmatrix} E_1 + E_2 & -E_1 - E_2 \\ -E_1 - E_2 & E_2 + E_2 \end{vmatrix} \tag{6.16}$$

$$S_{nm}{}^e{}_2 = \int_1^2 B \frac{d\phi_n}{dx} \phi_m dx = \frac{1}{6} \begin{vmatrix} 2B_1 + B_2 & B_1 + 2B_2 \\ -2B_1 - B_2 & -B_1 - 2B_2 \end{vmatrix} \tag{6.17}$$

$$S_{nm}{}^e{}_3 = \int_1^2 F \phi_m \phi_n dx = \frac{\Delta x}{12} \begin{vmatrix} 3F_1 + F_2 & F_1 + F_2 \\ F_1 + F_2 & F_1 + 3F_2 \end{vmatrix} \tag{6.18}$$

$$f_n{}^e = \int_1^2 G \phi_n dx = \frac{\Delta x}{6} \begin{vmatrix} 2G_1 + G_2 \\ G_1 + 2G_2 \end{vmatrix} \tag{6.19}$$

6.2. *Time Discretization*

The Galerkin method is used only for approximating the spatial derivatives while the time derivatives are discretized by means of finite differences as follows

$$\frac{[Q^1]^{j+1}\{c\}^{j+1} - [Q^1]^j\{c\}^j}{\Delta t} + [Q^2]^{j+\epsilon}\frac{\{c\}^{j+1} - \{c\}^j}{\Delta t} +$$
$$\epsilon\,[S]^{j+1}\{c\}^{j+1} + (1-\epsilon)[S]^j\{c\}^j = \epsilon\,\{f\}^{j+1} + (1-\epsilon)\{f\}^j \tag{6.20}$$

where j and j+1 indicate previous and actual time level and Δt is time step, and where ϵ is a temporal weighting coefficient. Different finite difference schemes results depending upon the value of ϵ (=0: explicit scheme, =0.5: Crank-Nicholson scheme, =1.: fully implicit scheme). Equation (6.20) can be rewritten as:

$$[P_s]\{c\}^{j+1} = [T]\{c\}^j + \{R\} \tag{6.21}$$

where

$$[P_s] = \frac{1}{\Delta t}\left([Q^1]^{j+1} + [Q^2]^{j+\epsilon}\right) + \epsilon\,[S]^{j+1}$$
$$[T] = \frac{1}{\Delta t}\left([Q^1]^j + [Q^2]^{j+\epsilon}\right) - (1-\epsilon)[S]^j \tag{6.22}$$
$$\{R\} = \epsilon\,\{f\}^{j+1} + (1-\epsilon)\{f\}^j$$

Notice that we separated the retardation factor R into two parts, R^1 and R^2, leading to two matrices, $[Q^1]$ and $[Q^2]$, which are evaluated at different time levels. This approach was found to lead to much faster convergence when nonlinear adsorption isotherm is considered. Matrix $[Q^1]$ is evaluated at the previous and current time levels, while matrix $[Q^2]$ is evaluated using weighted averages of the current and previous nodal values of θ and R.

Higher-order approximations for the time derivative in the transport equation were derived by *van Genuchten* [1976, 1978]. The higher-order approximations may be incorporated into the transport equation by introducing time-dependent dispersion corrections as follows

$$D^- = D - \frac{q^2\Delta t}{6\theta^2(R^1+R^2)}$$
$$D^+ = D + \frac{q^2\Delta t}{6\theta^2(R^1+R^2)} \tag{6.23}$$

where the superscripts + and - indicate evaluation at the old and the new time levels, respectively.

Evaluation of all integrals eventually leads to the following tridiagonal global matrices $[P_s]$ and $[T]$

$$[P_s] = \begin{vmatrix} d_1 & e_1 & 0 & & & & 0 \\ b_2 & d_2 & e_2 & 0 & & & 0 \\ 0 & b_3 & d_3 & e_3 & 0 & & 0 \\ & . & & & & . & \\ & . & & & & . & \\ & . & & & & . & \\ 0 & & 0 & b_{n-2} & d_{n-2} & e_{n-2} & 0 \\ 0 & & & 0 & b_{n-1} & d_{n-1} & e_{n-1} \\ 0 & & & & 0 & b_n & d_n \end{vmatrix} \tag{6.24}$$

with the individual entries of $[P_s]$ given in Table 6.1. In this table $\Delta x_{i-1}=x_i-x_{i-1}$, $\Delta x_i=x_{i+1}-x_i$, $\Delta x=(x_{i+1}-x_{i-1})/2$, $\Delta t=t_{j+1}-t_j$, i is the nodal index (increasing in the direction of the x-coordinate, $i=1,2,....,n$), and j is the time index. Individual entries of the vector $\{R\}$ have the following form

$$\begin{aligned} r_1 &= \Delta x_{i-1}(2s_1 + s_2) + \epsilon\, q_s(0,t^{j+1}) + (1-\epsilon) q_s(0,t^j) \\ r_i &= \Delta x_{i-1}(s_{i-1} + 2s_i) + \Delta x_i(2s_i + s_{i+1}) \\ r_n &= \Delta x_i(s_{n-1} + 2s_n) - \epsilon\, q_s(L,t^{j+1}) - (1-\epsilon) q_s(L,t^j) \\ s_i &= \frac{1}{6}[\epsilon\, G_i^{j+1} + (1-\epsilon) G_i^j] \end{aligned} \tag{6.25}$$

From equation (6.22) it follows that matrixes $[P_s]$ and $[T]$ are identical if the variables D^-, F, q and ϵ in $[P_s]$ are replaced by $-D^+$, $-F$, $-q$ and $(1-\epsilon)$ to yield $[T]$.

Table 6.1. Values of the diagonal entries d_i, and off-diagonal entries b_i and e_i of matrix $[P_s]$ for linear finite elements.

$$d_1 = \frac{\Delta x_1}{12\Delta t}(3\theta_1 R_1 + \theta_2 R_2) + \frac{\epsilon}{2\Delta x_1}(E_1 + E_2) + \frac{\epsilon}{6}(2B_1 + B_2) + \frac{\epsilon\,\Delta x_1}{12}(3F_1 + F_2) \tag{6.26}$$

$$b_i = \frac{\Delta x_{i-1}}{12\Delta t}(\theta_{i-1} R_{i-1} + \theta_i R_i) - \frac{\epsilon}{2\Delta x_{i-1}}(E_{i-1} + E_i) - \frac{\epsilon}{6}(2B_{i-1} + B_i) + \frac{\epsilon\,\Delta x_{i-1}}{12}(F_{i-1} + F_i) \tag{6.27}$$

$$\begin{aligned} d_i = {} & \frac{\Delta x_{i-1}}{12\Delta t}(\theta_{i-1} R_{i-1} + 3\theta_i R_i) + \frac{\Delta x_i}{12\Delta t}(3\theta_i R_i + \theta_{i+1} R_{i+1}) + \frac{\epsilon}{2\Delta x_{i-1}}(E_{i-1} + E_i) + \frac{\epsilon}{2\Delta x_i}(E_i + E_{i+1}) + \\ & \frac{\epsilon}{6}(B_{i+1} - B_{i-1}) + \frac{\epsilon\,\Delta x_{i-1}}{12}(F_{i-1} + 3F_i) + \frac{\epsilon\,\Delta x_i}{12}(3F_i + F_{i+1}) \qquad (i = 2,\ldots,n-1) \end{aligned} \tag{6.28}$$

$$e_i = \frac{\Delta x_i}{12\Delta t}(\theta_i R_i + \theta_{i+1} R_{i+1}) - \frac{\epsilon}{2\Delta x_i}(E_i + E_{i+1}) + \frac{\epsilon}{6}(2B_{i+1} + B_i) + \frac{\epsilon\,\Delta x_i}{12}(F_i + F_{i+1}) \tag{6.29}$$

$$d_N = \frac{\Delta x_{N-1}}{12\Delta t}(\theta_{N-1} R_{N-1} + 3\theta_N R_N) + \frac{\epsilon}{2\Delta x_{N-1}}(E_{N-1} + E_N) - \frac{\epsilon}{6}(B_{N-1} + 2B_N) + \frac{\epsilon\,\Delta x_{N-1}}{12}(F_{N-1} + 3F_N) \tag{6.30}$$

Table 6.2. Values of the diagonal entries d_i, and off-diagonal entries b_i and e_i of matrix $[P_s]$ for linear finite elements with upstream weighting.

$$d_1 = \frac{\Delta x_1}{12\Delta t}(3\theta_1 R_1 + \theta_2 R_2) + \frac{\epsilon}{2\Delta x_1}(E_1 + E_2) + \frac{\epsilon}{6}[(2+3\alpha^+)B_1 + B_2] + \frac{\epsilon\,\Delta x_1}{12}(3F_1 + F_2) \tag{6.31}$$

$$b_i = \frac{\Delta x_{i-1}}{12\Delta t}(\theta_{i-1} R_{i-1} + \theta_i R_i) - \frac{\epsilon}{2\Delta x_{i-1}}(E_{i-1} + E_i) - \frac{\epsilon}{6}[(2+3\alpha^-)B_{i-1} + B_i] + \frac{\epsilon\,\Delta x_{i-1}}{12}(F_{i-1} + F_i) \tag{6.32}$$

$$\begin{aligned} d_i = {} & \frac{\Delta x_{i-1}}{12\Delta t}(\theta_{i-1} R_{i-1} + 3\theta_i R_i) + \frac{\Delta x_i}{12\Delta t}(3\theta_i R_i + \theta_{i+1} R_{i+1}) + \frac{\epsilon}{2\Delta x_{i-1}}(E_{i-1} + E_i) + \frac{\epsilon}{2\Delta x_i}(E_i + E_{i+1}) + \\ & \frac{\epsilon}{6}[B_{i+1} + 3B_i(\alpha^+ + \alpha^-) - B_{i-1}] + \frac{\epsilon\,\Delta x_{i-1}}{12}(F_{i-1} + 3F_i) + \frac{\epsilon\,\Delta x_i}{12}(3F_i + F_{i+1}) \qquad (i = 2,\ldots,n-1) \end{aligned} \tag{6.33}$$

$$e_i = \frac{\Delta x_i}{12\Delta t}(\theta_i R_i + \theta_{i+1} R_{i+1}) - \frac{\epsilon}{2\Delta x_i}(E_i + E_{i+1}) + \frac{\epsilon}{6}[(2-3\alpha^+)B_{i+1} + B_i] + \frac{\epsilon\,\Delta x_i}{12}(F_i + F_{i+1}) \tag{6.34}$$

$$d_N = \frac{\Delta x_{N-1}}{12\Delta t}(\theta_{N-1} R_{N-1} + 3\theta_N R_N) + \frac{\epsilon}{2\Delta x_{N-1}}(E_{N-1} + E_N) - \frac{\epsilon}{6}[B_{N-1} + (2-\alpha^-)B_N] + \frac{\epsilon\,\Delta x_{N-1}}{12}(F_{N-1} + 3F_N) \tag{6.35}$$

6.3. *Numerical Solution for Linear Nonequilibrium Solute Transport*

The same solution procedure as described in Sections 6.1 and 6.2 is used here for either linear equilibrium or nonlinear (both equilibrium and nonequilibrium) solute transport. However, linear nonequilibrium transport is implemented somewhat differently. First, equation (3.8), simplified for linear adsorption, is discretized using finite differences as follows

$$\frac{s^{t+\Delta t} - s^{t}}{\Delta t} = \epsilon\,[\,\omega\,(1-f)k_s c - \omega s^{k} - \mu_s s^{k} + (1-f)\gamma]^{t+\Delta t} + (1-\epsilon)[\omega\,(1-f)k_s c - \omega s^{k} - \mu_s s^{k} + (1-f)\gamma]^{t} \tag{6.36}$$

The new adsorbed concentration for type-2 sorption sites follows directly from (6.36):

$$s^{t+\Delta t} = s^{t}\frac{2 - \Delta t(\omega + \mu_s)^{t}}{2 + \Delta t(\omega + \mu_s)^{t+\Delta t}} + \frac{\Delta t(1-f)[(\omega k_s c)^{t+\Delta t} + (\omega k_s c)^{t} + \gamma^{t+\Delta t} + \gamma^{t}]}{2 + \Delta t(\omega + \mu_s)^{t+\Delta t}} \tag{6.37}$$

This term is incorporated directly into F and G so that they have the following values:

$$F_*^{t} = F^{t} - \{\rho\omega(1-f)k_s\}^{t}$$

$$F_*^{t+\Delta t} = F^{t+\Delta t} - \left\{\rho\omega(1-f)k_s + \frac{\rho\omega\Delta t(1-f)\omega k_s}{2 + \Delta t(\omega + \mu_s)}\right\}^{t+\Delta t} \tag{6.38}$$

$$G_*^{t} = G^{t'} + (\rho\omega s^{k})^{t}$$

$$G_*^{t+\Delta t} = G^{\{t+\Delta t\}'} + \rho\omega^{t+\Delta t}\{s^{t}\frac{2 - \Delta t(\omega + \mu_s)^{t}}{2 + \Delta t(\omega + \mu_s)^{t+\Delta t}} + \frac{\Delta t(1-f)[(\omega k_s c)^{t} + \gamma^{t+\Delta t} + \gamma^{t}]}{2 + \Delta t(\omega + \mu_s)^{t+\Delta t}}\} \tag{6.39}$$

where F_*^t, $F_*^{t+\Delta t}$, G_*^t, and $G_*^{t+\Delta t}$ are the values of parameters F and G for linear nonequilibrium solute transport, and G^t', and $G^{t+\Delta t}$' are the original values of G without the term containing ω. The above procedure avoids having to solve two simultaneous equations for linear nonequilibrium transport. Once the transport equation with the modified F and G parameters is solved using the methods discussed earlier to yield the concentration $c^{t+\Delta t}$, equation (6.37) is used to update the adsorbed concentration $s^{t+\Delta t}$.

6.4. *Numerical Solution Strategy*

6.4.1. *Solution Process*

The solution process at each time step proceeds as follows. First, an iterative procedure is used to obtain the solution of the Richards' equation (2.1) (see Section 5.4.1). After achieving convergence, the solution of the transport equation (6.7) is implemented. This is done by first determining the nodal values of the fluid flux from nodal values of the pressure head by applying Darcy's law. Nodal values of the water content and the fluid flux at the previous time level are already known from the solution at the previous time step. Values for the water content and the fluid flux are subsequently used as input to the transport equations (first for heat transport and then for solute transport), leading to a system of linear algebraic equations given by (6.7). The structure of the final set of equations depends upon the value of the temporal weighing factor, ϵ. The explicit (ϵ=0) and fully implicit (ϵ=1) schemes for the transport equation require that the global matrices $[P_s]$ and $[T]$ and the vector $\{R\}$ be evaluated at only one time level (the previous or current time level). All other schemes require evaluation at both time levels. Also, all schemes except for the explicit formulation (ϵ=0) lead to an asymmetric banded matrix $[P_s]$.

Since the heat transport equation is linear, there is no need for an iterative solution process for heat flow. The same is true for the transport of solutes undergoing only linear sorption reactions. On the other hand, iteration is needed when a nonlinear reaction between the solid and liquid phase is considered. The iterative procedure for solute transport is very similar to that for water flow. The nonlinear coefficients in (6.7) are then re-evaluated at each iteration, and the new equations solved using results of the previous iteration. The iterative process continues until

a satisfactory degree of convergence is obtained, i.e., until at all nodes the absolute change in concentration between two successive iterations becomes less than some small value determined by the imposed relative and absolute concentration tolerances.

6.4.2. *Upstream Weighted Formulation*

Upstream weighing is provided as an option in the HYDRUS to minimize some of the problems with numerical oscillations when relatively steep concentration fronts are being simulated. For this purpose the fourth (flux) term of equation (6.4) is not weighted using regular linear basis functions ϕ_n, but instead with the nonlinear functions ϕ_n^u

$$\begin{aligned} \phi_1^u &= \phi_1 - 3\alpha^w \phi_1 \phi_2 \\ \phi_2^u &= \phi_2 + 3\alpha^w \phi_1 \phi_2 \end{aligned} \tag{6.40}$$

where α_i^w is a weighing factor associated with the length of the element size. The weighing factors are evaluated using the equation of *Christie et al.* [1976]:

$$\alpha^w = \coth\left(\frac{uL}{2D}\right) - \frac{2D}{uL} \tag{6.41}$$

where u, D and L are the flow velocity, dispersion coefficient and length associated with side i. The weighing functions ϕ^u ensure that relatively more weight is placed on the flow velocities of nodes located at the upstream side of an element. Evaluating the integrals in (6.17) shows that the following terms must replace the entries of the global matrix S_{nm}:

$$S_{nm}{}^e{}_2 = \int_1^2 B \frac{d\varphi_n}{dx} \phi_m dx = \frac{1}{6} \begin{vmatrix} B_1(2+3\alpha^w) + B_2 & B_1 + B_2(2-3\alpha^w) \\ -B_1(2+3\alpha^w) - B_2 & -B_1 - B_2(2-3\alpha^w) \end{vmatrix} \tag{6.42}$$

The coefficients of matrix $[P_s]$ (6.24) for upstream weighting formulation are given in Table 6.2.

6.4.3. *Mass Balance Calculations*

The total amount of mass in the entire flow domain, or in a preselected subregion, is given by

$$M = \sum_e \int_e (\theta c + a_v g + \rho s)\, dx = \sum_e \int_e [(\theta + a_v k_g + \rho f \frac{k_s c^{\beta-1}}{1 + \eta c^{\beta}})c + \rho s^k]\, dx \quad (6.43)$$

where summation is taken over all elements within the specified region.

The cumulative amounts M^0 and M^1 of solute removed from the flow region by zero- and first-order reactions, respectively, are calculated as follows

$$M_1^0 = -\int_0^t \sum_e \int_e (\gamma_{w,1}\theta + \gamma_{s,1}\rho + \gamma_{g,1}a_v)\, dx\, dt$$

$$M_k^0 = -\int_0^t \sum_e \int_e [(\mu'_{w,k-1}\theta + \mu'_{s,k-1}\rho f \frac{k_{s,k-1} c_{k-1}^{\beta_{k-1}-1}}{1 + \eta_{k-1} c_{k-1}^{\beta_{k-1}}} + \mu'_{g,k-1} a_v k_{g,k-1})c_{k-1} + \quad (6.44)$$

$$+ \mu'_{s,k-1}\rho s_{k-1}^k + \gamma_{w,k}\theta + \gamma_{s,k}\rho + \gamma_{g,k}a_v]\, dx\, dt \qquad k\varepsilon(2, n_s)$$

$$M^1 = \int_0^t \sum_e \int_e \{[(\mu_w + \mu'_w)\theta + (\mu_s + \mu'_s)\rho f \frac{k_s c^{\beta-1}}{1 + \eta c^{\beta}} + (\mu_g + \mu'_g)a_v k_g]c + \quad (6.45)$$

$$+ (\mu_s + \mu'_s)\rho s^k\}\, dx\, dt$$

whereas the cumulative amount, M_r, of solute taken up by plant roots is given by

$$M_r = \int_0^t \sum_{e_R} \int_e S c_r\, dx\, dt \quad (6.46)$$

where e_R represents the elements making up the root zone.

Finally, when all boundary material fluxes, decay reactions, and root uptake mass fluxes have been computed, the following mass balance should hold for the flow domain as a whole:

$$M_t - M_0 = + \int_0^t q_{s0}\,dt - \int_0^t q_{sL}\,dt - M^0 - M^1 - M_r \tag{6.47}$$

where M_t and M_0 are the amounts of solute in the flow region at times t and zero, respectively, as calculated with (6.43). The difference between the left- and right-hand sides of (6.47) represents the absolute error, ϵ_a^c, in the solute mass balance. Similarly as for water flow, the accuracy of the numerical solution for solute transport is evaluated by using the relative error, ϵ_r^c [%], in the solute mass balance as follows

$$\epsilon_r^c = \frac{100\,|\,\epsilon_a^c\,|}{\max\left[\sum_e |M_t^e - M_0^e|,\quad |M^0| + |M^1| + |M_r| + \int_0^t (|q_{s0}| + |q_{sL}|)\,dt\right]} \tag{6.48}$$

where M_0^e and M_t^e are the amounts of solute in element e at times 0 and t, respectively. Note again that HYDRUS does not relate the absolute error to the total amount of mass in the flow region. Instead, the program uses as a reference the maximum value of (1) the absolute change in element concentrations as summed over all elements, and (2) the sum of the absolute values of all cumulative solute fluxes across the flow boundaries including those resulting from sources and sinks in the flow domain.

The total amount of heat energy in the entire flow domain, or in a preselected subregion, is given by

$$W = \sum_e \int_e (C_n\theta_n + C_o\theta_o + C_w\theta + C_g a_v)\,T^A\,dx \tag{6.49}$$

where T^A is the absolute temperature [K]. The summation is again taken over all elements within the specified region.

6.4.4. *Oscillatory Behavior*

Numerical solutions of the transport equation often exhibit oscillatory behavior and/or excessive numerical dispersion near relatively sharp concentration fronts. These problems can

be especially serious for convection-dominated transport characterized by small dispersivities. One way to partially circumvent numerical oscillations is to use upstream weighing as discussed in Section 6.4.2. Undesired oscillations can often be prevented also by selecting an appropriate combination of space and time discretizations. Two dimensionless numbers may be used to characterize the space and time discretizations. One of these is the grid Peclet number, Pe^e, which defines the predominant type of the solute transport (notably the ratio of the convective and dispersive transport terms) in relation to coarseness of the finite element grid:

$$Pe^{\,e} = \frac{q\Delta x}{\theta D} \tag{6.50}$$

where Δx is the characteristic length of a finite element. The Peclet number increases when the convective part of the transport equation dominates the dispersive part, i.e., when a relatively steep concentration front is present. To achieve acceptable numerical results, the spatial discretization must be kept relatively fine to maintain a low Peclet number. Numerical oscillations can be virtually eliminated when the local Peclet numbers do not exceed about 5. However, acceptably small oscillations may be obtained with local Peclet numbers as high as 10 [*Huyakorn and Pinder*, 1983]. Undesired oscillations for higher Peclet numbers can be effectively eliminated by using upstream weighing (see Section 6.4.2).

A second dimensionless number which characterizes the relative extent of numerical oscillations is the Courant number, Cr^e. The Courant number is associated with the time discretization as follows

$$Cr^{\,e} = \frac{q\Delta t}{\theta R \Delta x} \tag{6.51}$$

Three stabilizing options are used in HYDRUS to avoid oscillations in the numerical solution of the solute transport equation [*Šimůnek and van Genuchten*, 1994]. One option is upstream weighing (see Section 6.4.2), which effectively eliminates undesired oscillations at relatively high Peclet numbers. A second option for minimizing or eliminating numerical oscillations uses the criterion developed by *Perrochet and Berod* [1993]

$$Pe \cdot Cr \leq \omega_s \quad (=2) \tag{6.52}$$

where ω_s is the performance index [-]. This criterion indicates that convection-dominated transport problems having large Pe numbers can be safely simulated provided Cr is reduced according to (6.52) [*Perrochet and Berod*, 1993]. When small oscillations in the solution can be tolerated, ω_s can be increased to about 5 or 10.

A third stabilization option implemented in HYDRUS also utilizes criterion (6.52). However, instead of decreasing Cr to satisfy equation (6.52), this option introduces artificial dispersion to decrease the Peclet number. The amount of additional longitudinal dispersion, $\bar{D}_L$ [L], is given by [*Perrochet and Berod*, 1993]

$$\bar{D}_L = \frac{|q|\Delta t}{R\theta\omega_s} - D_L - \frac{\theta D_w \tau}{|q|} \tag{6.53}$$

The maximum permitted time step is calculated for all three options, as well as with the additional requirement that the Courant number must remain less than or equal to 1. The time step calculated in this way is subsequently used as one of the time discretization rules (rule No. B) discussed in section 5.4.2.

7. PROBLEM DEFINITION

7.1. *Construction of Finite Element Mesh*

The finite element mesh is constructed by dividing the soil profile into linear elements whose sizes are defined by the x-coordinates of the nodes that form the element corners. Neighboring elements should have approximately the same size. The ratio of the sizes of two neighboring elements is not recommended to exceed about 1.5. The nodes are numbered sequentially from 1 to *NumNP* (total number of nodes) from the bottom of the soil profile to the soil surface.

The element dimensions must be adjusted to a particular problem. They should be made relatively small at locations where large hydraulic gradients are expected. Such a region is usually located close to the soil surface where highly variable meteorological factors can cause rapid changes in the soil water content and corresponding pressure heads. Therefore, it is usually recommended to use relatively small elements near the soil surface, and gradually larger sizes with depth. The element dimensions are also dependent on soil hydraulic properties. Coarse textured soils generally require a finer discretization than fine-textured soils (loams, clays). No special restrictions are necessary to facilitate the soil root zone.

7.2. *Coding of Soil Types and Subregions*

Soil Types - An integer code beginning with 1 and ending with *NMat* (the total number of soil materials) is assigned to each soil type in the flow region. The appropriate material code is subsequently assigned to each nodal point n of the finite element mesh.

Interior material interfaces do not coincide with element boundaries. When different material numbers are assigned to the nodes of a certain element, the finite element algorithm will assume that the material properties will change linearly over the element. This procedure will somewhat smooth soil interfaces. A set of soil hydraulic parameters, and solute and heat transport characteristics must be specified for each soil material.

Subregions - Water and solute mass balances are computed separately for each specified subregion. The subregions may or may not coincide with the material regions. Subregions are characterized by an integer code which runs from 1 to *NLay* (the total number of subregions). A subregion code is assigned to each element in the flow domain.

7.3. *Coding of Boundary Conditions*

Boundary codes *KodTop* and *KodBot* must be assigned to surface and bottom boundary nodes, respectively. If a boundary node is to have a prescribed pressure head during a time step (a Dirichlet boundary condition), *KodTop* and *KodBot* must be set positive during that time step. If the volumetric flux of water entering or leaving the system is prescribed during a certain time step (a Neumann boundary condition), *KodTop* and *KodBot* must be negative or zero.

Constant Boundary Conditions - The value of a constant boundary condition for a particular boundary node, n, is given by the initial value of the pressure head, $h(n)$, in case of Dirichlet boundary conditions, or by the initial value of the recharge/discharge flux, *rTop* or *rBot*, in case of Neumann boundary conditions. Table 7.1 summarizes the use of the variables *KodTop* (*KodBot*), *rTop* (*rBot*), and $h(n)$ for various types of nodes.

Table 7.1. Initial settings of *KodTop* (*KodBot*), *rTop* (*rBot*), and $h(n)$ for constant boundary conditions.

Node Type	*KodTop* (*KodBot*)	*rTop* (*rBot*)	$h(n)$
Specified Head Boundary	1	0.0	Prescribed
Specified Flux Boundary	-1	Prescribed	Initial Value

Variable Boundary Conditions - Three types of variable boundary conditions can be imposed:

1. Atmospheric boundary conditions for which *TopInf*=*AtmInf*=**.true.**,
2. Variable pressure head boundary conditions for which *TopInf*=**.true.** and *KodTop*=+3, or *BotInf*=**.true.** and *KodBot*=+3, or
3. Variable flux boundary conditions for which *TopInf*=**.true.** and *KodTop*=-3, or *BotInf*=**.true.** and *KodBot*=-3.

Initial settings of the variables *KodTop* (*KodBot*), *rTop* (*rBot*), and *h*(*n*) for the time-dependent boundary conditions are given in Table 7.2.

Table 7.2. Initial settings of *KodTop* (*KodBot*), *rTop* (*rBot*), and *h*(*n*) for time-variable boundary conditions.

Node Type	*KodTop* (*KodBot*)	*rTop* (*rBot*)	*h*(*n*)
Atmospheric Boundary	–4	0.0	Initial Value
Variable Head Boundary	+3	0.0	Initial Value
Variable Flux Boundary	–3	0.0	Initial Value

Atmospheric boundary conditions are implemented when *TopInf*=*AtmInf*=**.true.**, in which case time-dependent input data for the precipitation, *Prec*, and evaporation, *rSoil*, rates must be specified in the input file ATMOSPH.IN. The potential fluid flux across the soil surface is determined by *rAtm*=*rSoil*-*Prec*. The actual surface flux is calculated internally by the program. Two limiting values of surface pressure head must also be provided: *hCritS* which specifies the maximum allowed pressure head at the soil surface (usually 0.0), and *hCritA* which specifies the minimum allowed surface pressure head (defined from equilibrium conditions between soil water and atmospheric vapor). The program automatically switches the value of *KodTop* from -4 to +4 if one of these two limiting points is reached. Table 7.3 summarizes the use of the variables *rAtm*, *hCritS* and *hCritA* during program execution.

Table 7.3. Definition of the variables *KodTop*, *rTop*, and *h*(*n*) when an atmospheric boundary condition is applied.

KodTop	*rTop*	*h*(*n*)	Event
−4	*rAtm*	Unknown	*rAtm=rSoil-Prec*
+4	Unknown	*hCritA*	Evaporation capacity is exceeded
+4	Unknown	*hCritS*	Infiltration capacity is exceeded

Variable head or flux boundary conditions on the soil surface (bottom of the soil profile) are implemented when *KodTop* (*KodBot*)=+3 or -3 and *TopInf* (*BotInf*)=**.true.**, respectively. In that case, the input file ATMOSPH.IN must contain the prescribed time-dependent values of the pressure head, *hT* (*hB*), or the flux, *rT* (*rB*), imposed on the boundary. The values of *hT* (*hB*) or *rT* (*rB*) are assigned to particular nodes at specified times according to rules given in Table 7.4.

Table 7.4. Definition of the variables *KodTop* (*KodBot*), *rTop* (*rBot*), and *h*(*n*) when variable head or flux boundary conditions are applied.

Node Type	*KodTop* (*KodBot*)	*rTop* (*rBot*)	*h*(*n*)
Variable Head Boundary	+3	Unknown	*hT* (*hB*)
Variable Flux Boundary	−3	*rT* (*rB*)	Unknown

Water Uptake by Plant Roots - The program calculates the rate at which plants extract water from the root zone by evaluating equation (2.4). Values of the potential transpiration rate, *rRoot*, must be specified at preselected times in the input file ATMOSPH.IN. These time-dependent values must be provided by the user and can be calculated in various ways, such as from the temperature and crop coefficients. Actual transpiration rates are calculated internally by the program as discussed in Section 2.2. The root water uptake parameters are taken from

an input file, SELECTOR.IN. Values of the function *Beta*(n), which describes the potential water uptake distribution over the root zone, must be specified for each node in the flow domain. If the root growth model is considered, then the exponential function for the spatial distribution of the potential root water uptake is used (equation (2.12)). All parts of the flow region where *Beta*(n)>0 are treated as the soil root zone.

Root Growth Model - The program calculates the time variable rooting depth if the logical variable *lRoot* in input file SELECTOR.IN is equal to **.true.**. The classical Verhulst-Pearl logistic function (2.17) (see Section 2.2) is used to model the rooting depth. The exponential (2.12) spatial distribution function for the root water uptake function is always used along with the time-variable rooting depth option. The root growth factor, r, can be calculated either from the known value of root depth (*xRMed*) at a specified time (*tRMed*), or from the assumption that 50% of the rooting depth is reached after 50% of the growing season.

Deep Drainage from the Soil Profile - Vertical drainage, $q(h)$, across the lower boundary of the soil profile is sometimes approximated by a flux which depends on the position of the groundwater level [e.g., *Hopmans and Stricker*, 1989]. If available, such a relationship can be implemented in the form of a variable flux boundary condition; the code in that case internally sets the variable *KodBot* equal to -7. This boundary condition will be implemented in HYDRUS if the logical variable *qGWLF* in the input file SELECTOR.IN is set equal to **.true.**. The discharge rate $q(n)$ assigned to bottom node n is determined by the program as $q(n)=q(h)$, where h is the local value of the pressure head, and $q(h)$ is given by

$$q(h) = -A_{qh}\exp(B_{qh}\,|h - GWL0L|) \tag{7.1}$$

where A_{qh} and B_{qh} are empirical parameters which must be specified in input file SELECTOR.IN, together with *GWL0L* which represents the reference position of the groundwater level (sometimes set equal to the x-coordinate of the soil surface).

Free Drainage - Unit vertical hydraulic gradient boundary conditions can be implemented

in the form of a variable flux boundary condition. The program in that case will internally set the variable *KodBot* equal to -5. This boundary condition is implemented in HYDRUS by setting the logical variable *FreeD* in the input file SELECTOR.IN equal to **.true.**. The discharge rate $q(n)$ assigned to bottom node n is determined by the program as $q(n)=-K(h)$, where h is the local value of the pressure head, and $K(h)$ is the hydraulic conductivity corresponding to this pressure head.

Seepage Faces - The initial settings of the variables *KodBot*, *rBot* and $h(n)$ for node on a seepage face are summarized in Table 7.5. This boundary condition is implemented in HYDRUS by setting the logical variable *SeepF* in the input file SELECTOR.IN equal to **.true.**.

Table 7.5. Initial setting of *KodBot*, *rBot*, and $h(n)$ for seepage faces.

Node Type	*KodBot*	*rBot*	$h(n)$
Seepage Face (initially saturated)	+2	0.0	0.0
Seepage Face (initially unsaturated)	–2	0.0	Initial Value

Heat Transport Boundary Conditions - The type of applied boundary condition is specified by the input variables *kTopT* and *kBotT* for the upper and lower boundaries, respectively. Positive values for these variables means that a first-type boundary condition is used. When *kTopT* or *kBotT* is negative, then a third-type boundary condition is applied. On the other hand, when *kBotT* is equal to zero, a Neumann boundary condition with zero gradient is implemented. All initial and boundary conditions must be specified in °C.

Solute Transport Boundary Conditions - The type of applied boundary condition is specified by the input variables *kTopCh* and *kBotCh* for the upper and lower solute transport boundaries, respectively. Similarly as for heat transport, positive values for these variables means

that a first-type boundary condition will be assumed. When *kTopCh* or *kBotCh* is negative, then a third-type boundary condition is applied. When *kBotCh* is equal to zero, a Neumann boundary condition with zero gradient is used.

7.4. *Program Memory Requirements*

One single parameter statement is used at the beginning of the code to define the problem dimensions. All major arrays in the program are adjusted automatically according to these dimensions. This feature makes it possible to change the dimensions of the problem to be simulated without having to recompile all program subroutines. Different problems can be investigated by changing the dimensions in the parameter statement at the beginning of the main program, and subsequently linking all previously compiled subroutines with the main program when creating an executable file. Table 7.6 lists the array dimensions which must be defined in the parameter statement.

Table 7.6. List of the array dimensions.

Dimension	Current setting	Description
NumNPD	501	Maximum number of nodes in finite element mesh
NMatD	20	Maximum number of materials
NTabD	100	Maximum number of items in the table of hydraulic properties generated by the program for each soil material
NObsD	5	Maximum number of observation nodes

8. EXAMPLE PROBLEMS

Five example problems are presented in this section. The first two examples are identical to those described in the SWMS_2D manual [*Šimůnek et al.*, 1992]. Three other examples are identical to those discussed in the CHAIN_2D manual [*Šimůnek et al.*, 1994]. These three examples were included mainly for mathematical verification purposes, and for demonstrating new features of HYDRUS, i.e., non-equilibrium and nonlinear adsorption, and sequential first-order decay reactions.

Examples 1 and 2 provide comparisons of the water flow part of HYDRUS code with results from both the UNSAT2 code of *Neuman* [1972] and the SWATRE code of *Belmans et al.* [1983]. The results obtained with the HYDRUS code for these two examples were identical to those obtained with SWMS_2D. Example 3 serves to verify the accuracy of HYDRUS by comparing numerical results for a problem with three solutes involved in a sequential first-order decay reaction against results obtained with an analytical solution during one-dimensional steady-state water flow [*van Genuchten*, 1985]. Example 4 considers one-dimensional transport of a solute undergoing nonlinear cation adsorption. Numerical results are compared with experimental data and previous numerical solutions obtained with the MONOC code of *Selim et al.* [1987] and the previous version of HYDRUS code (version 5.0) of *Vogel et al.* [1996]. Example 5 serves to test the performance of HYDRUS for nonequilibrium adsorption by comparing numerical results against experimental data and previous numerical predictions during one-dimensional steady-state water flow [*van Genuchten*, 1981].

8.1. *Example 1 - Column Infiltration Test*

This example simulates a one-dimensional laboratory infiltration experiment initially discussed by *Skaggs et al.* [1970], and later used by *Davis and Neuman* [1983] as a test problem for the UNSAT2 code. Hence, the example provides a means of comparing results obtained with the HYDRUS and UNSAT2 codes.

The soil water retention and relative hydraulic conductivity functions of the sandy soil are presented in Figure 8.1. The sand was assumed to be at an initial pressure head of -150 cm. The soil was assumed to be homogenous and isotropic with a saturated hydraulic conductivity of 0.0433 cm/min. The column was subjected to ponded infiltration (a Dirichlet boundary condition) at the soil surface, resulting in one-dimensional vertical water flow. The open bottom boundary of the soil column was simulated by implementing a no-flow boundary condition during unsaturated flow ($h<0$), and a seepage face with $h=0$ when the bottom of the column becomes saturated (this last condition was not reached during the simulation).

The simulation was carried out for 90 min, which corresponds to the total time duration of the experiment. Figure 8.2 shows the calculated instantaneous (q_0) and cumulative (I_0) infiltration rates simulated with HYDRUS. The calculated results agree closely with those obtained by *Davis and Neuman* [1983] using their UNSAT2 code.

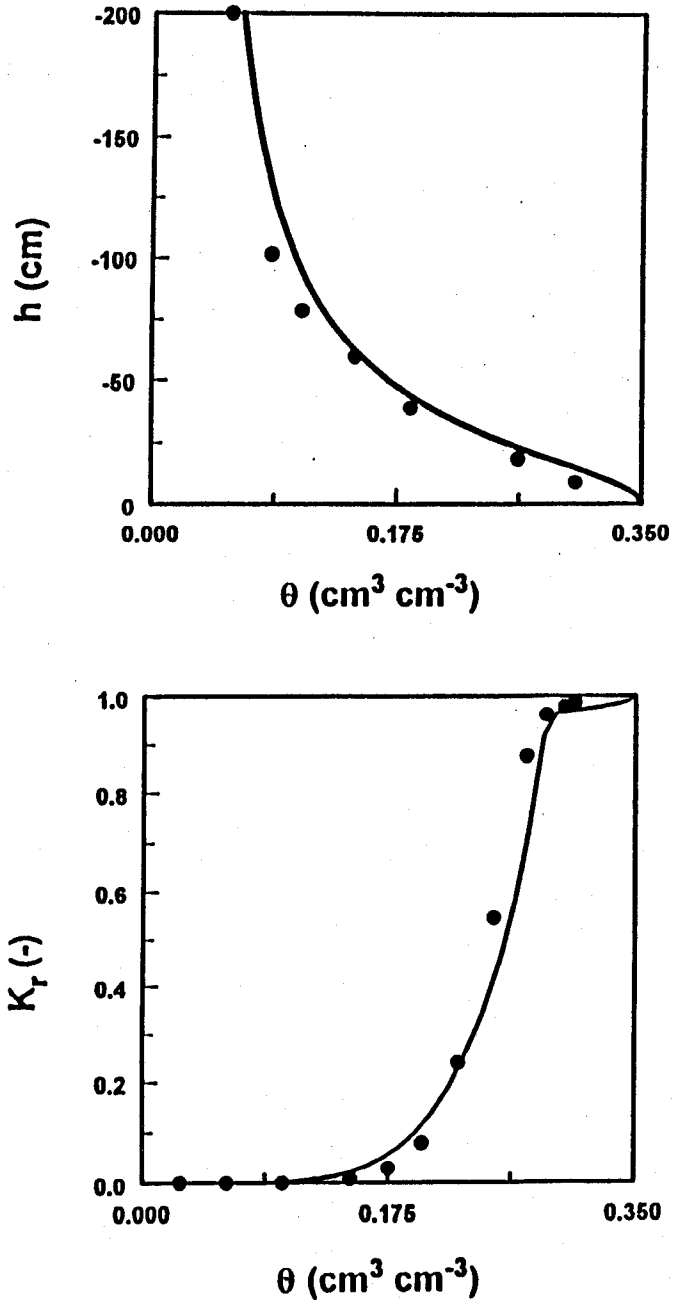

Fig. 8.1. Soil water retention and relative hydraulic conductivity functions for example 1. The solid circles are UNSAT2 input data [*Davis and Neuman*, 1983].

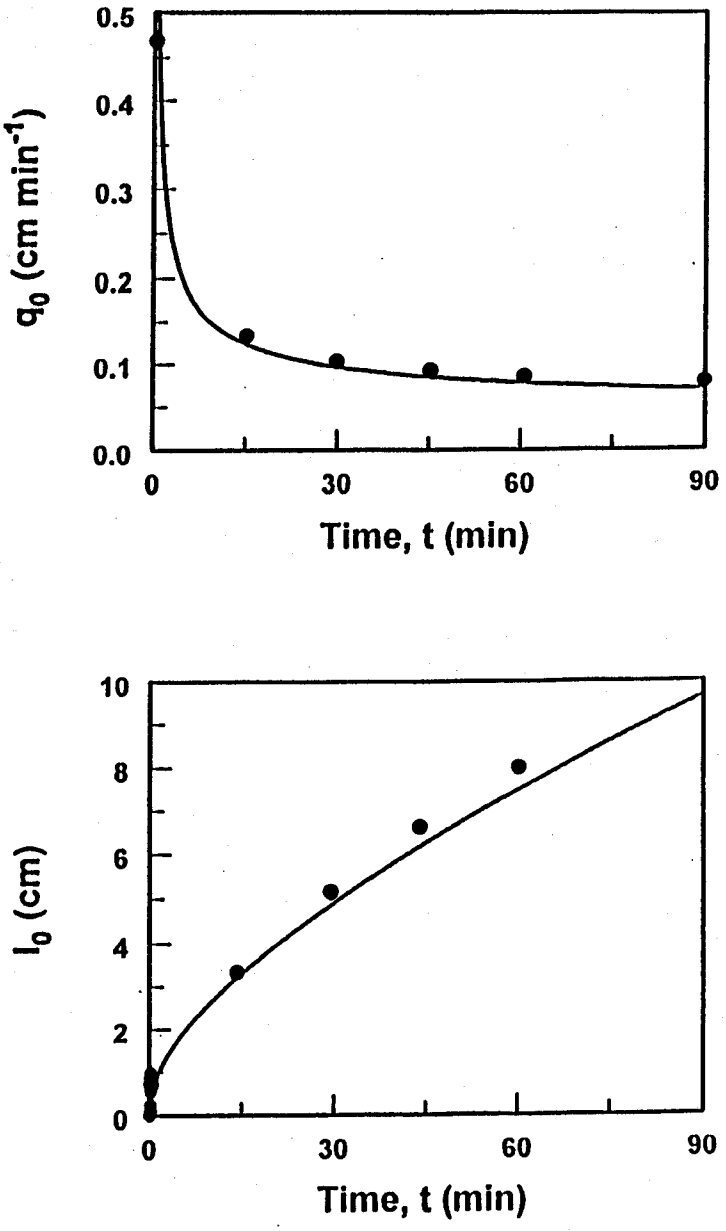

Fig. 8.2. Instantaneous, q_0, and cumulative, I_0, infiltration rates simulated with the HYDRUS (solid lines) and UNSAT2 (solid circles) computer codes (example 1).

8.2. *Example 2 - Water Flow in a Field Soil Profile Under Grass*

This example considers one-dimensional water flow in a field profile of the Hupselse Beek watershed in the Netherlands. Atmospheric data and observed ground water levels provided the required boundary conditions for the numerical model. Calculations were performed for the period of April 1 to September 30 of the relatively dry year 1982. Simulation results obtained with HYDRUS will be compared with those generated with the SWATRE computer program [*Feddes et al.*, 1978, *Belmans et al.*, 1983].

The soil profile consisted of two layers: a 40-cm thick A-horizon, and a B/C-horizon which extended to a depth of about 300 cm. The depth of the root zone was 30 cm. The mean scaled hydraulic functions of the two soil layers in the Hupselse Beek area [*Císlerová,* 1987; *Hopmans and Stricker*, 1989] are presented in Figure 8.3.

The soil surface boundary condition involved actual precipitation and potential transpiration rates for a grass cover. The surface fluxes were incorporated by using average daily rates distributed uniformly over each day. The bottom boundary condition consisted of a prescribed drainage flux - groundwater level relationship, $q(h)$, as given by equation (7.1). The groundwater level was initially set at 55 cm below the soil surface. The initial moisture profile was taken to be in equilibrium with the initial ground water level.

Figure 8.4 presents input values of the precipitation and potential transpiration rates. Calculated cumulative transpiration and cumulative drainage amounts as obtained with the HYDRUS and SWATRE codes are shown in Figure 8.5. The pressure head at the soil surface and the arithmetic mean pressure head of the root zone during the simulated season are presented in Figure 8.6. Finally, Figure 8.7 shows variations in the calculated groundwater level with time.

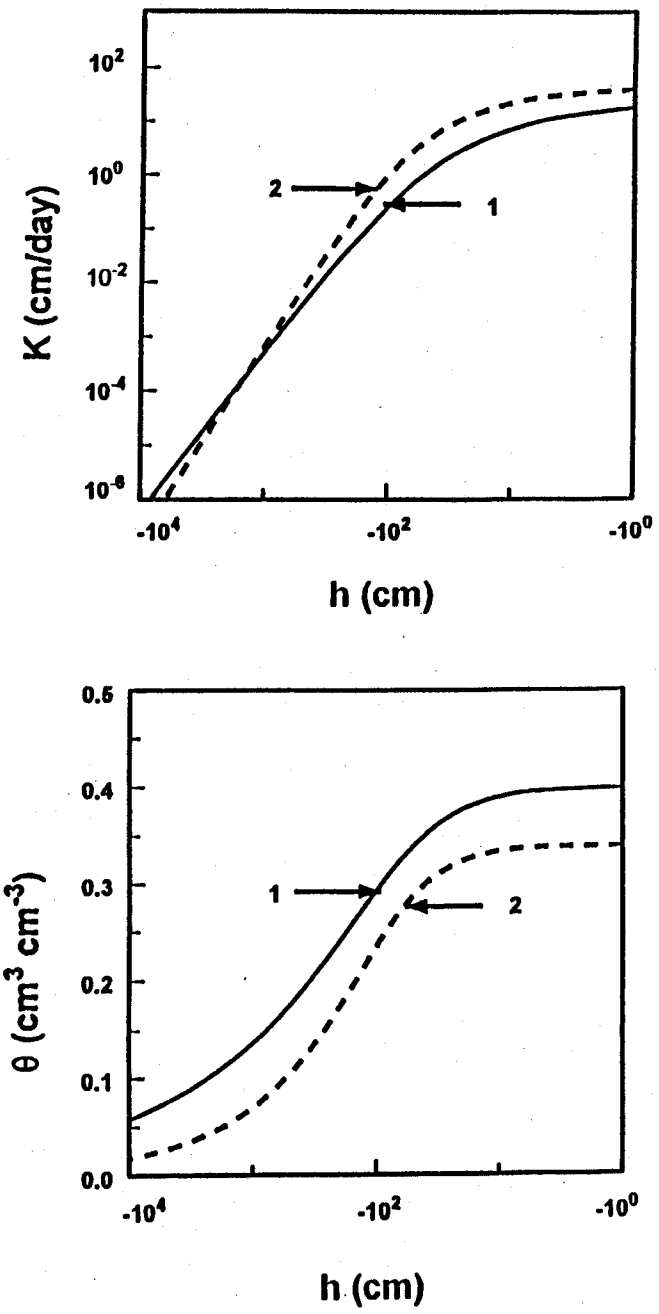

Fig. 8.3. Unsaturated hydraulic properties of the first and second soil layers (example 2).

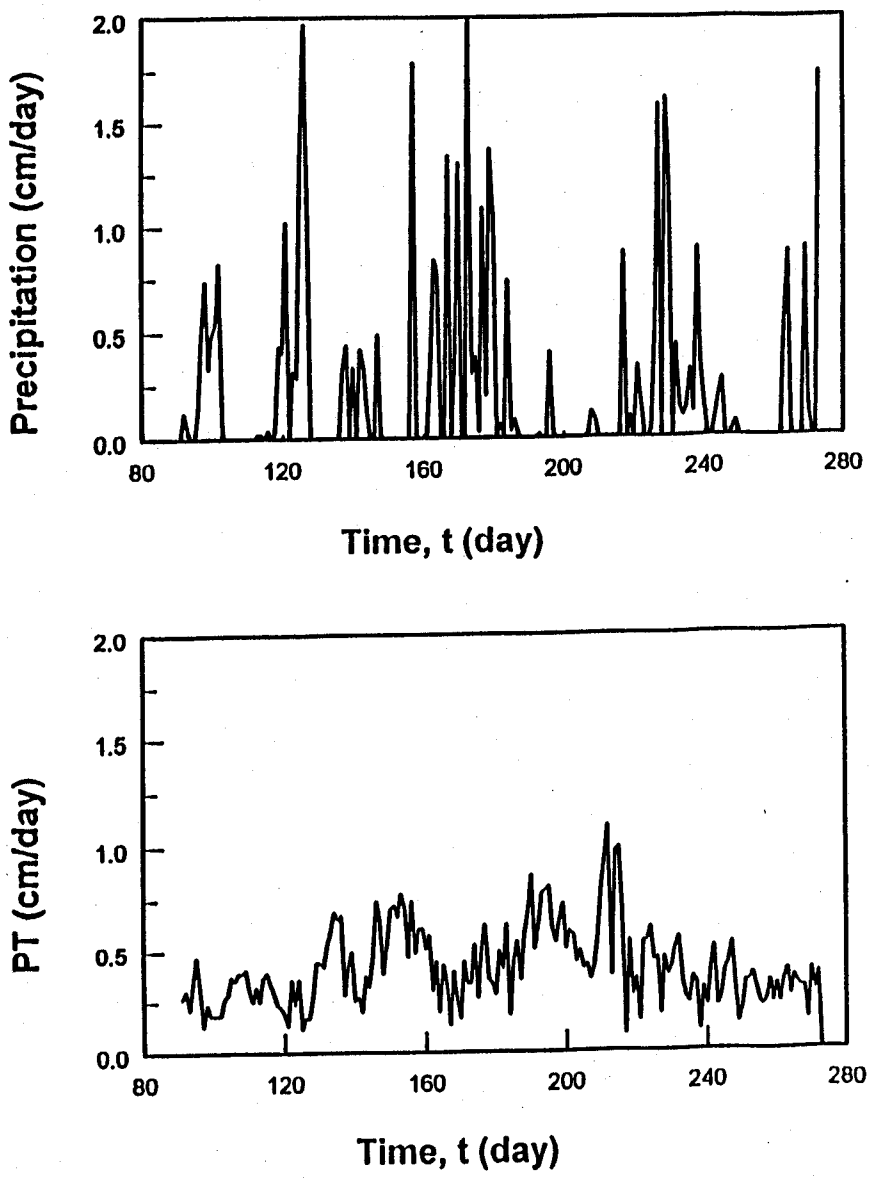

Fig. 8.4. Precipitation and potential transpiration rates (example 2).

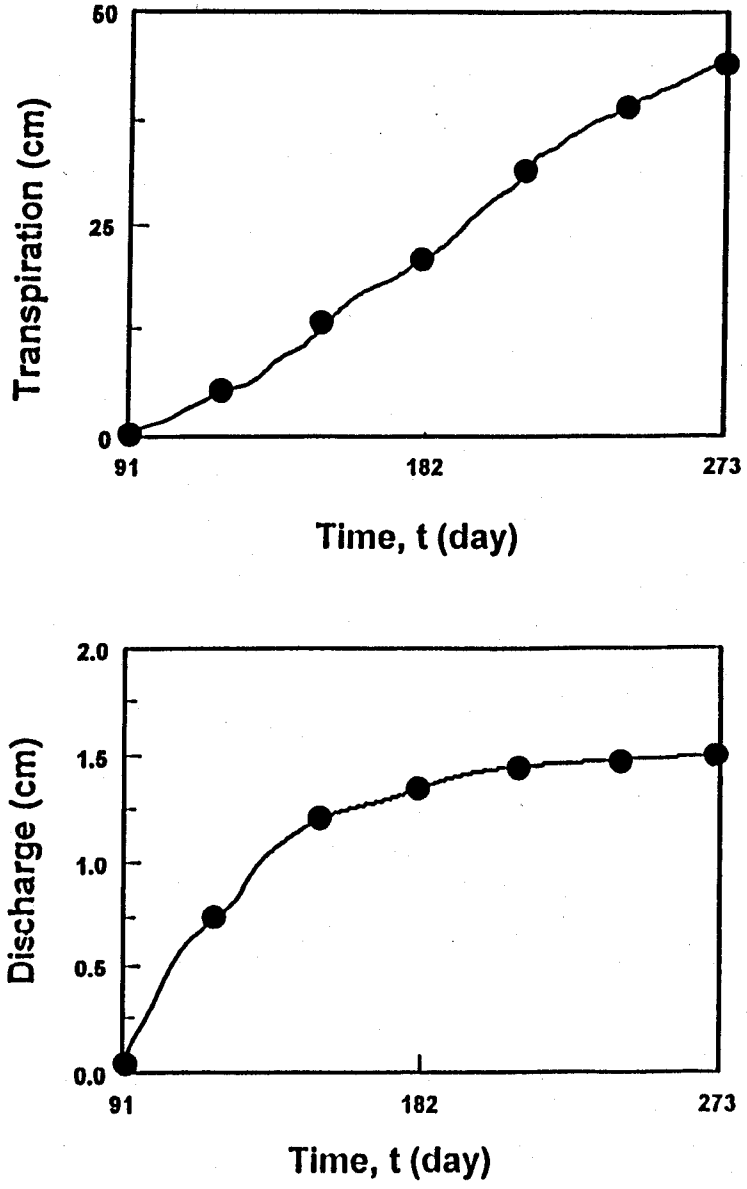

Fig. 8.5. Cumulative values for the actual transpiration and bottom leaching rates as simulated with the HYDRUS (solid line) and SWATRE (solid circles) computer codes (example 2).

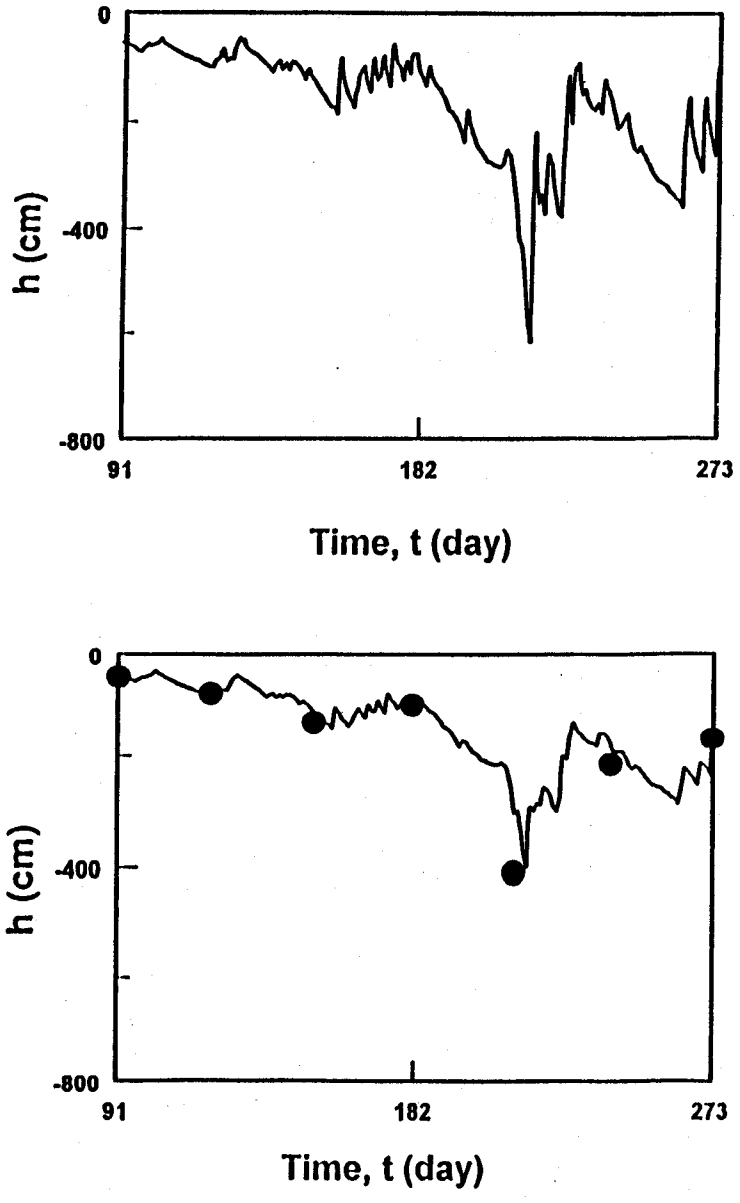

Fig. 8.6. Pressure head at the soil surface and mean pressure head of the root zone as simulated with the HYDRUS (solid lines) and SWATRE (solid circles) computer codes (example 2).

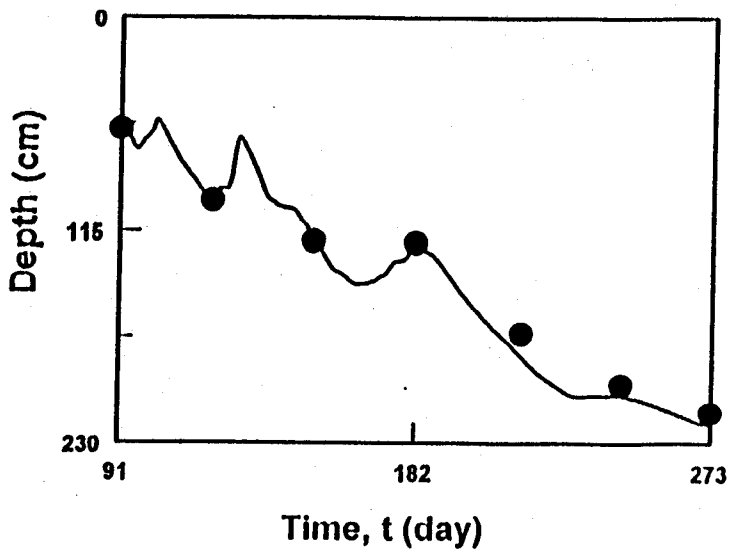

Fig. 8.7. Location of the groundwater table versus time as simulated with the HYDRUS (solid line) and SWATRE (solid circles) computer codes (example 2).

8.3. *Example 3 - Solute Transport with Nitrification Chain*

This example was used to verify in part the mathematical accuracy of the solute transport part of HYDRUS. Numerical results will be compared with results generated with an analytical solution published by *van Genuchten* [1985] for one-dimensional convective-dispersive transport of solutes involved in sequential first-order decay reactions. The analytical solution holds for solute transport in a homogeneous, isotropic porous medium during steady-state unidirectional groundwater flow. Solute transport equations (3.1) and (3.2) for this situation reduce to

$$R_1 \frac{\partial c_1}{\partial t} = D \frac{\partial^2 c_1}{\partial x^2} - v \frac{\partial c_1}{\partial x} - \mu_1 R_1 c_1 \tag{8.1}$$

$$R_i \frac{\partial c_i}{\partial t} = D \frac{\partial^2 c_i}{\partial x^2} - v \frac{\partial c_i}{\partial x} + \mu_{i-1} R_{i-1} c_{i-1} - \mu_i R_i c_i \qquad i = 2,3 \tag{8.2}$$

where μ is a first-order degradation constant, D is the dispersion coefficient, v is the average pore water velocity (q/θ) in the flow direction, x is the spatial coordinate in the direction of flow, and where it is assumed that 3 solutes participate in the decay chain. The specific example used here applies to the three-species nitrification chain

$$NH_4^+ \rightarrow NO_2^- \rightarrow NO_3^- \tag{8.3}$$

and is the same as described by *van Genuchten* [1985], and earlier by *Cho* [1971]. The boundary conditions may be written as:

$$\begin{aligned} \left[-D \frac{\partial c_1}{\partial x} + v c_1 \right] &= v c_{0,1}(0,t) \\ \left[-D \frac{\partial c_i}{\partial x} + v c_i \right] &= 0 \qquad i = 2,3 \\ \lim_{x \to \infty} \frac{\partial c_i}{\partial x} &= 0 \qquad i = 1,2,3 \end{aligned} \tag{8.4}$$

The experiment involves the application of a NH_4^+ solution to an initially solute-free medium ($c_i = 0$). The input transport parameters for the simulation are listed in Table 8.2.

Figure 8.8 shows concentration profiles for all three solutes at time 200 hours, calculated both numerically with HYDRUS and analytically with the CHAIN code of *van Genuchten* [1985]. Figure 8.9 shows the concentration profiles at three different times (50, 100, and 200 hours) for NH_4^+, NO_2^-, and NO_3^-, respectively. The numerical results in each case duplicated the analytical results.

Table 8.1. Input parameters for example 3.

Parameter	Value
v [cm/hour]	1.0
D [cm^2/hour]	0.18
μ_1 [hour^{-1}]	0.005
μ_2 [hour^{-1}]	0.1
μ_3 [hour^{-1}]	0.0
R_1 [-]	2.0
R_2 [-]	1.0
R_3 [-]	1.0
c_i [-]	0.0
$c_{0,1}$ [-]	1.0

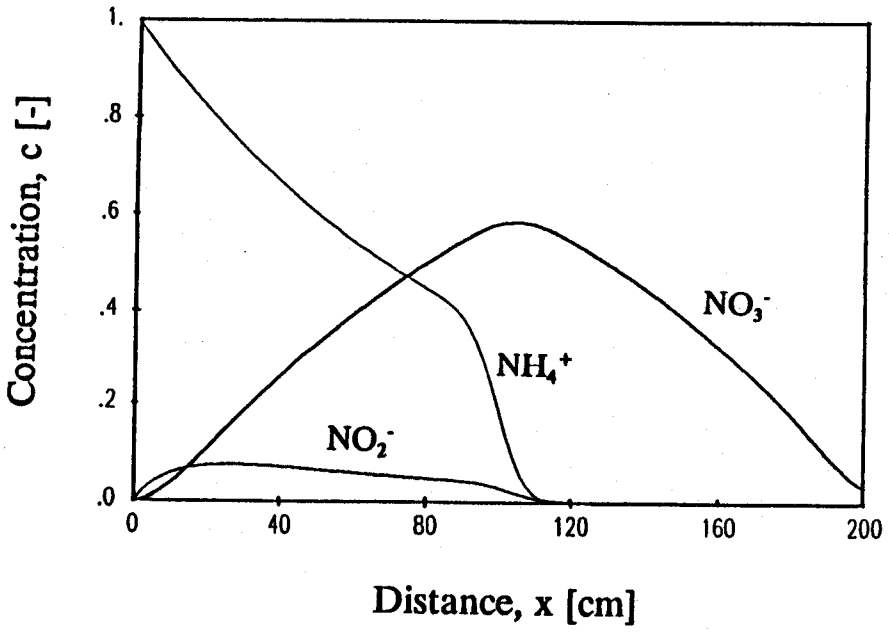

Fig. 8.8. Analytically and numerically calculated concentration profiles for NH_4^+, NO_2^-, and NO_3^- after 200 hours (example 3).

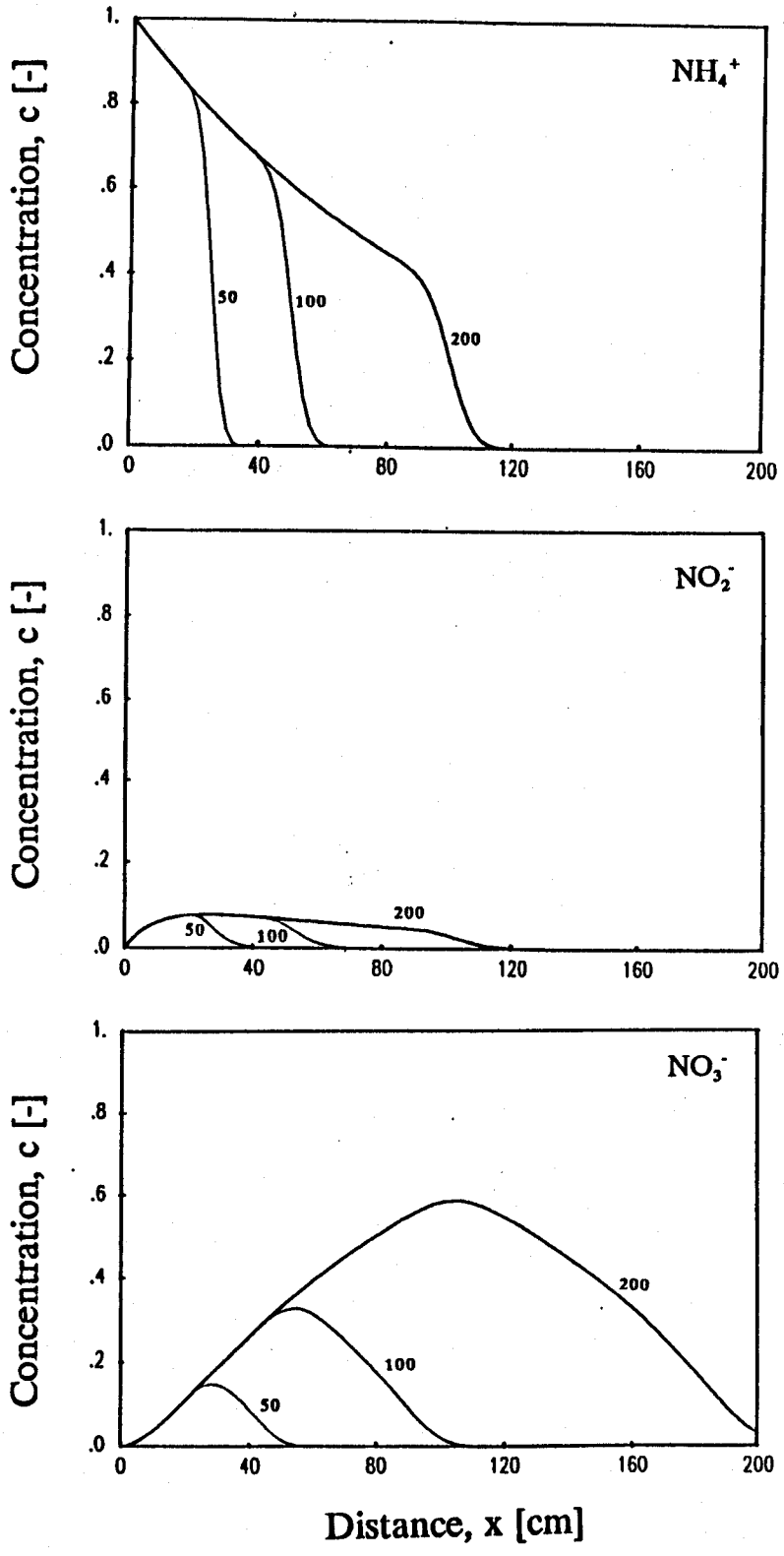

Fig. 8.9. Analytically and numerically calculated concentration profiles for NH_4^+ (top), NO_2^- (middle), NO_3^- (bottom) after 50, 100, and 200 hours (example 3).

8.4. *Example 4 - Solute Transport with Nonlinear Cation Adsorption*

The experiment discussed in this example was conducted by *Selim et al.* [1987], and used later for previous versions (version 3.1 and 5.0) of HYDRUS [*Kool and van Genuchten*, 1991; *Vogel et al.*, 1996]. The soil in this experiment was Abist loam. A 10.75-cm long soil column was first saturated with a 10 $mmol_c L^{-1}$ $CaCl_2$ solution. The experiment consisted of applying a 14.26 pore volume pulse (t = 358.05 hours) of a 10 $mmol_c L^{-1}$ $MgCl_2$ solution, followed by the original $CaCl_2$ solution. The adsorption isotherm was determined with the help of batch experiments [*Selim et al.*, 1987], and fitted with the Freundlich equation (3.3) [*Kool and van Genuchten*, 1991]. The Freundlich isotherm parameters, as well as other transport parameters for this problem, are listed in Table 8.2. First- and second-type boundary conditions were applied to the top and bottom of the soil column, respectively.

The observed Mg breakthrough curve is shown in Figure 8.10, together with simulated breakthrough curves obtained with HYDRUS, the MONOC code of *Selim et al.* [1987] and the previous versions of HYDRUS. The results indicate a reasonable prediction of the measured breakthrough curve using HYDRUS, and close correspondence between the simulated results obtained with the HYDRUS and MONOC models. The HYDRUS results became identical to those generated with previous versions of HYDRUS when a third-type boundary condition was invoked at the top of the soil column.

Table 8.2. Input parameters for example 4.

Parameter	Value
q [cm/hour]	0.271
D [cm^2/hour]	1.167
ρ [g/cm^3]	0.884
θ [-]	0.633
c_0 [$mmol_c/L$]	10.0
k_s [cm^3/g]	1.687
β [-]	1.615

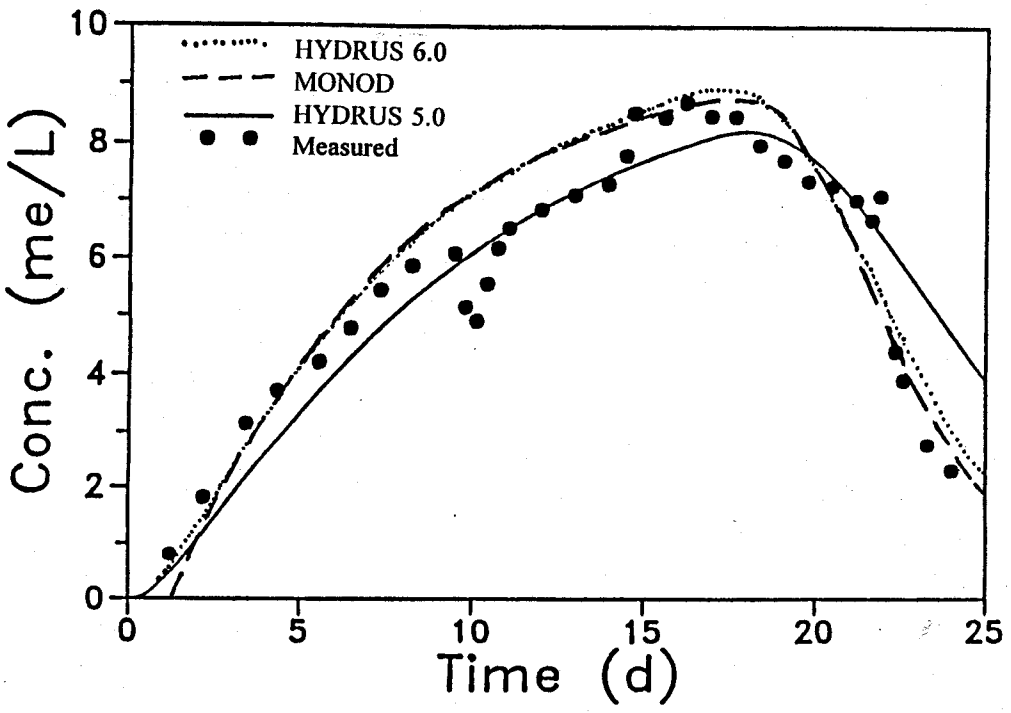

Fig. 8.10. Mg breakthrough curves for Abist loam calculated with the MONOD, HYDRUS, and new HYDRUS codes (data points from *Selim et al.*, 1978).

The Langmuir adsorption isotherm can also be used to model the exchange of homovalent ions. Parameters in the Langmuir adsorption isotherm for homovalent ion exchange may be derived as follows. Ion exchange for two ions with valences n and m can be expressed in a generalized form as [*Sposito*, 1981]

$$K_{ex} = \left[\frac{\bar{a}_1}{a_1}\right]^m \left[\frac{a_2}{\bar{a}_2}\right]^n \tag{8.5}$$

where K_{ex} is the dimensionless thermodynamic equilibrium constant, and a and $\bar{a}$ denote the ion activities in the soil solution and on the exchange surfaces [-], respectively:

$$a_i = \gamma_i c_i \qquad i = 1, 2$$
$$\overline{a}_i = \xi_i s_i \qquad i = 1, 2 \tag{8.6}$$

where c_i [ML^{-3}] (mmol/l) and s_i [MM^{-1}] (mmol/kg) are solution and exchangeable concentrations, respectively, and γ_i and ξ_i are activity coefficients in the soil solution [L^3M^{-1}] (l/mmol) and on the exchange surfaces [MM^{-1}] (kg/mmol), respectively. Substituting (8.6) into (8.5) gives

$$K_{12} = K_v \frac{{\gamma_1}^m}{{\gamma_2}^n} = K_{ex} \frac{{\xi_2}^n}{{\xi_1}^m} \frac{{\gamma_1}^m}{{\gamma_2}^n} = \frac{{s_1}^m}{{s_2}^n} \frac{{c_2}^n}{{c_1}^m} \tag{8.7}$$

where K_v denotes the Vanselow selectivity coefficient [-], while K_{12} will be simply referred to as the selectivity coefficient [-]. Assuming that both the total solution concentration, C_T [ML^{-3}] ($mmol_c/l$), and the cation exchange capacity, S_T [MM^{-1}] ($mmol_c/kg$), are time invariant, i.e.,

$$nc_1 + mc_2 = C_T$$
$$ns_1 + ms_2 = S_T \tag{8.8}$$

the Langmuir parameters k_s and η in (3.3) for the incoming solute become

$$k_s = \frac{K_{12} S_T}{C_T}$$
$$\eta = \frac{\vartheta(K_{12} - 1)}{C_T} \tag{8.9}$$

whereas for the solute initially in the soil column:

$$k_s = \frac{S_T}{K_{12} C_T}$$
$$\eta = \frac{\vartheta(1 - K_{12})}{K_{12} C_T} \tag{8.10}$$

The parameter ϑ in (8.9) and (8.10) equals 1 for monovalent ions, and 2 for divalent ions.

The selectivity coefficient K_{12} for example 4 was measured by *Selim et al.* [1987] (K_{12} = 0.51). From the total solution concentration (C_T = 10 mmol$_c$/l) and the known cation exchange capacity (S_T = 62 mmol$_c$/kg), it follows that the parameters in the Langmuir adsorption isotherm for the incoming solute (Mg) are k_s = 3.126 and η = -0.098, while those for the solute initially in the soil profile (Ca) the parameters are k_s = 12.157 and η = 0.192. The observed Ca breakthrough curve is shown in Figure 8.11, together with the simulated breakthrough curves obtained with the HYDRUS and MONOC codes [*Selim et al.*, 1987]. Notice the close agreement between the numerical results and the experimental data.

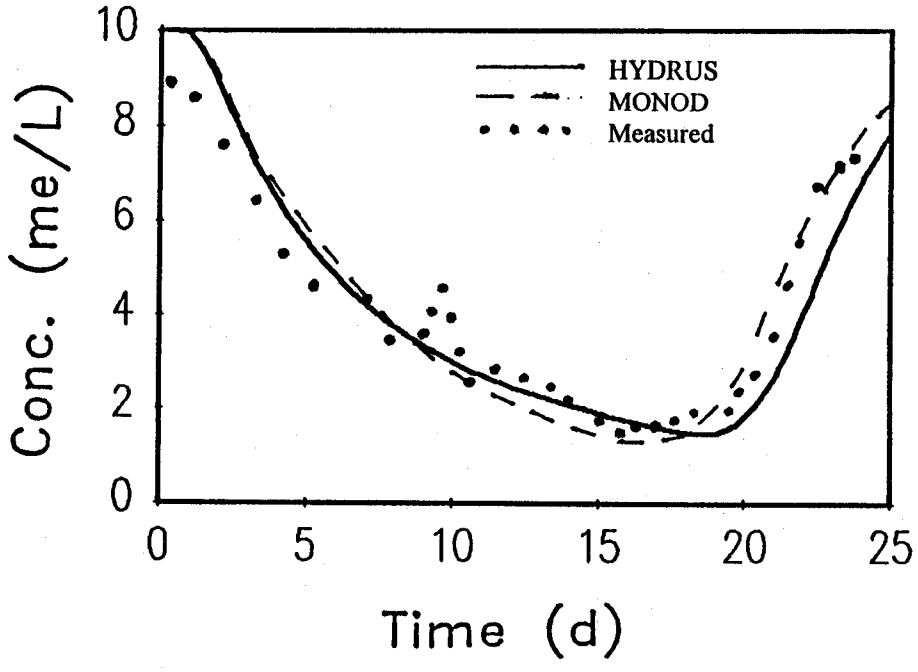

Fig. 8.11. Ca breakthrough curves for Abist loam calculated with the MONOD and HYDRUS codes (data points from *Selim et al.*, 1978) (example 4).

8.5. *Example 5 - Solute Transport with Nonequilibrium Adsorption*

This example considers the movement of a boron (H_3BO_4) pulse through Glendale clay loam [*van Genuchten*, 1981]. The numerical simulation uses solute transport parameters that were fitted to the breakthrough curve with the CFITIM parameter estimation model [*van Genuchten*, 1981] assuming a two-site chemical nonequilibrium sorption model analogous to the formulation discussed in Section 3, but for steady-state water flow. Input parameters for example 5 are listed in Table 8.3. Figure 8.12 compares HYDRUS numerical results with the experimental data, and with a numerical simulation assuming physical nonequilibrium and nonlinear adsorption [*van Genuchten*, 1981].

Table 8.3. Input parameters for example 5.

Parameter	Value
q [cm/day]	17.12
D [cm^2/day]	49.0
θ [-]	0.445
ρ [g/cm$_3$]	1.222
c_0 [mmol$_c$/L]	20.0
k_s [cm^3/g]	1.14
β [-]	1.0
η [-]	0.0
f [-]	0.47
ω [1/day]	0.320
t_p [day]	6.494

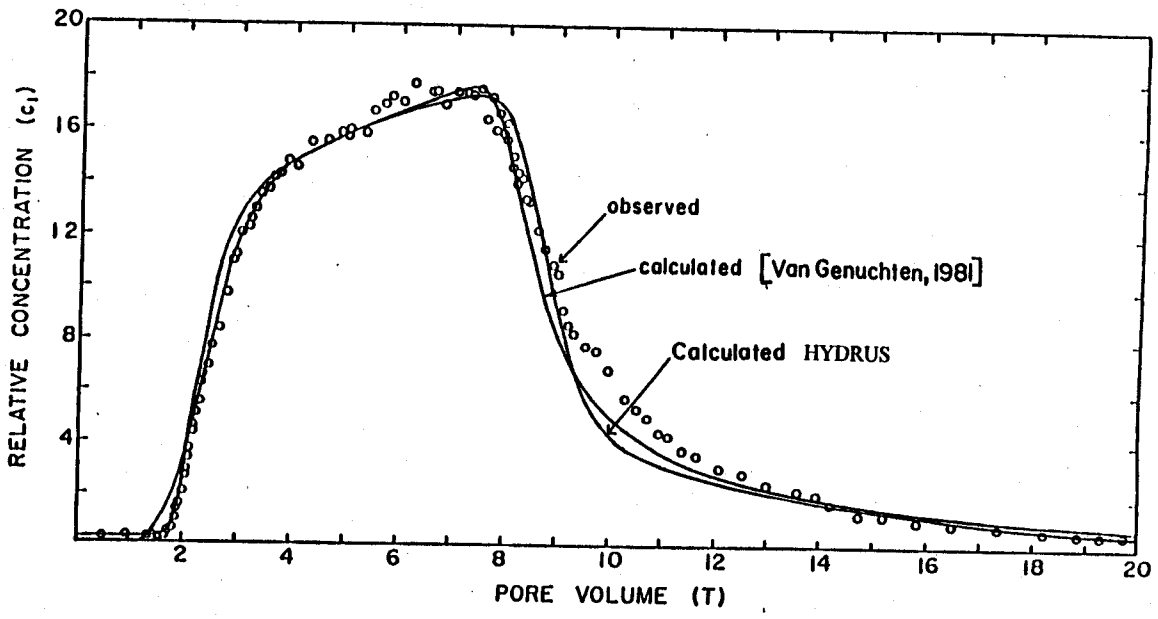

Fig. 8.12. Observed and calculated effluent curves for boron movement through Glendale clay (data points from *van Genuchten* [1981]) (example 5).

9. INPUT DATA

The input data for HYDRUS are given in three separate input files. These input files consist of one or more input blocks identified by the letters from A through I. The input files and blocks must be arranged as follows:

SELECTOR.IN

A. Basic Information
B. Water Flow Information
C. Time Information
D. Root Growth Information
E. Heat Transport Information
F. Solute Transport Information
G. Root Water Uptake Information

PROFILE.DAT

H. Nodal Information

ATMOSPH.IN

I. Atmospheric Information

All input files must be placed into one subdirectory. Output files are printed into the same subdirectory. An additional file **Level_01.dir** which specifies the path to the input and output file subdirectory must be given in the same directory as the executable **HYDRUS** code.

Tables 9.1 through 9.9 describe the data required for each input block. All data are read in using list-directed formatting (free format). Comment lines are provided at the beginning of, and within, each input block to facilitate, among other things, proper identification of the function of the block and the input variables. The comment lines are ignored during program execution; hence, they may be left blank but should not be omitted. The program assumes that all input data are specified in a consistent set of units for mass M, length L, and time T. The values of temperature should be specified in degrees Celsius.

Most of the information in Tables 9.1 through 9.9 should be self-explanatory. Table 9.8 (Block H) is used to define, among other things, the nodal coordinates and initial conditions for the pressure head, temperature and solute concentrations. One short-cut may be used when generating the nodal coordinates. The short-cut is possible when two nodes (e.g., N_1 and N_2), not

adjacent to each other, are located such that N_2 is greater than N_1+1. The program will automatically generate nodes between N_1 and N_2, provided all of the following conditions are met simultaneously: (1) all nodes between nodes N_1 and N_2 are spaced at equal intervals, (2) values of the input variables *hNew*(*n*), *Beta*(*n*), *Axz*(*n*), *Bxz*(*n*), *Dxz*(*n*), *Temp*(*n*), *Conc*(1,*n*) through *Conc*(*NS*,*n*), and *Sorb*(1,*n*) through *Sorb*(*NS*,*n*) vary linearly between nodes N_1 and N_2, and (3) values of *LayNum*(*n*) and *MatNum*(*n*) are the same for all $n = N_1, N_1+1,..., N_2-1$ (see Table 9.8).

Table 9.1. Block A - Basic Information.

Record	Type	Variable	Description
1,2	-	-	Comment lines.
3	Char	*Hed*	Heading.
4	-	-	Comment line.
5	Char	*LUnit*	Length unit (e.g., 'cm').
6	Char	*TUnit*	Time unit (e.g., 'min').
7	Char	*MUnit*	Mass unit for concentration (e.g., 'g', 'mol', '-').
8	-	-	Comment line.
9	Logical	*lWat*	Set this logical variable equal to **.true.** when transient water flow is considered. Set this logical variable equal to **.false.** when initial condition is to be kept constant during the simulation.
9	Logical	*lChem*	Set this logical variable equal to **.true.** if solute transport is to be considered.
9	Logical	*lTemp*	Set this logical variable equal to **.true.** if heat transport is to be considered.
9	Logical	*SinkF*	Set this logical variable equal to **.true.** if water extraction from the root zone occurs.
9	Logical	*lRoot*	Set this logical variable equal to **.true.** if root growth is to be considered.
9	Logical	*ShortF*	**.true.** if information is to be printed only at preselected times, but not at each time step (T-level information, see Section 10), **.false.** if information is to be printed at each time step.
9	Logical	*lWDep*	**.true.** if hydraulic properties are to be considered as temperature dependent. **.false.** otherwise (see Section 2.5).
9	Logical	*lScreen*	**.true.** if information is to be printed on the screen during code execution.
9	Logical	*AtmInf*	**.true.** if variable boundary conditions are supplied via the input file ATMOSPH.IN, **.false.** if the file ATMOSPH.IN is not provided (i.e., in case of time independent boundary conditions).
9	Logical	*lEquil*	**.true.** if equilibrium or no adsorption is considered in the solute transport equation. **.false.** if nonequilibrium adsorption is considered for at least one solute species.
10	-	-	Comment line.
11	Integer	*NMat*	Number of soil materials. Materials are identified by the material number, *MatNum*, specified in Block H.
11	Integer	*NLay*	Number of subregions for which separate water balances are being computed. Subregions are identified by the subregion number, *LayNum*, specified in Block H.

Table 9.1. (continued)

Record	Type	Variable	Description
11	Real	*CosAlfa*	Cosine of the angle between the flow direction and the vertical axis (i.e., cos α = 1 for vertical flow, cos α = 0 for horizontal flow, and 0 < cos α < 1 for inclined flow.

Table 9.2. Block B - Water Flow Information.

Record	Type	Variable	Description
1,2	-	-	Comment lines.
3	Integer	*MaxIt*	Maximum number of iterations allowed during any time step (usually 20).
3	Real	*TolTh*	Absolute water content tolerance for nodes in the unsaturated part of the flow region [-] (its recommended value is 0.0001). *TolTh* represents the maximum desired absolute change in the value of the water content, θ, between two successive iterations during a particular time step.
3	Real	*TolH*	Absolute pressure head tolerance for nodes in the saturated part of the flow region [L] (its recommended value is 0.1 cm). *TolH* represents the maximum desired absolute change in the value of the pressure head, h, between two successive iterations during a particular time step.
4	-	-	Comment line.
5	Logical	*TopInf*	**.true.** if time dependent boundary condition is to be imposed at the top of the profile; data are supplied via input file ATMOSPH.IN. **.false.** in the case of time independent surface boundary conditions.
5	Logical	*WLayer*	Set this variable equal to **.true.** if water can accumulate at the surface with zero surface runoff.
5	Integer	*KodTop*	Code specifying type of boundary condition (BC) for water flow at the surface. Code number is positive for Dirichlet BC and negative for Neumann BC. In the case of 'Atmospheric BC' set *KodTop*=-1.
6	-	-	Comment line.
7	Logical	*BotInf*	**.true.** if time dependent boundary condition is to be imposed at the bottom of the profile; control data are supplied via input file ATMOSPH.IN. **.false.** in the case of time independent bottom boundary conditions.
7	Logical	*qGWLF*	Set this variable equal to **.true.** if the discharge-groundwater level relationship $q(GWL)$ is applied as bottom boundary condition.
7	Logical	*FreeD*	**.true.** if free drainage is to be considered as bottom boundary condition.
7	Logical	*SeepF*	**.true.** if seepage face is to be considered as bottom boundary condition.
7	Integer	*KodBot*	Code specifying type of boundary condition for water flow at the bottom of the profile. Code number is positive for a Dirichlet BC and negative for a Neumann BC. In case of a seepage face or free drainage BC set *KodBot*=-1.
8a	-	-	Comment line.
9a	Real	*rTop*	Prescribed top flux [LT^{-1}] (in case of a Dirichlet BC set this variable equal to zero).
9a	Real	*rBot*	Prescribed bottom flux [LT^{-1}] (in case of a Dirichlet BC set this variable equal to zero).
9a	Real	*rRoot*	Prescribed potential transpiration rate [LT^{-1}] (if no transpiration occurs or if transpiration is variable in time set this variable equal to zero).

Table 9.2. (continued)

Record	Type	Variable	Description
			Records 8a and 9a are provided only when both boundary conditions are independent of time and at least one of them is a Neumann BC.
8b	-	-	Comment line.
9b	Real	*GWL0L*	Reference position of the groundwater table (e.g., the x-coordinate of the soil surface).
9b	Real	*Aqh*	Value of the parameter A_{qh} [$L T^{-1}$] in the $q(GWL)$-relationship, equation (7.1); set to zero if *qGWLF*=**.false.**
9b	Real	*Bqh*	Value of the parameter B_{qh} [L^{-1}] in the $q(GWL)$-relationship, equation (7.1); set to zero if *qGWLF* =**.false.**
			Records 8b and 9b are provided only when the logical variable *qGWLF*=**.true.**.
10	-	-	Comment line.
11	Real	*ha*	Absolute value of the upper limit [L] of the pressure head interval below which a table of hydraulic properties will be generated internally for each material (h_a must be greater than 0.0; e.g. 0.001 cm) (see Section 5.4.7).
11	Real	*hb*	Absolute value of the lower limit [L] of the pressure head interval for which a table of hydraulic properties will be generated internally for each material (e.g. 1000 m). One may assign to h_b the highest (absolute) expected pressure head to be expected during a simulation. If the absolute value of the pressure head during program execution lies outside of the interval $[h_a, h_b]$, then appropriate values for the hydraulic properties are computed directly from the hydraulic functions (i.e., without interpolation in the table).
12	-	-	Comment line.
13	Integer	*iModel*	Soil hydraulic properties model: = 0; *van Genuchten*'s [1980] model with five parameters. = 1; modified van Genuchten's model with nine parameters, *Vogel and Cislerová* [1988]. = 2; *Brooks and Corey*'s [1964] model with five parameters.
13	Integer	*iHyst*	Hysteresis in the soil hydraulic properties: = 0; No hysteresis = 1; Hysteresis in the retention curve only = 2; Hysteresis in both the retention and hydraulic conductivity functions
14	-	-	Comment line.
15	Integer	*iKappa*	= -1 if the initial condition is to be calculated from the main drying branch. = 1 if the initial condition is to be calculated from the main wetting branch.
			Records 14 and 15 are provided only when *iHyst* > 0.
16	-	-	Comment line.

Table 9.2. (continued)

Record	Type	Variable	Description
17	Real	*Par*(1,*M*)	Parameter θ_r for material *M* [-].
17	Real	*Par*(2,*M*)	Parameter θ_s for material *M* [-].
17	Real	*Par*(3,*M*)	Parameter α for material *M* [L^{-1}].
17	Real	*Par*(4,*M*)	Parameter *n* for material *M* [-].
17	Real	*Par*(5,*M*)	Parameter K_s for material *M* [LT^{-1}].
			The following four parameters are specified only when *iModel*=1.
17	Real	*Par*(6,*M*)	Parameter θ_m for material *M* [-].
17	Real	*Par*(7,*M*)	Parameter θ_a for material *M* [-].
17	Real	*Par*(8,*M*)	Parameter θ_k for material *M* [-].
17	Real	*Par*(9,*M*)	Parameter K_k for material *M* [LT^{-1}].
			The following four parameters are specified only when *iModel*=0 and *iHyst*>1.
17	Real	*Par*(6,*M*)	Parameter θ_m for material *M* [-].
17	Real	*Par*(7,*M*)	Parameter θ_{sw} for material *M* [-].
17	Real	*Par*(8,*M*)	Parameter α_w for material *M* [L^{-1}].
17	Real	*Par*(9,*M*)	Parameter K_{sw} for material *M* [LT^{-1}].
			Record 17 information is provided for each material *M* (from 1 to *NMat*). If *lWDep*=**.true.** (Block A) then the soil hydraulic parameters *Par*(*i*,*M*) must be specified at reference temperature T_{ref}=20°C.

Table 9.3. Block C - Time information.

Record	Type	Variable	Description
1,2	-	-	Comment lines.
3	Real	*dt*	Initial time increment, Δt [T]. Initial time step should be estimated in dependence on the problem being solved. For problems with high pressure gradients (e.g. infiltration into an initially dry soil), Δt should be relatively small.
3	Real	*dtMin*	Minimum permitted time increment, Δt_{min} [T].
3	Real	*dtMax*	Maximum permitted time increment, Δt_{max} [T].
3	Real	*dMul*	If the number of required iterations at a particular time step is less than or equal to *ItMin*, then Δt for the next time step is multiplied by a dimensionless number *dMul* $\geq$ 1.0 (its value is recommended not to exceed 1.3).
3	Real	*dMul2*	If the number of required iterations at a particular time step is greater than or equal to *ItMax*, then Δt for the next time step is multiplied by *dMul2* $\leq$ 1.0 (e.g. 0.33).
3	Integer	*ItMin*	If the number of required iterations at a particular time step is less than or equal to *ItMin*, then Δt for the next time step is multiplied by a dimensionless number *dMul* $\geq$ 1.0 (its value is recommended not to exceed 1.3).
3	Integer	*ItMax*	If the number of required iterations at a particular time step is greater than or equal to *ItMax*, then Δt for the next time step is multiplied by *dMul2* $\leq$ 1.0 (e.g. 0.33).
3	Integer	*MPL*	Number of specified print-times at which detailed information about the pressure head, water content, flux, temperature, concentrations, and the water and solute balances will be printed.
4	-	-	Comment line.
5	Real	*tInit*	Initial time of the simulation [T].
5	Real	*tMax*	Final time of the simulation [T].
6	-	-	Comment line.
7	Real	*TPrint*(1)	First specified print-time [T].
7	Real	*TPrint*(2)	Second specified print-time [T].
.	.	.	.
.	.	.	.
7	Real	*TPrint*(*MPL*)	Last specified print-time [T]. (Maximum six values on one line.)

Table 9.4. Block D - Root Growth Information.[†]

Record	Type	Symbol	Description
1,2	-	-	Comment lines.
3	Integer	*iRFak*	Method to calculate the root growth factor, *r*. = 0; the root growth factor is calculated from given data [*xRMed, tRMed*]. = 1; the root growth factor is calculated based on the assumption that 50% of the rooting depth, (*xRMax*+*xRMin*)/2., is reached at the midpoint of the growing season, (*tRMin*+*tRHarv*)/2.
3	Real	*tRMin*	Initial time of the root growth period [T].
3	Real	*tRMed*	Time of known rooting depth (set equal to zero if *iRFak*=0) [T].
3	Real	*tRHarv*	Time at the end of the root water uptake period [T].
3	Real	*xRMin*	Initial value of the rooting depth at the beginning of the growth period (recommended value = 1 cm) [L].
3	Real	*xRMed*	Value of known rooting depth (set equal to zero if *iRFak*=0) [L].
3	Real	*xRMax*	Maximum rooting depth which may be reached at infinite time [L].

[†] Block D is not needed if the logical variable *lRoot* (Block A) is set equal to **.false.**

Table 9.5. Block E - Heat transport information.[†]

Record	Type	Symbol	Description
1,2	-	-	Comment lines.
3	Real	*TPar*(1,*M*)	Volumetric solid phase fraction of material *M*, θ_n [-].
3	Real	*TPar*(2,*M*)	Volumetric organic matter fraction of material *M*, θ_o [-].
3	Real	*TPar*(3,*M*)	Longitudinal thermal dispersivity of material *M*, λ_L [L].
3	Real	*TPar*(4,*M*)	Coefficient b_1 in the thermal conductivity function [$MLT^{-3}K^{-1}$] (e.g.$Wm^{-1}K^{-1}$) (see equation (4.6)).
3	Real	*TPar*(5,*M*)	Coefficient b_2 in the thermal conductivity function [$MLT^{-3}K^{-1}$] (e.g.$Wm^{-1}K^{-1}$) (see equation (4.6)).
3	Real	*TPar*(6,*M*)	Coefficient b_3 in the thermal conductivity function [$MLT^{-3}K^{-1}$] (e.g.$Wm^{-1}K^{-1}$) (see equation (4.6)).
3	Real	*TPar*(7,*M*)	Volumetric heat capacity of solid phase of material *M*, C_n [$ML^{-1}T^{-2}K^{-1}$] (e.g. $Jm^{-3}K^{-1}$).
3	Real	*TPar*(8,*M*)	Volumetric heat capacity of organic matter of material *M*, C_o [$ML^{-1}T^{-2}K^{-1}$] (e.g. $Jm^{-3}K^{-1}$).
3	Real	*TPar*(9,*M*)	Volumetric heat capacity of liquid phase of material *M*, C_w [$ML^{-1}T^{-2}K^{-1}$] (e.g. $Jm^{-3}K^{-1}$).
			Record 3 is required for each soil material *M* (from 1 to *NMat*).
4	-	-	Comment line.
5	Real	*Ampl*	Temperature amplitude at the soil surface [K].
5	Real	*tPeriod*	Time interval for completion of one temperature cycle (usually 1 day) [T].
6	-	-	Comment line.
7	Integer	*kTopT*	Code which specifies the type of upper boundary condition =1: Dirichlet boundary condition, =-1: Cauchy boundary condition.
7	Real	*tTop*	Temperature of the upper boundary, or temperature of the incoming fluid [°C].
7	Integer	*kBotT*	Code which specifies the type of lower boundary condition =1: Dirichlet boundary condition, =0: continuous temperature profile, zero gradient, =-1: Cauchy boundary condition.
7	Real	*tBot*	Temperature of lower boundary, or temperature of the incoming fluid [°C].

[†] Block E is not needed if logical variable *lTemp* (Block A) is set equal to **.false.**

Table 9.6. Block F - Solute transport information.†

Record	Type	Variable	Description
1,2	-	-	Comment lines.
3	Real	*Epsi*	Temporal weighing coefficient. =0.0 for an explicit scheme. =0.5 for a Crank-Nicholson implicit scheme. =1.0 for a fully implicit scheme.
3	Logical	*lUpW*	**.true.** if upstream weighing formulation is to be used. **.false.** if the original Galerkin formulation is to be used.
3	Logical	*lArtD*	**.true.** if artificial dispersion is to be added in order to fulfill the stability criterion *PeCr* (see Section 6.4.4). **.false.** otherwise.
3	Logical	*lTDep*	**.true.** if at least one transport or reaction coefficient (*ChPar*) is temperature dependent. **.false.** otherwise. If *lTDep*=**.true.**, then all values of *ChPar*(*i,M*) should be specified at a reference temperature T_r=20°C.
3	Real	*cTolA*	Absolute concentration tolerance [ML^{-3}], the value is dependent on the units used (set equal to zero if nonlinear adsorption is not considered).
3	Real	*cTolR*	Relative concentration tolerance [-] (set equal to zero if nonlinear adsorption is not considered).
3	Integer	*MaxItC*	Maximum number of iterations allowed during any time step for solute transport - usually 20 (set equal to zero if nonlinear adsorption is not considered).
3	Real	*PeCr*	Stability criteria (see Section 6.4.4). Set equal to zero when *lUpW* is equal to **.true.**.
3	Integer	*NS*	Number of solutes.
4	-	-	Comment line.
5	Real	*ChPar*(1,*M*)	Bulk density of material *M*, ρ [ML^{-3}].
5	Real	*ChPar*(2,*M*)	Longitudinal dispersivity for material type *M*, D_L [L].
5	Real	*ChPar*(3,*M*)	Dimensionless fraction of the adsorption sites classified as type-1, i.e., sites with instantaneous sorption. Set equal to 1 if equilibrium transport is to be considered. Record 5 information is provided for each material *M* (from 1 to *NMat*).
6	-	-	Comment line.
7	Real	*ChPar*(4,*M*)	Ionic or molecular diffusion coefficient in free water, D_w [L^2T^{-1}].
7	Real	*ChPar*(5,*M*)	Ionic or molecular diffusion coefficient in gas phase, D_g [L^2T^{-1}].
8	-	-	Comment line.

Table 9.6. (continued)

Record	Type	Variable	Description
9	Real	*ChPar*(6,*M*)	Adsorption isotherm coefficient, k_s, for material type *M* [L^3M^{-1}]. Set equal to zero if no adsorption is to be considered.
9	Real	*ChPar*(7,*M*)	Adsorption isotherm coefficient, η, for material type M [L^3M^{-1}]. Set equal to zero if Langmuir adsorption isotherm is not to be considered.
9	Real	*ChPar*(8,*M*)	Adsorption isotherm coefficient, β, for material type M [-]. Set equal to one if Freundlich adsorption isotherm is not to be considered.
9	Real	*ChPar*(9,*M*)	Equilibrium distribution constant between liquid and gas phases, k_g, material type *M* [-].
9	Real	*ChPar*(10,*M*)	First-order rate constant for the dissolved phase, μ_w, material type *M* [T^{-1}].
9	Real	*ChPar*(11,*M*)	First-order rate constant for the solid phase, μ_s, material type *M* [T^{-1}].
9	Real	*ChPar*(12,*M*)	First-order rate constant for the gas phase, μ_g, material type *M* [T^{-1}].
9	Real	*ChPar*(13,*M*)	Rate constant, μ_w', representing a first-order decay for the first solute and zero-order production for the second solute in the dissolved phase, material type *M* [T^{-1}].
9	Real	*ChPar*(14,*M*)	Same as above for the solid phase, μ_s', material type *M* [T^{-1}].
9	Real	*ChPar*(15,*M*)	Same as above for the gas phase, μ_g', material type *M* [T^{-1}].
9	Real	*ChPar*(16,*M*)	Zero-order rate constant for the dissolved phase, γ_w, material type *M* [$ML^{-3}T^{-1}$].
9	Real	*ChPar*(17,*M*)	Zero-order rate constant for the solid phase, γ_s, material type *M* [T^{-1}].
9	Real	*ChPar*(18,*M*)	Zero-order rate constant for the gas phase, γ_g, material type *M* [$ML^{-3}T^{-1}$].
9	Real	*ChPar*(19,*M*)	First-order mass transfer coefficient for nonequilibrium adsorption, ω, material type M [T^{-1}].
			Record 9 information is provided for each material *M* (from 1 to *NMat*).
			Record 6 through 9 information is provided for each solute (from 1 to *NS*).
10,11	-	-	Comment lines.
12	Real	*TDep*(4)	Activation energy for parameter *ChPar*(4,*M*) [$ML^2T^{-2}M^{-1}$] (see Section 3.4). This parameter should be specified in J mol^{-1}. Set equal to 0 if *ChPar*(5,*M*) is temperature independent.
12	Real	*TDep*(5)	Same for parameter *ChPar*(5,*M*) [$ML^2T^{-2}M^{-1}$].
13	-	-	Comment line.
14	Real	*TDep*(6)	Same for parameter *ChPar*(6,*M*) [$ML^2T^{-2}M^{-1}$].
.	.	.	.
.	.	.	.
14	Real	*TDep*(19)	Same for parameter *ChPar*(19,*M*) [$ML^2T^{-2}M^{-1}$].
			Record 10 through 14 information is provided only when the logical variable *lTDep* of record 3 is set equal to **.true.**.
15	-	-	Comment line.
16	Integer	*kTopCh*	Code which specifies the type of upper boundary condition =1: Dirichlet boundary condition, =-1: Cauchy boundary condition.
16	Real	*cTop*(1)	Concentration of the upper boundary, or concentration of the incoming fluid, for the first solute [ML^{-3}].

Table 9.6. (continued)

Record	Type	Variable	Description
16	Real	*cTop*(2)	Concentration of the upper boundary, or concentration of the incoming fluid, for the second solute [ML^{-3}] (not specified if $NS < 2$).
.	.	.	.
.	.	.	.
16	Real	*cTop*(*NS*)	Concentration of the upper boundary, or concentration of the incoming fluid, for the *NS*th solute [ML^{-3}].
16	Integer	*kBotCh*	Code which specifies the type of lower boundary condition =1: Dirichlet boundary condition, =0: continuous concentration profile, =-1: Cauchy boundary condition.
16	Real	*cBot*(1)	Concentration of lower boundary, or concentration of the incoming fluid, for the first solute [ML^{-3}].
16	Real	*cBot*(2)	Concentration of lower boundary, or concentration of the incoming fluid, for the second solute [ML^{-3}] (not specified if $NS < 2$).
.	.	.	.
.	.	.	.
16	Real	*cBot*(*NS*)	Concentration of lower boundary, or concentration of the incoming fluid, for the *NS*th solute [ML^{-3}].
17	-	-	Comment line.
19	Real	*tPulse*	Time duration of the concentration pulse [T].

[†]Block F is not needed when the logical variable *lChem* in Block A is set equal to **.false.** .

Table 9.7. Block G - Root water uptake information.†

Record	Type	Variable	Description
1,2	-	-	Comment lines.
3	Integer	*iMoSink*	Type of root water uptake stress response function. = 0; *Feddes et al.* [1978] = 1; S-shaped, *van Genuchten* [1987]
4	-	-	Comment line.
			The following records (records 5a, 6a, 7a) are given only if *iMoSink*=0.
5a	Real	*P0*	Value of the pressure head, h_1 (Fig. 2.1), below which roots start to extract water from the soil.
5a	Real	*P2H*	Value of the limiting pressure head, h_3, below which the roots cannot extract water at the maximum rate (assuming a potential transpiration rate of *r2H*).
5a	Real	*P2L*	As above, but for a potential transpiration rate of *r2L*.
5a	Real	*P3*	Value of the pressure head, h_4, below which root water uptake ceases (usually equal to the wilting point).
5a	Real	*r2H*	Potential transpiration rate [LT^{-1}] (currently set at 0.5 cm/day).
5a	Real	*r2L*	Potential transpiration rate [LT^{-1}] (currently set at 0.1 cm/day).
			The above input parameters permit one to make the variable h_3 a function of the potential transpiration rate, T_p (h_3 presumably decreases at higher transpiration rates). HYDRUS currently implements the same linear interpolation scheme as used in several versions of the SWATRE code (e.g., *Wesseling and Brandyk* [1985]) and in the SWMS_2D [*Šimůnek et al.*, 1992] and HYDRUS 5.0 [*Vogel et al.*, 1996] codes. The scheme is based on the following interpolation: $$h_3 = P2H + \frac{P2L - P2H}{r2H - r2L}(r2H - T_p) \qquad for \;\; r2L < T_p < r2H$$ $$h_3 = P2L \qquad for \;\; T_a \le r2L$$ $$h_3 = P2H \qquad for \;\; T_a \ge r2H$$
6a	-	-	Comment line.
7a	Real	*POptm*(1)	Value of the pressure head, h_2, below which roots start to extract water at the maximum possible rate (material number 1).
7a	Real	*POptm*(2)	As above (material number 2).
.	.	.	.
.	.	.	.
7a	Real	*POptm*(*NMat*)	As above (for material number *NMat*).
			The following record (record 5b) is given only if *iMoSink*=1.

Table 9.7. (continued)

Record	Type	Variable	Description
5b	Real	*P50*	Value of the pressure head, h_{50} (Fig. 2.1), at which the root water uptake is reduced by 50%.
5b	Real	*P3*	Exponent, p, in the S-shaped root water uptake stress response function. Recommended value is 3.
			The following records are given only if *lChem*=**.true.** .
8	-	-	Comment line.
9	Logical	*lSolRed*	=**.true.** : root water uptake is reduced due to salinity. =**.false.**: otherwise.
			The following records are given only if *lSolRed*=**.true.** .
10	-	-	Comment line.
11	Logical	*lSolAdd*	=**.true.** if the effect of salinity stress is additive to the pressure head stress. =**.false.** if the effect of salinity stress is multiplicative to the pressure head stress.
12	-	-	Comment line.
13	Real	*c50*	Value of the osmotic head $h_{\phi 50}$, at which the root water uptake is reduced by 50%. This value is specified only when *lSolAdd*=**.false.**.
13	Real	*P3c*	Exponent, p, in the S-shaped root water uptake salinity stress response function. Recommended value is 3. This value is specified only when *lSolAdd*=**.false.**.
13	Real	*aOsm*(1)	Osmotic coefficient, a_1, for the first solute [L^4M^{-1}].
13	Real	*aOsm*(2)	Osmotic coefficient, a_2, for the second solute [L^4M^{-1}].
	.	.	.
	.	.	.
13	Real	*aOsm*(*NSD*)	Osmotic coefficient, a_n, for the last solute [L^4M^{-1}].

† Block G is not needed when the logical variable *SinkF* (Block L) is set equal to **.false.** .

Table 9.8. Block H - Nodal information.

Record	Type	Variable	Description
1	Integer	*NFix*	Number of fixed nodes.
2	Integer	*i*	Fixed node.
2	Real	*xFix(i)*	*x*-coordinate of the fixed node *i*.
2	Real	*wTop(i)*	Nodal density above fixed node *i*.
2	Real	*wBot(i)*	Nodal density below fixed node *i*.
			Record 2 must be specified for each fixed node.
			Records 1 and 2 have relevant information only for the module PROFILE of the user interface. When the code is used without the user interface, then only two fixed points (top and bottom of the soil profile) with unit nodal density have to be specified.
3	Integer	*NumNP*	Number of nodal points.
3	Integer	*NS*	Number of solutes (set equal to zero if *lChem* is equal to **.false.**).
3	Integer	*iTemp*	This variable is read only if the user interface is used. = 1; initial condition for the temperature is specified (must be equal to 1 when *lTemp* or *lChem* is equal to **.true.**). = 0; initial condition for the temperature is not specified.
3	Integer	*iEquil*	This variable is read only if the user interface is used. = 1; Equilibrium solute transport is considered. = 0; Nonequilibrium solute transport is considered. Set equal to 1 if *lChem* is equal to **.false.**.
4	Integer	*n*	Nodal number.
4	Real	*x(n)*	*x*-coordinate of node *n* [L].
4	Real	*hNew(n)*	Initial value of the pressure head at node *n* [L]. If *lWat*=**.false.** in Block A, then *hNew(n)* represents the pressure head which will be kept constant during simulation.
4	Integer	*MatNum(n)*	Index for material whose hydraulic and transport properties are assigned to node *n*.
4	Integer	*LayNum(n)*	Subregion number assigned to node *n*.
4	Real	*Beta(n)*	Value of the water uptake distribution, $b(x)$ [L^{-1}], in the soil root zone at node *n*. Set *Beta(n)* equal to zero if node *n* lies outside the root zone.
4	Real	*Ah(n)*	Nodal value of the dimensionless scaling factor α_h [-] associated with the pressure head.
4	Real	*Ak(n)*	Nodal value of the dimensionless scaling factor α_K [-] associated with the saturated hydraulic conductivity.

Table 9.8. (continued)

Record	Type	Variable	Description
4	Real	*Ath*(*n*)	Nodal value of the dimensionless scaling factor α_θ [-] associated with the water content.
4	Real	*Temp*(*n*)	Initial value of the temperature at node *n* [°C] (do not specify if both *lTemp* or *lChem* are equal to **.false.**; if *lTemp*=**.false.** and *lChem*=**.true.** then set equal to 0 or any other initial value to be used later for temperature dependent water flow and solute transport).
4	Real	*Conc*(1,*n*)	Initial value of the concentration of the first solute at node *n* [ML^{-3}] (omit if *lChem*=**.false.**).
4	Real	*Conc*(2,*n*)	Initial value of the concentration of the second solute at node *n* [ML^{-3}] (omit if *lChem*=**.true.** and *NS* < 2).
.	.	.	.
.	.	.	.
4	Real	*Conc*(*i*,*n*)	Initial value of the concentration of the last solute at node *n* [ML^{-3}] (omit if *lChem*=**.true.** and *NS* < *i*).
4	Real	*Sorb*(1,*n*)	Initial value of the adsorbed concentration on type-2 sites of the first solute at node *n* [ML^{-3}]. Omit this variable if *lChem*=**.false.**. or *lEquil*=**.true.** .
4	Real	*Sorb*(2,*n*)	Initial value of the adsorbed concentration on type-2 sites of the second solute at node *n* [ML^{-3}]. Omit this variable if *lChem*=**.false.** or *lEquil*=**.true.** or *NS* < 2.
.	.	.	.
.	.	.	.
4	Real	*Sorb*(*i*,*n*)	Initial value of the adsorbed concentration on type-2 sites of the *NS*th solute at node *n* [ML^{-3}]. This variable does not have to be specified if *lChem*=**.false.** or *lEquil*=**.true.** and *NS* < *i*). In general, record 4 information is required for each node *n*, starting with *n*=1 and continuing sequentially until *n*=*NumNP*. Record 4 information for certain nodes may be skipped if several conditions are satisfied (see beginning of this section).
5	Integer	*NObs*	Number of observation nodes for which values of the pressure head, the water content, temperature (for *lTemp*=**.true.**), and the solution and sorbed concentrations (for *lChem*=**.true.**) are printed at each time level.
6	Integer	*iObs*(1)	Nodal number of the first observation node.
6	Integer	*iObs*(2)	Nodal number of the second observation node.
.	.	.	.
.	.	.	.
6	Integer	*iObs*(*NObs*)	Nodal number of the last observation node.

Table 9.9. Block I - Atmospheric information.†

Record	Type	Variable	Description
1,2	-	-	Comment lines.
3	Integer	*MaxAl*	Number of atmospheric data records.
4	-	-	Comment line.
5	Real	*hCritS*	Maximum allowed pressure head at the soil surface [L].
6	-	-	Comment line.
7	Real	*tAtm*(*i*)	Time for which the *i*-th data record is provided [T].
7	Real	*Prec*(*i*)	Precipitation rate [LT^{-1}] (in absolute value).
7	Real	*rSoil*(*i*)	Potential evaporation rate [LT^{-1}] (in absolute value).
7	Real	*rRoot*(*i*)	Potential transpiration rate [LT^{-1}] (in absolute value).
7	Real	*hCritA*(*i*)	Absolute value of the minimum allowed pressure head at the soil surface [L].
7	Real	*rB*(*i*)	Bottom flux [LT^{-1}] (set equal to 0 if *KodBot* is positive, or if one of the logical variables *qGWLF*, *FreeD* or *SeepF* is **.true.**).
7	Real	*hB*(*i*)	Groundwater level [L], or any other prescribed pressure head boundary condition as indicated by a positive value of *KodBot* (set equal to 0 if *KodBot* is negative, or if one of the logical variables *qGWLF*, *FreeD* or *SeepF* is **.true.**).
7	Real	*hT*(*i*)	Prescribed pressure head [L] at the surface (set equal to 0 if *KodBot* is negative).
7	Real	*tTop*(*i*)	Soil surface temperature [°C] (omit if both *lTemp* and *lChem* are equal to **.false.**).
7	Real	*tBot*(*i*)	Soil temperature at the bottom of the soil profile [°C] (omit if both *lTemp* and *lChem* are equal to **.false.**, set equal to zero if *kBotT*=0).
7	Real	*Ampl*(*i*)	Temperature amplitude at the soil surface [K] (omit if both *lTemp* and *lChem* are equal to **.false.**).
7	Real	*cTop*(*i*,1)	Soil surface concentration [ML^{-3}] for the first solute (not needed if *lChem* is equal to **.false.**).
7	Real	*cTop*(*i*,2)	Soil surface concentration [ML^{-3}] for the second solute (not needed if *lChem* is equal to **.false.** or $NS < 2$).
.	.	.	.
.	.	.	.
7	Real	*cTop*(*i*,*NS*)	Soil surface concentration [ML^{-3}] for the *NS*th solute (not needed if *lChem* is equal to **.false.**).
7	Real	*cBot*(*i*,1)	Concentration at the bottom of the soil profile [ML^{-3}] for the first solute (not needed if *lChem* is equal to **.false.**, set equal to zero if *cBotSolute*=0).
7	Real	*cBot*(*i*,2)	Concentration at the bottom of the soil profile [ML^{-3}] for the second solute (not needed if *lChem* is equal to **.false.**, set equal to zero if *cBotSolute*=0 or $NS < 2$).
.	.	.	.

Table 9.9. (continued)

Record	Type	Variable	Description
7	Real	*cBot*(*i*,*NS*)	Concentration at the bottom of the soil profile [ML^{-3}] for the *NS*th solute (not needed if *lChem* is equal to **.false.**, set equal to zero if *cBotSolute*=0). The total number of atmospheric data records is *MaxAl* (i=1,2, ..,*MaxAl*).

† Block I is not needed if the logical variable *AtmInf* (Block A) is set equal to **.false.** .

10. OUTPUT DATA

The program output consists of $9+(n_s-1)$ output files, where n_s is the number of solutes considered in the first-order decay chain. The output is organized into 3 groups:

T-level information
- T_LEVEL.OUT
- RUN_INF.OUT
- SOLUTE.OUT
- OBS_NODE.OUT

P-level information
- NOD_INF.OUT
- BALANCE.OUT

A-level information
- A_LEVEL.OUT

In addition, some of the input data are printed to files I_CHECK.OUT and PROFILE.OUT. A separate output file SOLUTE.OUT is created for each solute. All output files are directed to the same directory as the input files, which must be created by the user prior to program execution (the directory is created automatically if the user interface is used). The various output files are described in detail in this section.

File I_CHECK.OUT contains a complete description of the space discretization, the hydraulic characteristic, and the transport properties of each soil material.

T-level information - This group of output files contains information which is printed at the end of each time step. Printing can be suppressed by setting the logical variable *ShortF* in input Block A equal to .true.; the information is then printed only at selected print times. Output files printed at the T-level are described in Tables 10.1 through 10.3. Output file OBS_NODE. OUT gives transient values of the pressure head, water content, temperature, and solution and sorbed concentrations, as obtained during the simulation at specified observation nodes.

P-level information - P-level information is printed only at prescribed print times. The following output files are printed at the P-level:

NOD_INF.OUT	Nodal values of the pressure head, the water content, the solution and sorbed concentrations, and temperature, etc. (Table 10.4).

BALANCE.OUT	This file gives the total amount of water, heat and solute inside each specified subregion, the inflow/outflow rates to/from each subregion, together with the mean pressure head (*hMean*), mean temperature (*TMean*) and the mean concentration (*cMean*) of each subregion (see Table 10.5). Absolute and relative errors in the water and solute mass balances are also printed to this file.

A-level information - A-level information is printed each time a time-dependent boundary condition is specified. The information is directed to output file A_LEVEL.OUT (Table 10.6).

Table 10.1. T_LEVEL.OUT - pressure heads and fluxes on the boundaries and in the root zone.

Time	Time, *t*, at current time-level [T].
rTop	Potential surface flux [LT^{-1}] (infiltration/evaporation: -/+).
rRoot	Potential transpiration rate [LT^{-1}].
vTop	Actual surface flux [LT^{-1}] (infiltration/evaporation: -/+).
vRoot	Actual transpiration rate [LT^{-1}].
vBot	Actual flux across the bottom of the soil profile [LT^{-1}] (inflow/outflow: +/-).
sum(rTop)	Cumulative value of the potential surface flux [L] (infiltration/evaporation: -/+).
sum(rRoot)	Cumulative value of the potential transpiration rate [L].
sum(vTop)	Cumulative value of the actual surface flux [L] (infiltration/evaporation: -/+).
sum(vRoot)	Cumulative value of the actual transpiration rate [L].
sum(vBot)	Cumulative value of the actual flux across the bottom of the soil profile [L] (inflow/outflow: +/-).
hTop	Pressure head at the soil surface [L].
hRoot	Mean value of the pressure head over the region for which *Beta(n)*>0 (i.e., within the root zone) [L].
hBot	Pressure head at the bottom of the soil profile [L].
TLevel	Time-level (current time-step number) [-].

Table 10.2. RUN_INF.OUT - time and iteration information.

TLevel	Time-level (current time-step number) [-].
Time	Time, t, at current time-level [T].
dt	Time step, Δt [T].
IterW	Number of iterations necessary for solution of the water flow equation [-].
IterC	Number of iterations necessary for solution of the solute transport equation [-].
ItCum	Cumulative number of iterations [-].
KodT	Code for the boundary condition at the soil surface.
KodB	Code for the boundary condition at the bottom of the soil profile.
Converg	Information whether or not the numerical convergence was achieved at the current time-level.
Peclet	Maximum local Peclet number [-].
Courant	Maximum local Courant number [-].

Table 10.3. SOLUTE.OUT - actual and cumulative concentration fluxes.†

Time	Time, *t*, at current time-level [T].
cvTop	Actual solute flux across the soil surface [$ML^{-2}T^{-1}$] (inflow/outflow: +/-).
cvBot	Actual solute flux across the bottom of the soil profile [$ML^{-2}T^{-1}$] (inflow/outflow: +/-).
sum(*cvTop*)	Cumulative solute flux across the soil surface [ML^{-2}] (inflow/outflow: +/-).
sum(*cvBot*)	Cumulative solute flux across the bottom of the soil profile [ML^{-2}] (inflow/outflow: +/-).
sum(*cvCh*0)	Cumulative amount of solute removed from the flow region by zero-order reactions (positive when removed from the system) [ML^{-2}].
sum(*cvCh*1)	Cumulative amount of solute removed from the flow region by first-order reactions [ML^{-2}].
sum(*cvChR*)	Cumulative amount of solute removed from the flow region by root water uptake *S* [ML^{-2}].
cTop	Solute concentration at the soil surface [ML^{-3}].
cRoot	Mean solute concentration of the root zone [ML^{-3}].
cBot	Solute concentration at the bottom of the soil profile [ML^{-3}].
TLevel	Time-level (current time-step number) [-].

† Similar output files are created for each solute from 1 to *NS*.

Table 10.4. NOD_INF.OUT - profile information.

Node	Number of nodal point *n*.
Depth	*x*-coordinate of node *n*.
Head	Nodal value of the pressure head [L].
Moisture	Nodal value of the water content [-].
K	Nodal value of the hydraulic conductivity [LT^{-1}].
C	Nodal value of the hydraulic capacity [L^{-1}].
Flux	Nodal value of the Darcian velocity [LT^{-1}].
Sink	Nodal value of the root water uptake [T^{-1}].
K/KsTop	Ratio between the local hydraulic conductivity and the saturated hydraulic conductivity at the soil surface [-].
v/KsTop	Ratio between the local velocity and the saturated hydraulic conductivity at the soil surface [-].
Temp	Nodal value of the temperature [K].
Conc(1,..,*NS*)	Nodal value of the concentration [ML^{-3}]. Only given when *lChem*=.true. .
Sorb(1,..,*NS*)	Nodal value of the sorbed concentration [MM^{3}]. Only given when *lChem*=.true. and *lEquil*=.false. .

Table 10.5. BALANCE.OUT - mass balance variables.

Area	Length of the entire flow domain or a specified subregion [L].
Volume	Volume of water in the entire flow domain or in a specified subregion [L].
InFlow	Inflow/outflow to/from the entire flow domain or a specified subregion [LT^{-1}].
hMean	Mean pressure head in the entire flow domain or a specified subregion [L].
TVol	Amount of heat in the entire flow domain or a specified subregion [MT^{-2}].
TMean	Mean temperature in the entire flow domain or a specified subregion [K].
ConcVol	Amount of solute in the entire flow domain or a specified subregion [ML^{-2}]. This variable is given for all solutes from 1 to *NS*.
cMean	Mean concentration in the entire flow domain or a specified subregion [ML^{-3}]. This variable is given for all solutes from 1 to *NS*.
Top Flux	Actual surface flux [LT^{-1}] (infiltration/evaporation: -/+).
Bot Flux	Actual flux across the bottom of the soil profile [LT^{-1}] (inflow/outflow: +/-).
WatBalT	Absolute error in the water mass balance of the entire flow domain [L].
WatBalR	Relative error in the water mass balance of the entire flow domain [%].
CncBalT	Absolute error in the solute mass balance of the entire flow domain [ML^{-2}]. This variable is given for all solutes from 1 to *NS*.
CncBalR	Relative error in the solute mass balance of the entire flow domain [%]. This variable is given for all solutes from 1 to *NS*.

Table 10.6. A_LEVEL.OUT - pressure heads and cumulative fluxes on the boundary and in the root zone.

Time	Time, *t*, at current time-level [T].
sum(rTop)	Cumulative potential surface flux [L] (infiltration/evaporation: -/+).
sum(rRoot)	Cumulative potential transpiration [L].
sum(vTop)	Cumulative value of the actual surface flux [L] (infiltration/evaporation: -/+).
sum(vRoot)	Cumulative value of the actual transpiration [L].
sum(vBot)	Cumulative value of the bottom boundary flux [L] (inflow/outflow: +/-).
hTop	Pressure head at the soil surface [L].
hRoot	Mean value of the pressure head in the soil root zone for which *Beta(n)*>0 [L].
hBot	Pressure head at the bottom of the soil profile [L].
ALevel	A-level number (current variable boundary condition number) [-].

11. PROGRAM ORGANIZATION

11.1. *Description of Program Units*

The program consists of a main program and 39 subprograms. The subprograms are organized by means of 9 source files which are stored and compiled separately and then linked together with the main program to form an executable program. Below is a list and brief description of the different source files and associated subprograms.

HYDRUS.FOR	(Main program unit)
INPUT.FOR	BasInf, NodInf, MatIn, GenMat, TmIn, SinkIn, RootIn, TempIn, Profil, ChemIn
WATFLOW.FOR	WatFlow, SetMat, Hyster, Reset, Shift, Gauss, Veloc, Fgh
TIME.FOR	TmCont, SetBC
MATERIAL.FOR	FK, FC, FQ, FH, FS
SINK.FOR	SetSnk, FSAlfa, FAlfa, SetRG
OUTPUT.FOR	TLInf, ALInf, SubReg, NodOut, ObsNod
SOLUTE.FOR	Solute, Coef, MatSet, BanSol
TEMPER.FOR	Temper

Main program unit HYDRUS.FOR

This is the main program unit of HYDRUS. This unit controls execution of the program and determines which optional subroutines are necessary for a particular application.

Source file INPUT.FOR

Subroutines included in this source file are designed to read data from different input blocks. The following table summarizes from which input file and input block (described in Section 9) a particular subroutine reads.

Table 11.1. Input subroutines/files.

Subroutine	Input Block	Input File
BasInf	A. Basic Information	
MatIn	B. Material Information	
TmIn	C. Time Information	
RootIn	D. Root Growth Information	SELECTOR.IN
TempIn	E. Heat Transport Information	
ChemIn	F. Solute Transport Information	
SinkIn	G. Root Water Uptake Information	
NodInf	H. Nodal Information	GRID.IN
SetBC	I. Atmospheric Information	ATMOSPH.IN

Subroutine **Profil** writes into output file I_CHECK.OUT information about the soil profile, such as residual and saturated water contents, saturated hydraulic conductivities, air-entry pressure heads, and the spatial distribution of the root water uptake term.

Subroutine **GenMat** generates for each soil type in the flow domain a table of water contents, hydraulic conductivities, and specific water capacities using the specified set of hydraulic parameters.

Source file WATFLOW.FOR

Subroutine **WatFlow** is the main subroutine for simulating water flow; this subroutine controls the complete iterative procedure of solving the Richards equation.

Subroutine **Reset** constructs the global matrix equation for water flow, including the right-hand side vector.

Subroutine **Gauss** solves the tridiagonal symmetric matrix equation for water flow by Gaussian elimination.

Subroutine **Shift** changes atmospheric or seepage face boundary conditions from Dirichlet type to Neumann type conditions, or vice versa, as needed. This subroutine also updates variable boundary fluxes (free and deep drainage).

Subroutine **Veloc** calculates nodal water fluxes.

Subroutine **SetMat** determines the nodal values of the hydraulic properties $K(h)$, $C(h)$ and $\theta(h)$ by interpolation between intermediate values in the hydraulic property tables.

Function **Fqh** describes the groundwater level - discharge relationship, $q(h)$, defined by equation (7.1). This function is called only from subroutine SetAtm.

Subroutine **Hyster** calculates scaling factors for the drying and wetting scanning curves, hysteresis reversal points, and other information connected with hysteresis in the soil hydraulic properties.

Source file TIME.FOR

Subroutine **TmCont** adjusts the current value of the time increment Δt.

Subroutine **SetBC** updates time-variable boundary conditions.

Source file MATERIAL.FOR

This file includes the functions **FK, FC, FQ**, **FH**, and **FS** which define the unsaturated hydraulic properties $K(h)$, $C(h)$, $\theta(h)$, $h(\theta)$, and $S_e(\theta)$ for each soil material.

Source file SINK.FOR

This file includes subroutine **SetSnk** and functions **FAlfa** and **FSAlfa**. These subroutines calculate the actual root water extraction rate as a function of water and salinity stress in the soil root zone. The file also includes subroutine **SetRG** which calculates the rooting depth using the invoked root growth model.

Source file OUTPUT2.FOR

Subroutines included in this file are designed to print data to different output files. Table 11.2 summarizes which output files are generated with a particular subroutine.

Table 11.2. Output subroutines/files.

Subroutine	Output File
TLInf	T_LEVEL.OUT SOLUTEx.OUT RUN_INF.OUT
NodOut	NOD_INF.OUT
SubReg	BALANCE.OUT
ALInf	A_LEVEL.OUT
ObsNod	OBS_NODE.OUT

Source file SOLUTE.FOR

Subroutine **Solute** is the main subroutine for simulating solute transport; this subroutine also controls the iterative procedure for solving the nonlinear nonequilibrium convection-dispersion equation.

Subroutine **Coeff** calculates solute transport parameters, nodal values of the dispersion coefficients, the optimum upstream weighing factors, the maximum local Peclet and Courant numbers, and the maximum permissible time step.

Subroutine **MatSel** constructs the global matrix equation for transport, including the right-hand side vector.

Subroutine **BanSol** solves the final asymmetric matrix equation for solute transport using Gaussian elimination.

Source file TEMPER.FOR

Subroutine **Temper** is the main subroutine for simulating heat transport; this subroutine constructs the global matrix equation for heat transport, including the right-hand side vector.

11.2. *List of Significant HYDRUS Program Variables.*

Table 11.3. List of significant integer variables.

ALevel	Time level at which a time-dependent boundary condition is specified.
iHyst	Code indicating whether or not hysteresis in the soil hydraulic functions is considered (Table 9.2).
iKappa	Code indicating whether the main drying or main wetting branch of the retention curve is to be used to calculate the initial condition (Table 9.2).
iModel	Type of the soil hydraulic property model (Table 9.2).
iMoSink	Code specifying which type of root water uptake stress response function is to be used (Table 9.7).
iRFak	Code specifying how to calculate the root growth factor (Table 9.4).
ItCum	Cumulative number of iterations (Table 10.2).
IterC	Number of iterations necessary for solution of the solute transport equation (Table 10.2).
IterW	Number of iterations necessary for solution of the water flow equation (Table 10.2).
ItMax	If the number of required iterations at a particular time step is more than or equal to *ItMax*, then Δt for the next time step is multiplied by a dimensionless number *dMul2* < 1.0 (Table 9.3).
ItMin	If the number of required iterations at a particular time step is less than or equal to *ItMin*, then Δt for the next time step is multiplied by a dimensionless number *dMul* ≥ 1.0 (Table 9.3).
kBotCh	Code specifying the type of boundary condition for solute transport imposed at the bottom of the soil profile (Table 9.6).
kBotT	Code specifying the type of boundary condition for heat transport imposed at the bottom of the soil profile (Table 9.5).
KodBot	Code specifying the type of boundary condition for water flow imposed at the bottom of the soil profile (Table 9.2).
KodTop	Code specifying the type of boundary condition for water flow imposed at the surface (Table 9.2).
kTopCh	Code specifying the type of boundary condition for solute transport imposed at the surface (Table 9.6).
kTopT	Code specifying the type of boundary condition for heat transport imposed at the surface (Table 9.5).
MaxAl	Number of atmospheric data records (Table 9.9).
MaxIt	Maximum number of iterations allowed during any time step for solution of water flow equation (Table 9.2).
MaxItC	Maximum number of iterations allowed during any time step for solution of solute transport equation (Table 9.6).
MPL	Number of specified print-times at which detailed information about the pressure head, the water content, flux, temperature, solute concentration, and the soil water, solute and energy balances are printed (Table 9.3).
NFix	Number of fixed points (Table 9.8). This parameter is used for the discretization of soil profile.

Table 11.4. (continued)

NLay	Number of subregions for which separate water balances are being computed (Table 9.1).
NLevel	Number of time levels at which the matrix A and vector B are assembled for solute transport.
NMat	Number of soil materials (Table 9.1).
NMatD	Maximum number of soil materials (Table 7.6).
NObs	Number of observation nodes for which the pressure head, the water content, temperature and concentration are printed at each time level (Table 9.8).
NObsD	Maximum number of observation nodes for which the pressure head, the water content, temperature and concentration are printed at each time level (Table 7.6).
NPar	Number of unsaturated soil hydraulic parameters specified for each material (Table 9.2).
NS	Number of solutes (Table 9.6).
NSD	Maximum number of solutes (Table 7.6).
NTab	Number of entries in the internally generated tables of the hydraulic properties (see Section 5.4.7).
NTabD	Maximum number of entries in the internally generated tables of the hydraulic properties (Table 7.6).
NumNP	Number of nodal points (Table 9.8).
NumNPD	Maximum number of nodes permitted in the finite element mesh (Table 7.6).
PLevel	Print time-level (current print-time number).
TLevel	Time-level (current time-step number) (Table 10.2).

Table 11.4. List of significant real variables.

Alf	1-*Epsi*, where *Epsi* is a temporal weighing coefficient [-].
Alfa	Parameter in the soil water retention function [L^{-1}] (see Section 2.3).
Ampl	Temperature amplitude at the soil surface [K] (Table 9.5).
Aqh	Parameter A_{qh} in equation (7.1) [LT^{-1}] (Table 9.2).
AT	Temperature scaling factor α_h^* associated with the pressure head [-].
ATot	Length of the entire flow domain [L] (*Area* in Table 10.5).
Bqh	Parameter B_{qh} in equation (7.1) [L^{-1}] (Table 9.2).
BT	Temperature scaling factor α_K^* associated with the hydraulic conductivity [-].
cBalR	Relative error in the solute mass balance of the entire flow domain [%] (see equation (6.48)) (*CncBalR* in Table 10.5).
cBalT	Absolute error in the solute mass balance of the entire flow domain [ML^{-2}] (see equation (6.47)) (*CncBalT* in Table 10.5).
cE	Average concentration of an element [ML^{-3}].
Change	Inflow/outflow to/from the flow domain [LT^{-1}] (*InFlow* in Table 10.5).
cMid	Arithmetic mean of the concentration at the old and new time level [ML^{-3}].
cNewE	Amount of solute in a particular element at the new time-level [ML^{-2}].
CosAlfa	Cosine of the angle between the flow direction and the vertical axis [-] (i.e., cos $\alpha = 1$ for vertical flow, cos $\alpha = 0$ for horizontal flow) (Table 9.1).
Courant	Maximum local Courant number [-] (Table 10.2).
cSink	Concentration of the sink term [ML^{-3}].
cTolA	Maximum desired absolute change in the value of the concentration, c [ML^{-3}], between two successive iterations for nonlinear adsorption (Table 9.6).
cTolR	Maximum desired relative change in the value of the concentration, c [ML^{-3}], between two successive iterations for nonlinear adsorption (Table 9.6).
CumQrR	Cumulative total potential transpiration from the entire flow domain [L] (*sum*(*rRoot*) in Tables 10.1 and 10.6).
CumQrT	Cumulative total potential flux across the atmospheric boundary [L] (*sum*(*rTop*) in Tables 10.1 and 10.6).
CumQvR	Cumulative total actual transpiration from the entire flow domain [L] (*sum*(*vRoot*) in Tables 10.1 and 10.6).
CumR	Amount of solute removed from the entire flow domain by root water uptake during one time step [ML^{-2}].
*Cum*0	Amount of solute removed from the entire flow domain by zero-order reactions during one time step [ML^{-2}].
*Cum*1	Amount of solute removed from the entire flow domain by first-order reactions during one time step [ML^{-2}].

Table 11.4. (continued)

c50	Osmotic head at which root water uptake is reduced by 50 % [L] (Table 9.7).
DeltC	Sum of the absolute changes in concentrations as summed over all elements [ML^{-2}], (see equation (6.48)).
DeltW	Sum of the absolute changes in water content as summed over all elements [L], (see equation (5.20)).
dHenry	Change in the value of the equilibrium distribution constant, k_g, during one time step [T^{-1}].
dlh	Spacing (logarithmic scale) between consecutive pressure heads in the internally generated tables of the hydraulic properties [-], (see equation (5.23)).
dMul	Dimensionless number by which Δt is multiplied if the number of iterations is less than or equal to 3 [-] (Table 9.3).
dMul2	Dimensionless number by which Δt is multiplied if the number of iterations is greater than or equal to 7 [-] (Table 9.3).
dt	Time increment, Δt [T] (Table 9.3).
dtMax	Maximum permitted time increment, Δt_{max} [T] (Table 9.3).
dtMaxC	Maximum permitted time increment, Δt_{max} for solute transport [T] (see equation (6.51)).
dtMin	Minimum permitted time increment, Δt_{min} [T] (Table 9.3).
dtOld	Old time increment [T].
dtOpt	Optimal time increment [T].
EI	Potential surface flux per unit atmospheric boundary [LT^{-1}] (=*rTop*).
Epsi	Temporal weighing coefficient [-] (Table 9.6).
EpsH	Absolute change in the nodal pressure head between two successive iterations [L].
EpsTh	Absolute change in the nodal water content between two successive iterations [-].
fExp	Adsorption isotherm coefficient, β [-] (Table 9.6).
Frac	Dimensionless fraction of the adsorption sites classified as Type-1, i.e., sites with instantaneous sorption (Table 9.6).
GamG	First-order rate constant for gaseous phase, μ_g [T^{-1}] (Table 9.6).
*GamG*1	Rate constant, μ_g [T^{-1}], representing first-order decay for the first solute and zero-order production for the second solute in the gaseous phase (Table 9.6).
GamL	First-order rate constant for dissolved phase, μ_w [T^{-1}] (Table 9.6).
*GamL*1	Rate constant, μ_w [T^{-1}], representing first-order decay for the first solute and zero-order production for the second solute in the dissolved phase (Table 9.6).
GamS	First-order rate constant for the solid phase concentration, μ_s [T^{-1}] (Table 9.6).
*GamS*1	Rate constant, μ_s [T^{-1}], representing first-order decay for the first solute and zero-order production for the second solute in the solid phase (Table 9.6).
GWL0L	Parameter in equation (7.1) [L] (Table 9.2).

Table 11.4. (continued)

ha	Absolute value of the upper limit of the pressure head interval below which a table of hydraulic properties will be generated [L] (Table 9.2).
hb	Absolute value of the lower limit of the pressure head interval above which a table of hydraulic properties will be generated [L] (Table 9.2).
hB	Time-dependent prescribed head boundary condition [L] for the lower boundary (Table 9.9).
hCritA	Minimum allowed pressure head at the soil surface [L] (Table 9.9).
hCritS	Maximum allowed pressure head at the soil surface [L] (Table 9.9).
hE	Mean element value of the pressure head [L].
Henry	Equilibrium distribution constant between liquid and gas phase, k_g [-] (Table 9.6).
hMeanR	Mean value of the pressure head within the root zone [L] (*hRoot* in Table 10.1 and 10.6).
*hTab*1	Lower limit [L] of the pressure head interval for which tables of hydraulic properties are generated internally for each material (*ha* in Table 9.2).
hTabN	Upper limit [L] of the pressure head interval for which tables of hydraulic properties are generated internally for each material (*hb* in Table 9.2).
hTot	Mean pressure head of the entire flow domain [L] (*hMean* in Table 10.5).
Kk	Unsaturated hydraulic conductivity corresponding to θ_k [LT^{-1}] (see Section 2.3) (Table 9.2).
Ks	Saturated hydraulic conductivity [LT^{-1}] (Table 9.2).
m	Parameter in the soil water retention function [-] (see Section 2.3) (Table 9.2).
n	Parameter in the soil water retention function [-] (see Section 2.3) (Table 9.2).
Omega	Mass transfer coefficient for nonequilibrium adsorption, ω [T^{-1}] (Table 9.6).
Peclet	Maximum local Peclet number [-] (Table 10.2).
PeCr	Stability criteria (see Section 6.4.4) (Table 9.6).
Prec	Precipitation [LT^{-1}] (Table 9.9).
P0	Value of the pressure head [L], h_1, below which roots start to extract water from the soil (Table 9.7).
P2H	Value of the limiting pressure head [L], h_3, below which the roots cannot extract water at the maximum rate (assuming a potential transpiration rate of *r2P*) (Table 9.7).
P2L	As above, but for a potential transpiration rate of *r2L* (Table 9.7).
P3	Value of the pressure head [L], h_4, below which root water uptake ceases (usually equal to the wilting point) (Table 9.7).
P3c	Exponent p [-] in the S-shaped root water uptake salinity reduction function (Table 9.7).
P50	Pressure head at which the root water uptake is reduced by 50 % [L] (Table 9.7).
Qa	Parameter in the soil water retention function [-] (see Section 2.3) (Table 9.2).
Qk	Volumetric water content corresponding to K_k [-] (see Section 2.3) (Table 9.2).

Table 11.4. (continued)

Qm	Parameter in the soil water retention function [-] (see Section 2.3) (Table 9.2).
Qr	Residual soil water content [-] (Table 9.2).
Qs	Saturated soil water content [-] (Table 9.2).
R	Universal gas constant [$ML^2T^{-2}K^{-1}M^{-1}$] (8.314 kg m^2 $s^{-2}K^{-1}mol^{-1}$).
rB	Time-dependent prescribed flux at the bottom of the soil profile [LT^{-1}] (Table 9.9).
rBot	Time-independent boundary flux [LT^{-1}] prescribed at the bottom of the soil profile (Table 9.2).
ro	Bulk density of material *M* [ML^{-3}] (Table 9.6).
RootCh	Amount of solute removed from a particular subelement during one time step by root water uptake, [ML^{-2}].
rRoot	Potential transpiration rate [LT^{-1}] (Table 9.2).
rSoil	Potential evaporation rate [LT^{-1}] (Table 9.9).
rT	Time-dependent boundary flux [LT^{-1}] prescribed at the top of the soil profile (Table 9.9).
rTop	Potential surface flux across soil surface [LT^{-1}] (Table 10.1).
r2H	Potential transpiration rate [LT^{-1}] (see Table 9.7).
r2L	Potential transpiration rate [LT^{-1}] (see Table 9.7).
t	Time, *t*, at current time-level [T].
tAtm	Time for which the *i*-th data record is provided [T] (Table 9.9).
TauG	Tortuosity factor in the gas phase [-].
TauW	Tortuosity factor in the liquid phase [-].
tBot	Temperature for the lower boundary condition [K] (Table 9.5).
TE	Average temperature of an element [K].
tFix	Next time resulting from time discretization rules 2 and 3 [T] (see Section 5.4.2).
tInit	Starting time of the simulation [T] (Table 9.3).
tMax	Maximum duration of the simulation [T] (Table 9.3).
TNewE	Amount of heat in a particular element [MT^{-2}].
tOld	Previous time-level [T].
TolH	Maximum desired absolute change in the pressure head, *h* [L], between two successive iterations during a particular time step (Table 9.2).
TolTh	Maximum desired absolute change in the water content, θ [-], between two successive iterations during a particular time step (Table 9.2).
tPeriod	Time interval for completion of one temperature cycle [T] (Table 9.5).
tPulse	Time duration of the applied concentration pulse [T] (Table 9.6).
Tr	Reference temperature 293.15 K (20°C).

Table 11.4. (continued)

tRHarv	Time at the end of the root water uptake period [T] (Table 9.4).
tRMed	Time of known root depth [T] (Table 9.4).
tRMin	Initial time of the root growth period [T] (Table 9.4).
tTop	Temperature for the upper boundary condition [K] (table 9.5).
TTot	Average temperature in the entire flow domain [K] (*TMean* in Table 10.5).
TVol	Amount of heat in the entire flow domain [MT^{-2}] (Table 10.5).
Vabs	Absolute value of the nodal Darcy fluid flux density [LT^{-1}].
vMeanR	Actual transpiration rate [LT^{-1}] (*vRoot* in Table 10.1).
vNewE	Amount of water in a particular element at the new time-level [L].
vOldE	Amount of water in a particular element at the old time-level [L].
Volume	Amount of water in the entire flow domain [L] (Table 10.5).
wBalR	Relative error in the water mass balance of the entire flow domain [%] (see equation (5.20)).
wBalT	Absolute error in the water mass balance of the entire flow domain [L] (see equation (5.19)).
wCumA	Sum of the absolute values of all fluxes across the flow boundaries, including those resulting from sources and sinks in the region [L] (see equation (5.20)).
wCumT	Sum of all cumulative fluxes across the flow boundaries, including those resulting from sources and sinks in the region [L] (see equation (5.19)).
WLayer	Logical variable indicating whether or not water can accumulate at the soil surface with zero surface runoff (Table 9.2).
wVolI	Initial amount of water in the flow domain [L].
xKs	Adsorption isotherm coefficient, k_s [L^3M^{-1}] (Table 9.6).
xMuG	Zero-order rate constant for the gaseous phase concentration, γ_g [$ML^{-3}T^{-1}$] (Table 9.6).
xMuL	Zero-order rate constant for the liquid phase concentration, γ_w [$ML^{-3}T^{-1}$] (Table 9.6).
xMuS	Zero-order rate constant for the solid phase concentration, γ_s [T^{-1}] (Table 9.6).
xNu	Adsorption isotherm coefficient, η [L^3M^{-1}] (Table 9.6).
xRMax	Maximum rooting depth [L] (Table 9.4).
xRMed	Value of the known root depth [L] (Table 9.4).
xRMin	Initial value of rooting depth at the beginning of the growth period [L] (Table 9.4).

Table 11.5. List of significant logical variables.

AtmBC	Logical variable indicating whether or not the input file ATMOSPH.IN is provided (Table 9.1).
BotInf	Logical variable indicating whether a time-dependent or time-independent boundary condition is to be imposed at the bottom of the profile (Table 9.2).
ConvgF	Logical variable indicating whether or not convergence was achieved for water flow.
FreeD	Logical variable indicating whether a unit hydraulic gradient (free drainage) is, or is not, invoked at the bottom of the transport domain (Table 9.2).
ItCrit	Logical variable indicating whether or not convergence was achieved for water flow.
lArtD	Logical variable indicating whether or not artificial dispersion is to be added in order to satisfy the stability criteria *PeCr* (see Section 6.4.4) (Table 9.6).
lChem	Logical variable indicating whether or not the solute transport equation is to be solved (Table 9.1).
lConv	Logical variable indicating whether or not convergence was achieved in case of nonlinear adsorption (Table 9.1).
lEquil	Logical variable indicating whether equilibrium or nonequilibrium adsorption is to be considered (Table 9.1).
lMoSink	Logical variable indicating whether the *Feddes et al.* [1978] or S-shaped stress response function is to be used (Table 9.7).
lRoot	Logical variable indicating whether or not root growth is to be considered (Table 9.1).
lScreen	Logical variable indicating whether or not the selected output is to be sent to the monitor screen during program execution (Table 9.1).
lSolAdd	Logical variable indicating whether or not root water uptake reduction due to salinity is additive or multiplicative to the pressure head stress (Table 9.7).
lSolRed	Logical variable indicating whether or not root water uptake is reduced due to salinity (Table 9.7).
lTDep	Logical variable indicating whether or not the solute transport properties are considered to be temperature dependent (Table 9.6).
lTemp	Logical variable indicating whether or not the heat transport equation is to be solved (Table 9.1).
lUpW	Logical variable indicating if upstream weighing or the standard Galerkin formulation is to be used (Table 9.6).
lWat	Logical variable indicating if steady-state or transient water flow is to be considered (Table 9.1).
lWDep	Logical variable indicating whether or not the soil hydraulic properties are considered to be temperature dependent (Table 9.1).
qGWLF	Logical variable indicating whether or not the discharge-groundwater level relationship is to be used as bottom boundary condition (Table 9.2).
SeepF	Logical variable indicating whether or not a seepage face is to be invoked at the bottom of the transport domain (Table 9.2).
ShortO	Logical variable indicating whether or not the printing of time-level information is to be suppressed at each time level (Table 9.1).

Table 11.5. (continued)

SinkF	Logical variable indicating whether or not plant water uptake will take place (Table 9.1).
TopInf	Logical variable indicating whether a time-dependent or time-independent boundary condition is to be imposed on the top of the profile (Table 9.2).
WLayer	Logical variable indicating whether or not water can accumulate at the soil surface with zero surface runoff (Table 9.2).

Table 11.6. List of significant arrays.

Ah(NumNPD)	Nodal values of the dimensionless scaling factor α_h associated with the pressure head [-] (Table 9.8).
AhW(NMatD)	Ratio between parameters α^d and α^w of the main drying and wetting branches of the retention curve [-], respectively (see Section 2.6).
AK(NumNPD)	Nodal value of the dimensionless scaling factor α_K associated with the saturated hydraulic conductivity [-] (Table 9.8).
AKS(NumNPD)	Nodal value of the dimensionless scaling factor α_K associated with a particular scanning curve of a hysteretic model of soil hydraulic properties (see Section 2.6).
AKW(NMatD)	Ratio between the saturated hydraulic conductivities K_s^w and K_s^d of the main wetting and drying branches of the hydraulic conductivity function [-], respectively.
aOsm(NSD)	Osmotic coefficients a_i [L^4M^{-1}] (Table 9.7).
Area(10)	Length of the specified subregions [L] (Table 10.5).
Ath(NumNPD)	Nodal values of the dimensionless scaling factor α_θ associated with the water content (Table 9.8).
AthS(NumNPD)	Nodal values of the dimensionless scaling factor α_θ associated with a particular scanning curve of a hysteretic model of soil hydraulic properties (see Section 2.6).
AThW(NMatD)	Ratio between differences θ_s^w-θ_r^w and θ_s^d-θ_r^d of the main wetting and drying branches of the retention curve [-], respectively (see Section 2.6).
B(NumNPD)	Coefficient vector in the global solute transport matrix equation [LT^{-1}].
Beta(NumNPD)	Nodal values of the normalized rootwater uptake distribution [L^{-1}] (Table 9.8).
Cap(NumNPD)	Nodal values of the soil water capacity [L^{-1}].
CapTab(NTabD,NMatD)	Internally generated table of the soil water capacity [L^{-1}].
cB(NSD)	Time-dependent boundary concentration for the soil surface [ML^{-3}] (Table 9.9).
cBot(NSD)	Concentration associated with the lower boundary condition [ML^{-3}] (Table 9.6).
cCumA(NSD)	Sum of the absolute values of all cumulative solute fluxes across the flow boundaries, including those resulting from sources and sinks in the flow domain [ML^{-2}] (see equation (6.48)).
cCumT(NSD)	Sum of all cumulative solute fluxes across the boundaries, including those resulting from sources and sinks in the flow domain [ML^{-2}] (see right hand side of equation (6.47)).
*ChPar(NSD*16+3,NMatD)*	Parameters which describe the solute transport properties of the porous medium (Table 9.6).
cMean(8,10)	Mean concentrations of specified subregions [ML^{-3}] (Table 10.5).
cNew(NumNPD)	Nodal values of the concentration at the new time level [ML^{-3}].
Con(NumNPD)	Nodal values of the hydraulic conductivity [LT^{-1}].
Conc(NSD,NumNPD)	Nodal values of the concentration [ML^{-3}] (Table 9.8).

Table 11.6. (continued)

ConD(NumNPD)	Nodal values of the thermal conductivity [$MLT^{-3}K^{-1}$] ($Wm^{-1}K^{-1}$).
ConO(NumNPD)	Nodal values of the hydraulic conductivity at old time level [LT^{-1}].
ConR(NumNPD)	Nodal values of the fictitious residual hydraulic conductivity for a wetting scanning curve [LT^{-1}].
ConSat(NMatD)	Saturated hydraulic conductivities of materials [LT^{-1}].
ConSub(8,10)	Amounts of solute in the specified subregions [ML^{-2}] (Table 10.5).
ConTab(NTabD,NMatD)	Internally generated table of the hydraulic conductivities [LT^{-1}].
ConVol(8)	Amount of solute in the entire flow domain [ML^{-2}] (*ConVol* in Table 10.5).
cPrevO(NumNPD)	Nodal values of the concentration of the previous solute in the decay chain at the old time-level [ML^{-3}].
cT(NSD)	Time-dependent concentration boundary condition for the soil surface [ML^{-3}] (Table 9.9).
cTemp(NumNPD)	Nodal values of the concentration at the previous iteration [ML^{-3}].
cTop(NSD)	Concentration associated with the upper boundary condition [ML^{-3}] (Table 9.6).
cTot(8)	Mean concentration in the flow domain [ML^{-3}] (*cMean* in Table 10.5).
CumCh(4,*NSD*)	Cumulative boundary solute fluxes and amounts of solute removed from the entire flow domain by zero- and first-order reactions [ML^{-2}] (Table 10.2).
CumQ(NumKD)	Cumulative boundary fluxes [L] (Table 10.1).
cvBot(NSD)	Solute boundary fluxes across the bottom of the soil profile [$ML^{-2}T^{-1}$] (Table 10.3).
*cvCh*0(*NSD*)	Amount of solute removed from the entire flow domain by zero-order reactions [$ML^{-2}T^{-1}$] (Table 10.3).
*cvCh*1(*NSD*)	Amount of solute removed from the entire flow domain by first-order reactions [$ML^{-2}T^{-1}$] (Table 10.3).
cvChR(NSD)	Amount of solute removed from the entire flow domain by root water uptake [$ML^{-2}T^{-1}$] (Table 10.3).
cVolI(NSD)	Initial amount of solute in the entire flow domain [ML^{-2}].
cvTop(NSD)	Solute boundary fluxes across the soil surface [$ML^{-2}T^{-1}$] (Table 10.3).
D(NumNPD)	Coefficient vector in the global solute transport matrix equation [LT^{-1}].
Disp(NumNPD)	Nodal values of the dispersion coefficient D [L^2T^{-1}].
E(NumNPD)	Coefficient vector in the global solute transport matrix equation [LT^{-1}].
F(NumNPD)	Coefficient vector in the global solute transport matrix equation [$ML^{-2}T^{-1}$].
*g*0(*NumNPD*)	Nodal values of parameter G [$ML^{-3}T^{-1}$] (see equation (3.14)).
*g*1(*NumNPD*)	Nodal values of parameter F [T^{-1}] (see equation (3.13)).
hMean(10)	Mean values of the pressure head in specified subregions [L] (Table 10.5).
hNew(NumNPD)	Nodal values of the pressure head [L] at the new time-level (Table 9.8).

Table 11.6. (continued)

hOld(*NumNPD*)	Nodal values of the pressure head [L] at the old time-level.
hSat(*NMatD*)	Air-entry values for each material [L].
hTab(*NTabD*)	Internal table of the pressure head [L].
hTemp(*NumNPD*)	Nodal values of the pressure head [L] at the previous iteration.
iObs(*NObsD*)	Observation nodes for which the pressure head, the water content, temperature and concentration are printed at each time level (Table 9.8).
iUnit(13)	Vector which contains identification numbers of the different output files.
Kappa(*NumNPD*)	Code indicating whether the local process is drying or wetting at the new time level.
KappaO(*NumNPD*)	Code indicating whether the local process is drying or wetting at the old time level.
LayNum(*NumNPD*)	Subregion numbers assigned to each element (Table 9.8).
lLinear(*NSD*)	Array of logical variables indicating whether a linear or nonlinear adsorption to be considered.
MatNum(*NumNPD*)	Index for material whose hydraulic and transport properties are assigned to a particular node (Table 9.8).
Node(*NObsD*)	Observation nodes for which the pressure head, the water content, temperature and concentration are printed at each time level (Table 9.8).
P(*NumNPD*)	Coefficient vector in the global water flow matrix equation [T^{-1}].
ParD(10,*NMatD*)	Parameters describing the drying branch of the hydraulic properties of the medium (Table 9.2).
ParW(10,*NMatD*)	Parameters describing the wetting branch of the hydraulic properties of the medium (Table 9.2).
POptm(*NMatD*)	Values of the pressure head [L], h_2, below which roots start to extract water at the maximum possible rate (Table 9.4).
*q*0(*NumNPD*)	Nodal values of part of parameter G representing zero-order reactions [$ML^{-3}T^{-1}$] (see equation (3.14)).
*q*1(*NumNPD*)	Nodal values of part of parameter F representing first-order reactions [T^{-1}] (see equation (3.13)).
R(*NumNPD*)	Coefficient vector in the global water flow matrix equation [T^{-1}].
Retard(*NumNPD*)	Nodal values of the retardation factor R [-].
S(*NumNPD*)	Coefficient vector in the global water flow matrix equation [T^{-1}].
Sink(*NumNPD*)	Nodal values of the sink term [T^{-1}] (see equation (2.3)).
SolIn(*NumNPD*)	Element values of the initial amount of solute [ML^{-2}].
Sorb(*NSD*,*NumNPD*)	Nodal values of the sorbed concentration for type-2 sorption sites [-] (Table 9.8).
SorbN(*NumNPD*)	Nodal values of the sorbed concentration for type-2 sorption sites during the last iteration [-] (Table 9.8).
SubCha(10)	Inflow/outflow to/from specified subregions [LT^{-1}] (Table 10.5).

Table 11.6. (continued)

SubT(10)	Amount of heat in specified subregions [MT^{-2}] (Table 10.5).
SubVol(10)	Volume of water in specified subregions [L] (Table 10.5).
TDep(*NSD**16+3)	Activation energy for transport and chemical parameters [$ML^2T^{-2}M^{-1}$] (see Section 3.4).
TempN(*NumNPD*)	Nodal values of the temperature at the new time level [K].
TempO(*NumNPD*)	Nodal values of the temperature at the old time level [K].
TheTab(*NTabD*,*NMatD*)	Internal table of the soil water content [-].
ThNew(*NumNPD*)	Nodal values of the water content at the new time level [-].
ThOld(*NumNPD*)	Nodal values of the water content at the old time level [-].
thr(*NMatD*)	Residual water contents for specified materials [-].
ThRR(*NumNPD*)	Nodal values of the residual water content for a wetting scanning retention curve [L^3 L^{-3}] (see Section 2.6).
thSat(*NMatD*)	Saturated water contents for specified materials [-].
TMean(10)	Average temperature in a specified subregion [K] (Table 10.5).
TPar(10,*NMatD*)	Parameters which describe the heat transport properties of the porous media (Table 9.5).
TPrint(*MPL*)	Specified print-times [T] (Table 9.3).
vN(*NumNPD*)	Nodal values of the Darcian velocity vector at the new time level [LT^{-1}].
vO(*NumNPD*)	Nodal values of the Darcian velocity vector at the old time level [LT^{-1}].
WatIn(*NumNPD*)	Element values of the initial volume of water [L].
wBot(10)	Nodal density below fixed points (Table 9.8). Variable is used for discretizing the soil profile.
wc(*NumNPD*)	Weighing factors associated with the element [-].
wTop(10)	Nodal density above fixed points (Table 9.8). Variable is used for discretizing the soil profile.
x(*NumNPD*)	*x*-coordinates [L] of the nodal points (Table 9.8).
xFix(10)	Coordinate of fixed points (Table 9.8). Variable is used for discretizing the soil profile.

12. REFERENCES

Alexander, M., and K. M. Scow. 1989. Kinetics of biodegradation in soil, In *Reactions and Movement of Organic Chemicals in Soils*, edited by B. L. Sawhney and K. Brown, Spec. Publ. No. 22, 243-270, Soil Science Society of America, Madison, WI.

Aziz, K., and A. Settari. 1979. *Petroleum Reservoir Simulation.* pp. 395-401, Applied Science, Barking, United Kindom.

Bear, J. 1972. *Dynamics of Fluid in Porous Media.* Elsevier, New York, NY.

Belmans, C., J. G. Wesseling and R. A. Feddes. 1983. Simulation model of the water balance of a cropped soil: SWATRE, *J. Hydrol., 63*, 271- 286.

Bromilow, R. H., and M. Leistra. 1980. Measured and simulated behavior of aldicarb and its oxidation products in fallow soils, *Pestic. Sci., 11*(4), 389-395.

Brooks, R. H., and A. T. Corey. 1966. Properties of porous media affecting fluid flow. *J. Irrig. Drainage Div.*, ASCE Proc. 72(IR2), 61-88.

Castro, C. L., and D. E. Rolston. 1977. Organic phosphate transport and hydrolysis in soil: theoretical and experimental evaluation, *Soil Sci. Soc. Am. J., 41*(6), 1085-1092.

Celia, M. A., and E. T. Bououtas, R. L. Zarba. 1990. A general mass-conservative numerical solution for the unsaturated flow equation, *Water Resour. Res., 26*, 1483-1496.

Chiou, C. T. 1989. Theoretical consideration of the partition uptake of nonionic organic compounds by soil organic matter, In *Reactions and Movement of Organic Chemicals in Soils*, edited by B. L. Sawhney and K. Brown, Spec. Publ. Number 22, 1-30, Soil Science Society of America, Madison, WI.

Chung S.-O., and R. Horton. 1987. Soil heat and water flow with a partial surface mulch, *Water Resour. Res., 23*(12), 2175-2186.

Cho, C. M. 1971. Convective transport of ammonium with nitrification in soil, *Can. Jour. Soil Sci., 51*(3), 339-350.

Christie, L. D., D. F. Griffiths, A. R. Mitchell, and O. C. Zienkiewicz. 1976. Finite element methods for second order differential equations with significant first derivatives, *Int. J. Num. Methods in Engineering, 10*, 1389-1396.

Císlerová, M. 1987. Comparison of simulated water balance for ordinary and scaled soil hydraulic characteristics, *Publ. No. 82*, Dept. of Hydraulics and Catchment Hydrology, Agricultural Univ., Wageningen, The Netherlands.

Cleary, R. W., and M. J. Ungs. 1978. Groundwater pollution and hydrology, Mathematical models and computer programs, *Research Rep. No. 78-WR-15*, Water Resour. Program, Princeton Univ. Princeton, NJ.

Constantz, J. 1982. Temperature dependence of unsaturated hydraulic conductivity of two soils. *Soil Sci. Soc. Am. J., 46*(3), 466-470.

Davis, L. A., and S. P. Neuman. 1983. Documentation and user's guide: UNSAT2 - Variably saturated flow model, *Final Rep., WWL/TM-1791-1,* Water, Waste & Land, Inc., Ft. Collins, CO.

de Marsily, G. 1986. *Quantitative Hydrogeology*, Academic Press, London.

de Vries, D. A. 1963. The thermal properties of soils, In *Physics of Plant Environment*, edited by R. W. van Wijk, pp. 210-235, North Holland, Amsterdam.

Feddes, R. A., E. Bresler, and S. P. Neuman. 1974. Field test of a modified numerical model for water uptake by root systems, *Water Resour. Res., 10*(6), 1199-1206.

Feddes, R. A., P. J. Kowalik, and H. Zaradny. 1978. *Simulation of Field Water Use and Crop Yield*, John Wiley & Sons, New York, NY.

Glotfelty, D. E., and C. J. Schomburg. 1989. Volatilization of pesticides from soil, In *Reactions and Movement of Organic Chemicals in Soils*, edited by B. L. Sawhney and K. Brown, Spec. Publ. Number 22, 181-208, Soil Science Society of America, Madison, WI.

Gureghian, A. B. 1981. A two-dimensional finite-element solution for the simultaneous transport of water and multi-solutes through a nonhomogeneous aquifer under transient saturated-unsaturated flow conditions, *Sci. Total Environ., 21*, 329-337.

Gureghian, A. B., and G. Jansen. 1983. LAYFLO: A one-dimensional semianalytical model for the migration of a three-member decay chain in a multilayered geologic medium, *Tech. Rep. ONWI-466*, Office of Nuclear Waste Isolation, Battelle Memorial Institute, Columbus, OH.

Harada, M., P. L. Chambre, M. Foglia, K. Higashi, F. Iwamoto, D. Leung, T. H. Pigford, and D. Ting. 1980. Migration of radionuclides through sorbing media, analytical solutions - I, *Rep. no. LBL-10500 (UC-11)*, Lawrence Berkeley Laboratory, Univ. of California, Berkeley, CA.

Higashi, K., and T. H. Pigford. 1980. Analytical models for migration of radionuclides in geologic sorbing media, *J. Nucl. Sci. and Techn., 7*(9), 700-709.

Hopmans, J. W., and J. N. M. Stricker. 1989. Stochastic analysis of soil water regime in a watershed, *J. Hydrol., 105*, 57-84.

Huyakorn, P. S., and G. F. Pinder. 1983. *Computational Methods in Subsurface Flow*, Academic Press, London, United Kingdom.

Javandel, I., Ch. Doughty, Chin-Fu Tsang. 1984. *Groundwater Transport: Handbook of Mathematical Models*, Water Resour. Monograph No. 10, Am. Geophys. Union, Washington, D.C.

Jury, W. A., W. F. Spencer, and W. J. Farmer. 1983. Behavior assessment model for trace organics in soil, I. Model description, *J. Environ. Qual., 12*, 558-564.

Kirkham, D., and W. L. Powers. 1972. *Advanced Soil Physics*, John Wiley & Sons, New York, NY.

Kool, J. B., and J. C. Parker. 1987. Development and evaluation of closed-form expressions for hysteretic soil hydraulic properties. *Water Resour. Res., 23*(1), 105-114.

Kool, J. B., M. Th. van Genuchten. 1991. HYDRUS - One-dimensional variably saturated flow and transport model, including hysteresis and root water uptake, Version 3.3, *Research Report No. 124*, U. S. Salinity Laboratory, USDA, ARS, Riverside, CA.

Leij, F. J., T. H. Skaggs, and M. Th. van Genuchten. 1991. Analytical solutions for solute transport in three-dimensional semi-infinite porous media, *Water Resour. Res., 27*(10), 2719-2733.

Leij, F. J., and S. A. Bradford. 1994. 3DADE: A computer program for evaluating three-dimensional equilibrium solute transport in porous media, *Research Report No. 134*, U. S. Salinity Laboratory, USDA, ARS, Riverside, CA.

Lester, D. H., G. Jansen, and H. C. Burkholder. 1975. Migration of radionuclide chains through an adsorbing medium, In: *Adsorption and Ion Exchange,* Am. Inst. Chem. Eng., Symp. Series no. 152, 71, 202-213.

Luckner, L., M. Th. van Genuchten, and D. R. Nielsen. 1989. A consistent set of parametric models for the two-phase flow of immiscible fluids in the subsurface. *Water Resour. Res., 25*(10), 2187-2193.

Lynch, D. 1984. Mass conservation in finite element groundwater models. *Adv. Water Resour., 7*, 67-75.

Miller, E. E., and R. D. Miller. 1956. Physical theory for capillary flow phenomena, *J. Appl. Phys., 27*, 324-332.

Millington, R. J., and J. M. Quirk. 1961. Permeability of porous solids, *Trans. Faraday Soc., 57*, 1200-1207.

Misra, C., D. R. Nielsen, J. W. Biggar. 1974. Nitrogen transformations in soil during leaching: I. Theoretical considerations, *Soil Sci. Soc. Am. Proc., 38*(2), 289-293.

Mls, J. 1982. Formulation and solution of fundamental problems of vertical infiltration, *Vodohosp. Čas., 30*, 304-313 (in Czech).

Mohammad, F. S., and R. W. Skaggs. 1983. Drain tube opening effects on drain inflow, *J. Irrig. Drain. Div., Am. Soc. Civ. Eng., 109*(4), 393-404.

Mualem, Y. 1976. A new model for predicting the hydraulic conductivity of unsaturated porous media, *Water Resour. Res., 12*(3), 513-522.

Neuman, S. P. 1972. Finite element computer programs for flow in saturated-unsaturated porous media, *Second Annual Report, Project No. A10-SWC-77*, Hydraulic Engineering Lab., Technion, Haifa, Israel.

Neuman, S. P. 1973. Saturated-unsaturated seepage by finite elements, *J. Hydraul. Div.*, ASCE, 99 (HY12), 2233-2250.

Neuman, S. P., R. A. Feddes, and E. Bresler. 1974. Finite element simulation of flow in saturated-unsaturated soils considering water uptake by plants, *Third Annual Report, Project No. A10-SWC-77*, Hydraulic Engineering Lab., Technion, Haifa, Israel.

Neuman, S. P. 1975. Galerkin approach to saturated-unsaturated flow in porous media, Chapter 10 in *Finite Elements in Fluids, Vol. I, Viscous Flow and Hydrodynamics*, edited by R. H. Gallagher, J. T. Oden, C. Taylor, and O.C. Zienkiewicz, John Wiley & Sons, London, pp. 201-217.

Nielsen, D. R., and L. M. Luckner. 1992. Theoretical aspects to estimate reasonable initial parameters and range limits in indentification procedures for soil hydraulic properties. In, Proc. Intl. Workshop on *Indirect Methods for Estimating the Hydraulic Properties of Unsaturated Soils,* edited by M. Th van Genuchten, F. J. Leij, and L. J. Lund, University of California, Riverside, pp. 147-160.

Ou, L. T., P. S. C. Rao, K. S. V. Edvardson, R. E. Jessup, A. G. Hornsby, and R. L. Jones. 1988. Aldicarb degradation in sandy soils from different depths, *Pesticide Sci., 23*, 1-12.

Perrochet, P., and D. Berod. 1993. Stability of the standard Crank-Nicolson-Galerkin scheme applied to the diffusion-convection equation: some new insights, *Water Resour. Res., 29*(9), 3291-3297.

Philip, J. R., and D. A. de Vries. 1957. Moisture movement in porous media under temperature gradients, *Eos Trans. AGU, 38*(2), 222-232.

Pignatello, J. J. 1989. Sorption dynamics of organic compounds in soils and sediments, In *Reactions and Movement of Organic Chemicals in Soils*, edited by B. L. Sawhney and K. Brown, Spec. Publ. Number 22, 45-80, Soil Science Society of America, Madison, WI.

Pinder, G. F., W. G. Gray. 1977. *Finite Element Simulation in Surface and Subsurface Hydrology*, Academic Press, New York, N.Y.

Raats, P. A. C., Steady flows of water and salt in uniform soil profiles with plant roots, *Soil Sci. Soc. Am. Proc., 38*, 717-722, 1974.

Rogers, V. C. 1978. Migration of radionuclide chains in groundwater, *Nucl. Techn., 40*(3), 315-320.

Rogers, J. S., J. L. Fouss. 1989. Hydraulic conductivity determination from vertical and horizontal drains in layered soil profiles, *Transaction of the ASAE, 32*(2), 589-595.

Scott, P. S., G. J. Farquhar, and N. Kouwen. 1983. Hysteresis effects on net infiltration, Advances in Infiltration, *Publ. 11-83*, pp.163-170, Am. Soc. Agri. Eng., St. Joseph, Mich.

Selim, H. M., R. Schulin, H. Flühler. 1987. Transport and ion exchange of calcium and magnesium in an aggregated soil, *Soil Sci. Soc. Am. J., 51*(4), 876-884.

Simmons, C. S., D. R. Nielsen, J. W. Biggar. 1980. Scaling of field-measured soil water properties, *Hilgardia, 47*, 101-122.

Šimůnek, J., T. Vogel and M. Th. van Genuchten. 1992. The SWMS_2D code for simulating water flow and solute transport in two-dimensional variably saturated media, Version 1.1., *Research Report No. 126*, U. S. Salinity Laboratory, USDA, ARS, Riverside, CA.

Šimůnek, J. 1993. *Numerical modeling of transport processes in unsaturated porous media,* Dissertation, Czech Academy of Sciences, Prague (in Czech).

Šimůnek, J., and D. L. Suarez. 1993a. Modeling of carbon dioxide transport and production in soil: 1. Model development, *Water Resour. Res., 29*(2), 487-497.

Šimůnek, J., and D. L. Suarez. 1993b. UNSATCHEM-2D code for simulating two-dimensional variably saturated water flow, heat transport, carbon dioxide production and transport, and multicomponent solute transport with major ion equilibrium and kinetic chemistry, Version 1.1., *Research Report No. 128*, U. S. Salinity Laboratory, USDA, ARS, Riverside, CA.

Šimůnek, J., and M. Th. van Genuchten. 1994. The CHAIN_2D code for simulating two-dimensional movement of water flow, heat, and multiple solutes in variably-saturated porous media, Version 1.1, *Research Report No 136*, U.S. Salinity laboratory, USDA, ARS, Riverside, California.

Šimůnek, J., and M. Th. van Genuchten. 1995. Numerical model for simulating multiple solute transport in variably-saturated soils, *Proc. "Water Pollution III: Modelling, Measurement, and Prediction*, Ed. L. C. Wrobel and P. Latinopoulos, Computation Mechanics Publication, Ashurst Lodge, Ashurst, Southampton, UK, pp. 21-30.

Šír, M., T. Vogel, and M. Císlerová. 1985. Analytical expression of the retention curve and hydraulic conductivity for porous material, *Vodohosp. Čas., 33*(1), 74-85 (in Czech).

Sisson, J. B. 1987. Drainage from layered field soils: Fixed gradient models, *Water Resour. Res., 23*(11), 2071-2075.

Skaggs, R. W., E. J. Monke, and L. F. Huggins. 1970. An approximate method for determining the hydraulic conductivity function of an unsaturated soil, *Techn. Rep. No. 11*, Water Resour. Res. Center, Purdue University, Lafayette, IN.

Sophocleous, M. 1979. Analysis of water and heat flow in unsaturated-saturated porous media, *Water Resour. Res., 15*(5), 1195-1206.

Spencer, W. F. 1991. Volatilization of pesticides from soil: processes and measurement, *Pesticide Res. J., 3*(1), 1-14.

Sposito, G. 1981. *The Thermodynamics of Soil Solutions*. Oxford University Press, New York, NY.

Stumm, W., and J. J. Morgan. 1981. *Aquatic Chemistry: An Introduction Emphasizing Chemical Equilibria in Natural Waters*, John Wiley & Sons, New York, NY.

Sudicky, E. A., and P. S. Huyakorn. 1991. Contaminant migration in imperfectly known heterogeneous groundwater systems, *Review of Geophysics*, Supplement, U. S. National Rep. to Inter. Union of Geodesy and Geophysics 1987-1990, 240-253.

Tillotson, W. R., C. W. Robbins, R. J. Wagenet, R. J. Hanks. 1980. Soil water, solute and plant growth simulation, *Bulletin 502,* Utah Agricultural Experiment Station, 53 p.

Toride, N., F. J. Leij, and M. Th. van Genuchten. 1993. A comprehensive set of analytical solutions for nonequilibrium solute transport with first-order decay and zero-order production, *Water Resour. Res., 29*(7), 2167-2182.

van Genuchten, M. Th. 1976. On the accuracy and efficiency of several numerical schemes for solving the convective-dispersive equation, in *Finite Elements in Water Resources*, edited by W. G. Gray et al., Pentech Press, London, pp. 1.71-1.90.

van Genuchten, M. Th. 1978. Mass transport in saturated-unsaturated media: one-dimensional solutions, *Research Rep. No. 78-WR-11*, Water Resources Program, Princeton Univ., Princeton, NJ.

van Genuchten, M. Th. 1980. A closed-form equation for predicting the hydraulic conductivity of unsaturated soils, *Soil Sci. Soc. Am. J., 44*, 892-898.

van Genuchten, M. Th. 1981. Non-equilibrium transport parameters from miscible displacement experiments. *Research Report No. 119*, U.S. Salinity Laboratory, Riverside, CA.

van Genuchten, M. Th. 1985. Convective-dispersive transport of solutes involved in sequential first-order decay reactions, *Computers & Geosciences, 11*(2), 129-147.

van Genuchten, M. Th., and J. Parker. 1984. Boundary conditions for displacement experiment through short laboratory soil columns, *Soil Sci. Soc. Am. J., 48*, 703-708.

van Genuchten, M. Th., 1987. A numerical model for water and solute movement in and below the root zone. *Research Report No 121*, U.S. Salinity laboratory, USDA, ARS, Riverside, California.

van Genuchten, M. Th., and R. J. Wagenet. 1989. Two-site/two-region models for pesticide transport and degradation: Theoretical development and analytical solutions, *Soil Sci. Soc. Am. J., 53*, 1303-1310.

Vimoke, B. S., and G. S. Taylor. 1962. Simulating water flow in soil with an electric resistance network, *Report No. 41-65*, 51 p., Soil and Water Conserv. Res. Div., U. S. Agric. Res. Serv., Columbus, OH.

Vimoke, B. S., T. D. Tura, T. J. Thiel, and G. S. Taylor. 1963. Improvements in construction and use of resistance networks for studying drainage problems, *Soil Sci. Soc. Am. Proc., 26*(2), 203-207.

Vogel, T. 1987. SWMII - Numerical model of two-dimensional flow in a variably saturated porous medium, *Research Rep. No. 87*, Dept. of Hydraulics and Catchment Hydrology, Agricultural Univ., Wageningen, The Netherlands.

Vogel, T., M. Císlerová. 1988. On the reliability of unsaturated hydraulic conductivity calculated from the moisture retention curve, *Transport in Porous Media, 3*, 1-15.

Vogel, T. 1990. *Numerical modeling of water flow in non-homogeneous soil profile*, Dissertation, Czech Technical Univ., Prague (in Czech).

Vogel, T., M. Císlerová, and J. W. Hopmans. 1991. Porous media with linearly variable hydraulic properties, *Water Resour. Res., 27*(10), 2735-2741.

Vogel, T., K. Huang, R. Zhang, and M. Th. van Genuchten. 1996. The HYDRUS code for simulating one-dimensional water flow, solute transport, and heat movement in variably-saturated media, Version 5.0, *Research Report No 140*, U.S. Salinity laboratory, USDA, ARS, Riverside, CA.

Wagenet, R. J., J. W. Biggar, and D. R. Nielsen. 1976. Analytical solutions of miscible displacement equations describing the sequential microbiological transformations of urea, ammonium and nitrate, *Research Rep. no 6001,* Dept. of Water Science and Engineering, Univ. California, Davis, CA.

Wagenet R. J., and J. L. Hutson. 1987. LEACHM: Leaching Estimation And CHemistry Model, A process-based model of water and solute movement, transformations, plant uptake and chemical reactions in the unsaturated zone, *Continuum 2*, Dept. of Agronomy, Cornell University, Ithaca, New York, NY.

Wesseling, J. G., and T. Brandyk. 1985. Introduction of the occurrence of high groundwater levels and surface water storage in computer program SWATRE, *Nota 1636*, Institute for Land and Water Management Research (ICW), Wageningen, The Netherlands.

Yeh, G. T., and V. S. Tripathi. 1990. HYDROGEOCHEM: A coupled model of HYDROlogic transport and GEOCHEMical equilibria in reactive multicomponent systems, *Environs Sci. Div., Publ. No. 3170.*, Oak Ridge National Lab., Oak Ridge, TN.

Zienkiewicz, O.C. 1977. *The Finite Element Method*, 3rd ed., McGraw-Hill, London, United Kingdom.